RSC Advances

REVIEW

Cite this: *RSC Adv.*, 2022, **12**, 10950

Gold nanoparticle-based optical nanosensors for food and health safety monitoring: recent advances and future perspectives

Nguyen Ha Anh,†*[a] Mai Quan Doan,†[a] Ngo Xuan Dinh,[a] Tran Quang Huy,[ab] Doan Quang Tri,[c] Le Thi Ngoc Loan,[d] Bui Van Hao[e] and Anh-Tuan Le*[ae]

Modern society has been facing serious health-related problems including food safety, diseases and illness. Hence, it is urgent to develop analysis methods for the detection and control of food contaminants, disease biomarkers and pathogens. As the traditional instrumental methods have several disadvantages, including being time consuming, and having high cost and laborious procedures, optical nanosensors have emerged as promising alternative or complementary approaches to those traditional ones. With the advantages of simple preparation, high surface-to-volume ratio, excellent biocompatibility, and especially, unique optical properties, gold nanoparticles (AuNPs) have been demonstrated as excellent transducers for optical sensing systems. Herein, we provide an overview of the synthesis of AuNPs and their excellent optical properties that are ideal for the development of optical nanosensors based on local surface plasmon resonance (LSPR), colorimetry, fluorescence resonance energy transfer (FRET), and surface-enhanced Raman scattering (SERS) phenomena. We also review the sensing strategies and their mechanisms, as well as summarizing the recent advances in the monitoring of food contaminants, disease biomarkers and pathogens using developed AuNP-based optical nanosensors in the past seven years (2015–now). Furthermore, trends and challenges in the application of these nanosensors in the determination of those analytes are discussed to suggest possible directions for future developments.

Received 12th November 2021
Accepted 29th March 2022

DOI: 10.1039/d1ra08311b

rsc.li/rsc-advances

1. Introduction

Never in the history of humanity have food and health not been major global concerns. In the Christian Bible, the Four Horsemen of the Apocalypse are figures representing four heart-struck fears of human: Pestilence, War, Famine and Death. Nowadays, by virtue of the rapid developments of agriculture and food processing industry, the worries of famine are less serious in most areas of the world, instead, people have to deal with the threat of unsafe food and drinks. There have been incidents of heavy metal contaminants in wheat,[1] melamine in milk,[2] fipronil in chicken eggs and poultry products,[3] Cholera outbreaks,[4] *etc.* Food contamination may lead to serious gastrointestinal infections,[5] malnutrition,[6] and even cancers.[6,7] Moreover, humanity has been fighting against diseases such as cancer and diabetes for decades. Besides, the continuous appearance of new pathogenic viruses such as Severe Acute Respiratory Syndrome coronaviruses (SARS-CoV) and Middle East respiratory syndrome coronavirus (MERS-CoV) keeps challenging every medical system. Recently, the COVID-19 outbreak has proved that human beings have never escaped from the threat of fatal diseases and pathogens. All of these problems have been putting human health in serious dangers. Therefore, it is essential to develop rapid and accurate tools and techniques to detect food contaminants, as well as diseases and pathogens.

The traditional methods such as high performance liquid chromatography (HPLC),[8] mass spectrometry (MS),[9] liquid chromatography-MS,[10] gas chromatography-MS,[11] and polymerase chain reactions (PCR)[12] are powerful techniques to detect different kinds of chemical compounds and biological elements. Despite their high sensitivity, accuracy and stability, they are time consuming, laborious and require expensive instruments.[13,14] Therefore, sensing systems have been investigated to develop rapid, convenient, effective and less expensive detecting tools. In general, a sensor requires a target recognition element to ensure the selectivity and a transducer element to signal the binding events and manage the sensitivity of the detection.[15] Antibodies,[16] enzymes[17] and aptamers[18] are obviously effective for specific recognitions. A useful transducer element has to possess the ability to convert physical and

[a]*Phenikaa University Nano Institute (PHENA), Phenikaa University, Hanoi 12116, Vietnam. E-mail: anh.nguyenha@phenikaa-uni.edu.vn*
[b]*Faculty of Electric and Electronics, Phenikaa University, Hanoi 12116, Vietnam*
[c]*Advanced Institute for Science and Technology (AIST), Hanoi University of Science and Technology (HUST), 1st Dai Co Viet Road, Hanoi, Vietnam*
[d]*Faculty of Natural Sciences, Quy Nhon University, Quy Nhon 55113, Vietnam*
[e]*Faculty of Materials Science and Engineering, Phenikaa University, Hanoi 12116*
† N. H. Anh and M. Q. Doan contributed equally to this work.

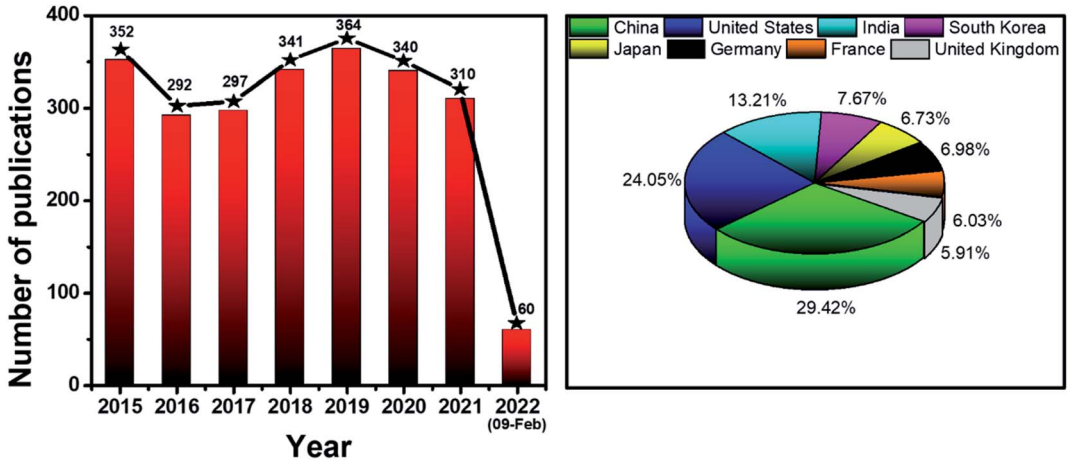

Fig. 1 Statistics of publications about AuNPs-based optical sensors (2015 – February 2022). Data source: Scopus. Keywords: gold nanoparticles optical sensors.

chemical changes into detectable or measurable signals.[15] Gold nanoparticles (AuNPs) have been attracting considerable attention as excellent scaffolds for the development of advanced sensing systems.[19] With the sizes in the range of ~1–100 nm, AuNPs possess unique physical and/or chemical properties in comparison with either the bulk state or the atomic level. Stable AuNPs can be easily prepared in either chemical or physical approaches.[20,21] Moreover, their excellent biocompatibility and high surface-to-volume ratio allow the binding of various organic and biological ligands.[22] Furthermore, their unique

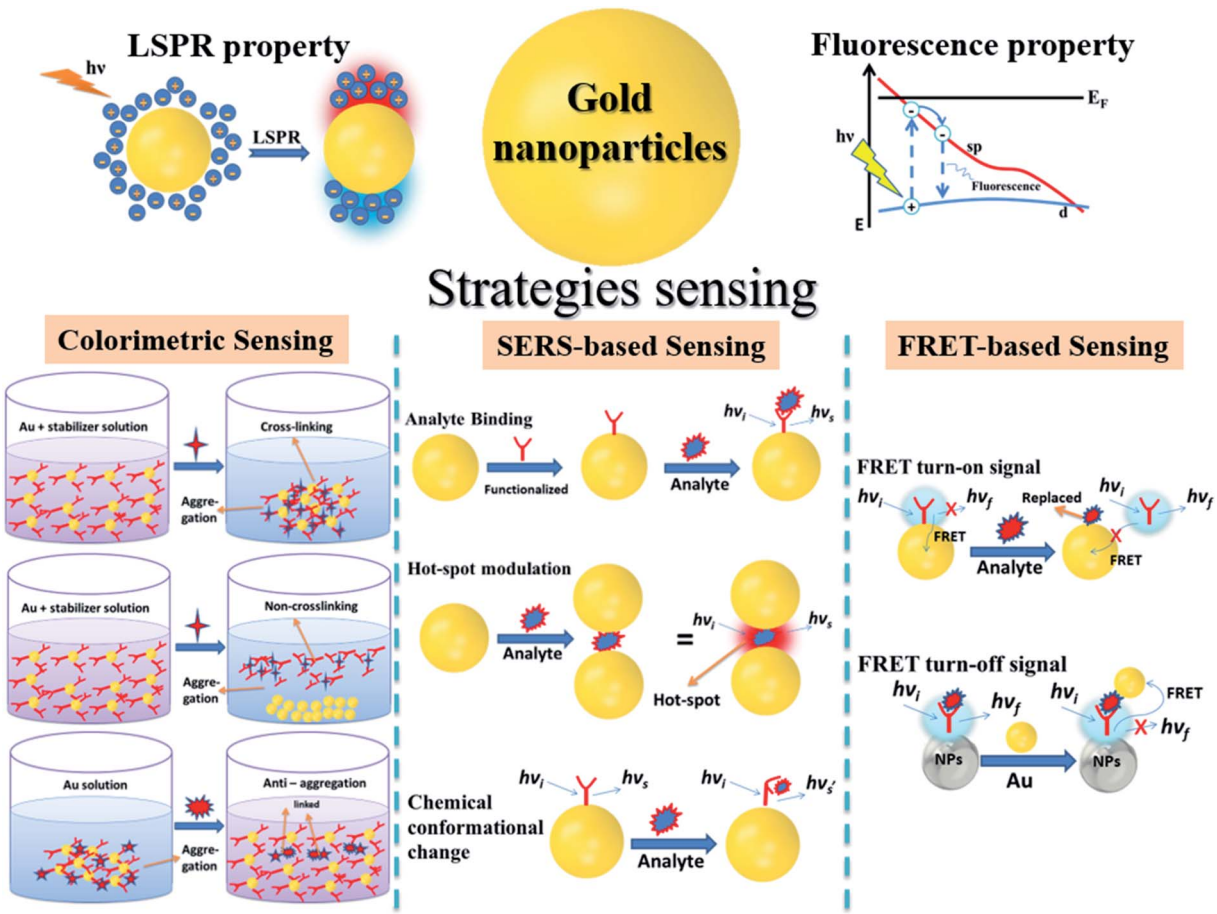

Fig. 2 Illustration of gold nanoparticles, their optical properties and strategies to develop AuNPs-based optical nanosensors.

electrical, electrochemical, catalytic and especially, optical properties are remarkable.[21,23,24] Every modification of size, shape, analyte binding, aggregation, *etc.* leads to change(s) in optical behaviors of AuNPs such as wavelength shift, color change, and enhancement of Raman scattering.[25,26] They are detectable response signals that researchers are always looking for in an appropriate transducer. Therefore, it is not surprising that AuNPs-based optical sensors have attracted their interest for several years. Fig. 1 demonstrates the statistics of publications about AuNPs-based optical sensors over the last seven years (2015 – February 2022) according to Scopus data. Even after many years of investigation, it is still a well-concerned topic of researchers all around the world without any sign of stop. Possessing the properties of local surface plasmon resonance (LSPR), fluorescence quenching and surface-enhanced Raman scattering (SERS), AuNPs have been employed to develop different kinds of optical sensing systems including LSPR, colorimetric, fluorescence resonance energy transfer (FRET)-based and SERS-based sensors (Fig. 2). In this review, we focus on the strategies to develop those sensors, especially for the applications in food safety monitoring, and *in vitro* disease diagnosis. Recent advances in optical nanosensors for those analytes will be highlighted, focusing on the use of monometallic AuNPs, however, potential of multi-metallic gold-based optical nanosensors will be also introduced. Trends and challenges will be discussed to consider the future perspectives.

Recently, several reviews relating AuNPs-based sensors for food safety[14,27] and disease diagnosis[28–30] have been established. However, most of them only focused on colorimetric sensors.[14,27–30] Other types of AuNPs-based optical sensors were mentioned in a few reviews but only as an introduction without full discussion.[28–30] This review exhibits a systematic look of AuNPs-based optical sensors for food and health safety monitoring with three kinds of sensors including colorimetric, FRET and SERS sensors. Further discussion about the sensing strategies developed for each kind of those optical sensors would provide readers more choices when considering designing a AuNPs-based optical sensor for their desired analyte. On the other hand, instead of focusing on the sensing mechanism for each kind of analytes as in the literature,[28–30] this review shows several comparisons of sensing strategies for different selection of analyte for one identical target, for example, nucleic acid or protein biomarker for cancer detection; nucleic acid, capsid protein or antibody for virus determination; *etc.*, which is useful for researchers when selecting a suitable analyte for their study. Therefore, this review would give researchers who are working on AuNPs-based sensors some suggestions to develop their sensing strategies to their designed targets in the future.

2. Gold nanoparticles

2.1. Synthesis and modifications

Analogously to other nanomaterials, AuNPs can be prepared by both "top-down" and "bottom-up" methods. In general, the "top-down" fabrication of AuNPs involves breaking down the bulk Au into nanoparticles, while the "bottom-up" method is based on the assembly of precursor molecules or atoms. For the "top-down" approach, various techniques have been developed, such as chemical etching, lithography, pyrolysis, laser ablation, sputtering, *etc.*[20,21,31] Despite their advantages of fast and simple fabrication procedures, these "top-down" methods commonly encounter the limitations in controlling the particle size and shape.[32] In addition, some of these synthesis procedures require extreme conditions, including high vacuum, high temperature, and large amount of energy as well as expensive instruments.[21]

In contrast, the "bottom-up" methods commonly involve the reduction of Au ions into Au atoms, followed by the assembly of the atoms to form NPs. In this case, the formation of AuNPs normally follows two steps: the nucleation and the subsequent growth.[32,33] In the first step, under certain circumstance, Au atoms are assembled to form small clusters, which function as nuclei. The addition of the incident atoms to the surface of the nuclei leads to the formation of AuNPs in the second step. An isotropic growth normally results in spherical nanoparticles. In order to tailor the particle morphology, surfactants such as cetyltrimethylammonium bromide (CTAB),[34] sodium dodecylsulfonate (SDS),[35] and poly(vinylpyrrolidone) (PVP)[36] are usually added. This is due to the fact that surfactants may suppress the growth in certain directions and promote the growth in the other directions, resulting in the anisotropic growth of the NPs.[37,38] Therefore, by choosing an appropriate surfactant, the particle size and shape can be controlled. This is a great advantage of the "bottom-up" methods over the "top-down". Nevertheless, the use of toxic chemicals and solvents is a major drawback of this approach.[39]

The era of size- and shape-controlled synthesis of AuNPs started with the method developed by Turkevich in 1951, in which AuNPs were synthesized by reducing hydrogen tetrachloroaurate ($HAuCl_4$) in the presence of sodium citrate.[40] This method was further improved by Frens *et al.* in 1957, who demonstrated the size control of AuNPs by varying the ratio between $HAuCl_4$ and sodium citrate.[41] Although this protocol requires a high dilution of the Au salt that leads to the low AuNP concentration, its simplicity is a great advantage that retains it as the first choice of researchers for the synthesis of spherical and monodispersed AuNPs with diameters in the range of 10–20 nm. In 1994, Brust and co-workers developed a novel approach for the synthesis of ultra-small AuNPs, namely two-phase liquid–liquid reduction of $AuCl_4^-$ by sodium borohydride in the presence of alkanethiol, which is nowadays known as the Schiffrin-Brust method.[42] In this method, $HAuCl_4$ was transferred from the aqueous solution to toluene using tetraoctylammonium bromide as the phase-transfer reagent. The addition of dodecanethiol and aqueous sodium borohydride facilitated the reduction of $AuCl_4^-$. In this process, the growth of Au clusters was accompanied by the simultaneous attachment of self-assembled thiol monolayers on Au surface. This provided an excellent control of the particle size, which allowed the synthesis of AuNPs with diameters in the range of 1–3 nm.[42] These are the pioneering works that paved the way for the tremendous development in AuNPs synthesis in the last several decades.[42–44]

At the same time, the shape-controlled growth has also received enormous attention due to the shape-dependent properties of AuNPs.[45,46] In this regard, the most common approach is utilizing surfactants to promote the anisotropic growth of AuNPs. A diversity of AuNPs such as nanorods, nanostars, nanoflowers, and many others has been fabricated by adding CTAB as a surfactant.[37,38] PVP has been reported to be useful to control the formation of star-like Au nanoplates.[47] Recently, surfactant-free techniques have been developed to control the shape of AuNPs. Wall *et al.* demonstrated the fabrication of AuNPs with different morphologies, including nanostars, nanospheres, nanorods, and nanoplates without using any surfactant. Instead, the morphology was controlled by varying the ratio between the reactants, pH, temperature and reaction time.[48]

As the environmental issues raise the concerns, chemical solvents are gradually replaced by other environmentally benign reducing and capping agents such as biomolecules like lactic acids and chitosan,[49] or other biological agents such as extracts from *Citrus maxima* fruit or alfalfa plants.[50] Alternative approaches used physical agents to assist the reduction of Au ions, such as UV irradiation or electrical current in the electrochemical and photochemical methods.[33,51,52] Laser ablation is another popular physical method of synthesis as it can be employed to synthesize AuNPs in both aqueous and organic solvents.[53,54] Moreover, this process does not require the removal of excess reagents after the synthesis. It also helps avoid the contamination on the surface of the nanoparticles and reduce the toxicity of the prepared nanoparticles. Vinod *et al.* demonstrated a successful synthesis of AuNPs by pulsed laser ablation.[55] The obtained AuNPs exhibited excellent SERS and photothermal properties.[55] Electron-beam-induced reduction method has also been employed for the synthesis of AuNPs with a diameter of less than 20 nm that can be used as bioimaging probes in mammalian cells.[56] However, in comparison with the chemical synthesis methods, the physical approaches are less convenient and provide a lower yield.

For technological sensing applications, AuNPs are usually modified by appropriate chemical or biological elements for target recognition. Binding a self-assembled monolayer (SAM) to the AuNPs surface is a common technique to functionalize AuNPs. In general, SAM involves the adsorption of organic molecules onto the solid surface.[57,58] Thiol, amides and carboxylic acids are ideal candidates for SAM due to their affinities to the AuNPs surface. Among them, thiols are most used because the Au–S bond is the strongest ($\sim$40 kcal mol^{-1}) in comparison with Au–N ($\sim$8 kcal mol^{-1}) and Au–COO ($\sim$2 kcal mol^{-1}).[59] Thanks to these interactions, a wide range of molecules can be anchored to AuNPs. For example, peptides or proteins can be attached.[60] Kumar and coworkers used cysteinylated peptide to modified AuNPs and developed a sensor for Newcastle disease virus.[61] Similarly, thiolated aptamers were bound to AuNPs in a colorimetric sensor for interleukin-6, a biomarker for acute inflammation.[62] Thanks to this great biocompatibility, AuNPs can be the scaffold for many kinds of recognition elements, leading to the ability to sense various targets, from inorganic to organic and from molecules to cells.

2.2. Optical properties of gold nanoparticles for sensing applications

2.2.1. Localized surface plasmon resonance: LSPR-based and colorimetric sensors & sensing mechanism. Localized surface plasmon resonance (LSPR) is one of the most important optical properties of AuNPs. LSPR is a phenomenon in which a collective coherent oscillation of the surface conduction electrons of the AuNPs is induced by the electric field of the incident light. The interaction between the electric field and the free electrons induces a charge separation, leading to the accumulation of charges on the surface of NPs.[25,26,63,64] LSPR is highly dependent on shape and size of AuNPs. Sharp corners of the NPs lead to the rise of charge polarization, resulting in the red-shifts of LSPR spectra while highly symmetric structures increase the intensity of dipole resonances, followed by the increase in LSPR intensities.[65] In addition, AuNPs may exhibit multiple resonance absorption peaks depending on the number of modes that they are polarized.[25,66] Therefore, nonspherical NPs usually exhibit multiple, red-shifted peaks in comparison to spherical particles.[67] For example, with two axis, transverse and longitudinal, gold nanorods can be polarized along them, leading to the appearance of two absorption peaks.[65] In contrast, spherical AuNPs exhibit only one peak of absorption.[65] Moreover, the longitudinal LSPR peak of gold nanorods is usually found at the longer wavelength region in comparison to the absorption band of spherical AuNPs.[25] The wavelength-shift of LSPR peak is also observed with the change in size of AuNP. It was reported that for spherical AuNPs, changing the size from 10 to 100 nm results in a red-shift of 47 nm.[68] In addition, the interaction among NPs is also an influencing factor to LSPR. Interacting particles, either in a dimer or in an aggregation, would result in red shifts of the LSPR spectra as well as the appearance of an absorption band at the region of lower energy (larger wavelength).[25,26] Furthermore, wavelength shifts in LSPR spectra can also be the results of changes in refractive index at the surface of NPs. The relationship between the LSPR wavelength shift, $\Delta\lambda$ (in nm), and the change in refractive index Δn (in refractive index unit, RIU) is described by the equation:[25,63]

$$\Delta\lambda = m\Delta n\left[1 - \exp\frac{-2d}{l_d}\right] \quad (1)$$

in which m is the bulk refractive index response of the nanoparticles (in nm/RIU), d is the thickness of adsorbed layer (in nm) and l_d is the characteristic electromagnetic field decay length (in nm). Eqn (1) expresses the influence of the changes in the surrounding medium as well as the attachment of other molecules onto the surface of the NPs through Δn on their LSPR spectra. Therefore, every change in size, shape, interparticle interaction, surrounding environment and surface modification may result in LSPR wavelength shifts. This is the underlying mechanism of optical sensors based on inherent LSPR property of AuNPs.

Due to their strong LSPR absorption in the green region, AuNP solutions usually exhibit a characteristic ruby red color. In most cases, an LSPR wavelength-shift can lead to a change in color of the solution. For example, an aggregation of AuNPs that

caused a red shift of the LSPR spectra was also observed as a red-to-purple/blue change in the solution color.[69] Therefore, the changes in LSPR spectra can be detected by either using an UV-visible spectrophotometer or bare-eyes. Hence, from the LSPR characteristics of AuNPs, two typical types of optical sensors have been developed: LSPR-based and colorimetric sensors. Importantly, the shift of LSPR spectra is strongly correlated with the aggregation of AuNPs. This correlation has been utilized in many sensing systems that are related to the aggregation of AuNPs (Fig. 3).

The aggregation state of AuNPs can be triggered through either crosslinking or non-crosslinking strategies. In the crosslinking method, ligand-functionalized AuNPs are assembled in the addition of a target element. Herein, the ligand acts as recognition probes for the target compound, which binds to this compound, decreases the interparticle distance and triggers aggregation of the AuNPs (Fig. 2). For instance, in the study of Megarajan and Veerapan, the aggregation of *N*-lauryltyramine (NLTA) capped AuNPs was induced in the addition of Al^{3+}, which led to a pink-to-purple change in the solution color as well as a red-shift from 538 nm to 670 nm of the LSPR peak. The mechanism was suggested to be the chelation effect between NLTA and Al^{3+}.[70] In contrast, the non-crosslinking approach, which is also known as de-protection method, is based on the removal of stabilizing agent on the surface of AuNPs due to the presence of the target element. In this strategy, AuNPs are well-protected with the stabilizing agent to avoid aggregation. However, in the addition of the target element, which has higher affinity to the stabilizing agent, the AuNPs lose their coating agent (*i.e.* they are "de-protected"). This loss of electrosteric stabilizations results in AuNP aggregation. Aptamer-anchored AuNPs are widely used to develop colorimetric sensors based on this mechanism. In the addition of salts and the target elements, the aptamers are disassociated from AuNPs to "capture" the targets while high-salt condition induced the aggregation of the AuNPs. Wu *et al.* have applied this strategy and designed aptasensors for detection of *Escherichia coli* O157:H7 and *Salmonella typhimurium* with the specificity of 100%.[71]

On the contrary, a change of color from blue to red is observed in another strategy of colorimetric sensing called anti-aggregation. In this method, a linking molecule (or linker) induces aggregation of NPs by crosslinking mechanism. However, as the target element has a higher affinity to the linker, their interaction inhibits the binding of the linker to the ligand on AuNP surface and consequently prevents the aggregation of those AuNPs. For example, Gao's group introduced a sensing system for Ag^{+}, in which thiamazole played the role of a linking molecule to induce aggregation of AuNPs.[72] The presence of Ag^{+} ions triggered the formation of preferential combination between the pyrimidic nitrogen of thiamazole and Ag^{+} ions. Moreover, thiol group of thiamazole was also oxidized by Ag^{+}. Therefore, the aggregation of AuNPs was inhibited, which resulted in a blue-to-red change in the solution color[72]

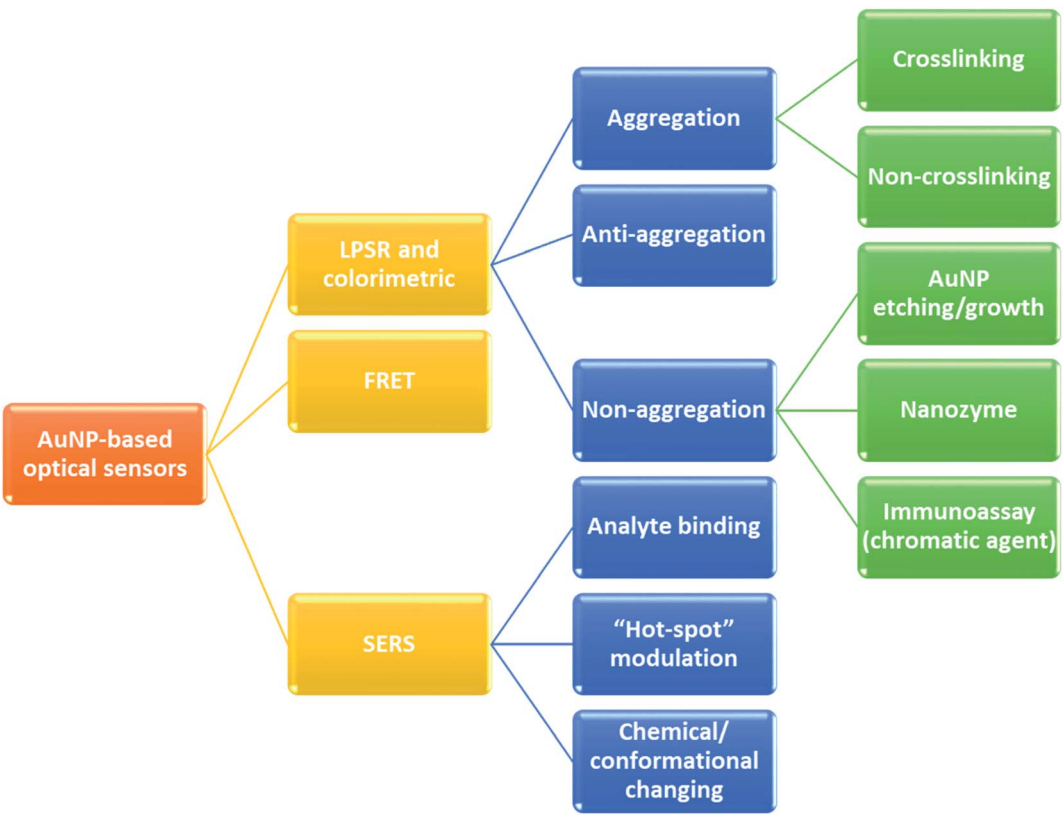

Fig. 3 AuNPs-based optical sensors and their sensing strategies.

(Fig. 4). The same strategy has been utilized to detect other heavy metals, food additives, *etc.*[14,73,74]

Mainly concerning the aggregation of AuNPs (either formation or destruction), all strategies mentioned above do not require any specific shape of the AuNPs. Therefore, any kind of AuNPs can be employed to develop these colorimetric sensors, however, spherical AuNPs are the most selected in practice.[75] The choice of isotropic AuNPs helps simplify the fabrication procedures of the sensors, consequently, it is more time- and cost-effective to develop these sensors. Brief information about AuNPs-based colorimetric sensors and their particle shapes can be found in Table 1 and 2, and further discussion about those sensors will be presented in the following sections.

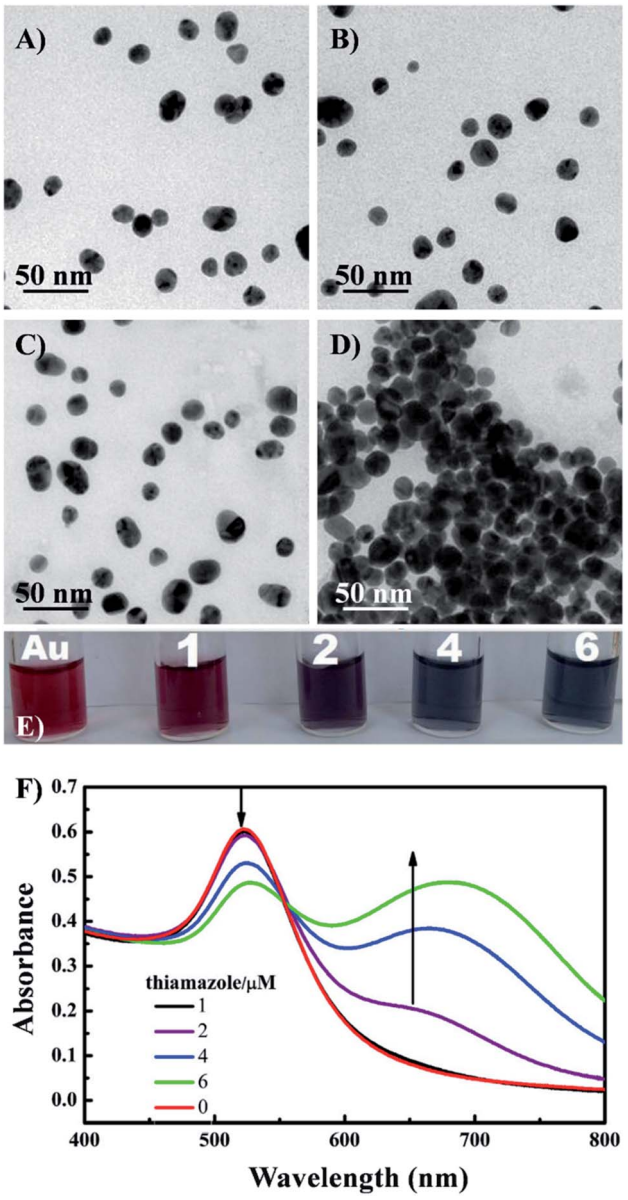

Fig. 4 TEM images of the AuNPs under different conditions: (A) AuNPs, (B) AuNPs + Ag^+ ions (1 nM), (C) AuNPs + thiamazole (2 μM) + Ag^+ (1 nM), (D) AuNPs + thiamazole (2 μM); (E) photographs and (F) UV-VIS absorption spectra of AuNPs and AuNPs (200 μL) mixed with different concentrations of thiamazole (1–6 μM). Reprinted from ref. 72 Copyright 2021, with permission from Elsevier.

Based on the aggregation of AuNPs, the colorimetric sensing strategies mentioned above are fast and simple with only a few steps of preparation and testing. Moreover, the obvious color change can be observed with bare-eye without any complicated instrument. However, the main limitation of these approaches is that AuNPs can be aggregated due to numerous factors, including pH, temperature and ionic forces that can lead to false positive/negative results. Therefore, researchers have investigated AuNPs-based sensors applying non-aggregation mechanisms, including etching, growth and nanozyme.[76] Etching techniques focus on the effect of enchants such as H_2O_2 and I^- ions to change the sizes and shapes of AuNPs, which leads to a shift in LSPR peak and a subsequent color change of reaction solution. Thus, etching is the only strategy, in which anisotropic NPs, such as Au nanorods and multibranched AuNPs, are preferable when designing colorimetric sensors.[66,77] An example of this strategy is a urine glucose sensor established by Zhang *et al.*, in which glucose oxidase enzymatic reaction led to the release of H_2O_2 that oxidized I^- to I_2 rapidly.[66] Au nanorods were etched by I_2, especially at their tips, thus, a longitudinal LSPR blue-shift and a blue-to-red color change were observed for glucose detection.[66] Besides, tetracycline, one of the over-used antibiotics for farm animals, could reduce Au^{3+} ions to trigger the growth of AuNPs and introduce the characteristic red color to the solutions. Hence, it has become the principle to develop tetracycline sensing systems.[78] However, it is worth mentioning that the selectivity of this method is low among other antibiotics in the same family (with tetracycline) due to their similar phenolic structures.[78] In another approach, the peroxidase-like activity of AuNPs allows them to oxidize TMB in the presence of H_2O_2 to achieve the colorless-to-blue color change in solutions. Hence, target elements that enhance the catalytic activity such as Hg^{2+} (ref. 79) and Fe^{2+},[80] or induce the formation of H_2O_2 such as glucose[81] (in the interaction with glucose oxidase) can be detected. In another study, the color change was reversed upon the addition of glutathione, which suggested another principle to sense this disease marker.[82] Furthermore, AuNPs can mimic the catalytic activity of several other enzymes such as glucose oxidase and peroxidase.[76,83] With the highest surface area-to-volume ratio, there is no surprise that spherical AuNPs are the most selected material for this approach (see Tables 1 and 2).

AuNPs-based sensors using non-aggregation approaches are more complicated than those using aggregation or anti-aggregation methods. For instance, to detect zearalenone, a mycotoxin, the sensors fabricated based on the catalytic activity of AuNPs to convert 4-nitrophenol (yellow) into 4-aminophenol (colorless) needed to be functionalized with two kinds of single stranded DNA (ssDNA), including one aptamer and its complementary strand. Moreover, the detecting procedure required two steps of adding exonuclease III and 4-nitrophenol.[84] Nevertheless, these novel methods have helped researchers to escape from the "red-to-blue" trap as with every kind of target element, the aggregation methods only exhibit the colors in that range. The novel indirect colorimetric

Table 1 Recently reported AuNPs-based optical nanosensors for food safety (2015–now)

Target	Nanomaterials	Sensing principle	LOD	Linear range	Real sample	Ref.
Heavy metals						
Hg^{2+}	Aptamer-spherical AuNP	Colorimetric (crosslinking)	3.4 nM	5 nM to 10 μM	Tap water	200
Hg^{2+}	Aptamer-spherical AuNP	FRET	60 nM	0.2–20 μM	Tap water, milk	201
Hg^{2+}	cDNA-spherical AuNP	FRET	7.5×10^{-13} M	1.3×10^{-12} to 2.4×10^{-5} M	Fish	145
Hg^{2+}	ssDNA-spherical AuNP	SERS (hot-spot formation)	0.45 pg mL^{-1}	0.001–0.5 ng mL^{-1}	Drinking water	117
Hg^{2+}	DNAzyme contained ssDNA-spherical AuNP	Colorimetric (anti-aggregation)	59.59 nM	0–1 nM 1–15 nM	Tap water	148
Cr^{3+}	4-Amino hippuric acid (PAH)-spherical AuNP	Colorimetric (crosslinking)	1.17 μM	5.0–120 μM	Liquid milk, milk power	202
Cd^{2+}	2,6-Dimecartopurine-spherical AuNP	Colorimetric (crosslinking)	32 nM	0.75–3.0 μM	Milk, honey	203
Cu^{2+}	Dipicolylamine-spherical AuNP	SERS (change in ligand)	5×10^{-8} M	5×10^{-8} to 5×10^{-4} M	White wine	120
Pb^{2+}	Citrate-spherical AuNP	Colorimetric (crosslinking)	0.5 μM	0.5–100 μM	Water	204
Pb^{2+}	DNAzyme-spherical AuNP	Colorimetric (anti-aggregation)	8.0 nM	0–500 nM	Tap water	205
Pb^{2+}	Maleic acid-spherical AuNP	Colorimetric (crosslinking)	0.5 μg L^{-1} (~2.4 nM)	0.0–10.0 μg L^{-1} (~0.0–48 nM)	Breast milk	206
Pb^{2+}	GSH-spherical AuNP	LSPR (change in refractive index)	5×10^{-11} M	10^{-10} to 10^{-5} M	Preserved egg	207
As^{3+}	Citrate-spherical AuNP	Colorimetric (crosslinking)	1.8 ppb	4–100 ppb	Drinking water	152
Pesticides						
Phorate	Hyaluronan-tyrosine-spherical AuNP	Colorimetric (non-crosslinking)	0.005 μg mL^{-1} (~0.006 mg kg^{-1})	0.001–10 μg mL^{-1}	Tomato	155
Organophosphorus pesticides	Spherical AuNP	Colorimetric (AuNP growth)	0.7 ppb (~2.4 nM)	25–65 ppb	Tap water, apple washing solution	157
Dichlorvos Trichlorfon Paraoxon	Citrate-spherical AuNP	Colorimetric (crosslinking) + enzyme inhibitor	0.0120 mg kg^{-1}, 0.0224 mg kg^{-1}, 0.0106 mg kg^{-1}	0–1000 μg L^{-1}	Pear, Chinese cabbage	208
Triazophos Parathion Chlorpyrifos	Fluorophore-ssDNA-spherical AuNP	FRET	0.007 μg L^{-1} 0.009 μg L^{-1} 0.089 μg L^{-1}	0.01–20 μg L^{-1} 0.05–50 μg L^{-1} 0.5–1000 μg L^{-1}	Homogenized rice, wheat, cucumber, cabbage, apple	158
Parathio-methyl Thiram Chlorpyrifos	Spherical AuNP on sticky side of adhesive tape	SERS	2.60 ng cm^{-2} 0.24 ng cm^{-2} 3.51 ng cm^{-2}	—	Vegetable, cucumber, orange, apple	161
Parathio-methyl Triazophos Phosmet	C_{14}PDB-snowflake-like AuNP	SERS (analyte binding)	0.026 ng cm^{-2} 0.031 ng cm^{-2} 0.032 ng cm^{-2} (apple peel)	—	Cucumber, apple, mango, green pepper, tomato peel	159
Malathion	Citrate-spherical AuNP	Colorimetric (anti-aggregation)	11.8 nM	0.05–0.8 μM	Tap water, apple juice, vegetable juice	209
Chlorsulfuron	Acetamiprid-spherical AuNP	Colorimetric (anti-aggregation)	0.025 mg L^{-1}	0.1–100 mg L^{-1}	Tap water	210

Table 1 (*Contd.*)

Target	Nanomaterials	Sensing principle	LOD	Linear range	Real sample	Ref.
Thiram	Citrate-spherical AuNP	SERS	5×10^{-10} M	10^{-8} to 10^{-5} M	Tap water, orange juice	114
Thiram	Multi-branched Au nanostar	SERS	10^{-10} M 0.24 ng cm^{-2} (apple peel)	0.24 ng cm^{-2} to 2 μg cm^{-2}	Apple peel	112
Carbendazim	Citrate-spherical AuNP	SERS (analyte binding)	0.1 ppm	—	Oolong tea	160
Dimethoate	Citrate-spherical AuNP	FRET	0.004 ppm	0.005–1.0 ppm	Water, fruit	211
Herbicides						
Paraquat	Citrate-spherical AuNP	SERS (analyte binding)	0.1 μg mL^{-1}	—	Apple juice	212
Metsulfuron-methyl	Melamine-spherical AuNP	Colorimetric (anti-aggregation)	0.05 mg L^{-1}	0.1–100 mg L^{-1}	Tap water	125
Farm animal drugs						
Ractopamine	Aptamer-spherical AuNP	Colorimetric (crosslinking)	10 ng mL^{-1}	10–400 ng mL^{-1}	Beef	163
Ractopamine	Spherical AuNP	AuNP growth (aggregate or not)	0.35 ng mL^{-1}	2–512 ng mL^{-1}	Sheep urine	164
Kanamycin	DNA-spherical AuNP	Colorimetric (crosslinking)	10 pM	20 pM to 5 nM	Milk, honey	213
Chloramphenicol tetracycline	Multifunctional aptamer-spherical AuNP	Colorimetric (crosslinking)	7.0 nM 32.9 nM	0.05–1.8 μM 0.05–3.0 μM	Chicken, milk	132
Chloramphenicol	Citrate-AuNP	SERS	5.5×10^{-8} M	10^{-7} **to** 10^{-5} M	Beef, shrimp	114
Dopamine	Aptamer-spherical AuNP	FRET	2 nM	26–2.90 × 10^3 nM	Swine feeds, chicken livers	91
Bacteria						
E. coli	Aptamer-spherical AuNP	FRET	3 CFU mL^{-1}	5–10^6 CFU mL^{-1}	Tap/pond water, milk	187
Shigella flexneri	Aptamer-spherical AuNP	Colorimetric (non-crosslinking)	80 CFU mL^{-1}	10^2–10^6 CFU mL^{-1}	Salmon	191
E. coli *S. pollorum* *S. aureus* *E. faecalis* *S. mutants*	4-MPBA-spherical AuNP	Colorimetric (anti-aggregation)	—	10^4 to 10^7 CFU mL^{-1}	Drinking water	192
S. aureus	Vancomycin-spherical AuNP	FRET	10 CFU mL^{-1}	20 to 10^8 CFU mL^{-1}	Milk, orange juice	195
S.aureus	Teicoplainin-spherical AuNP	FRET	2 CFU mL^{-1}	10 to 5 × 10^8 CFU mL^{-1}	Milk, orange juice	190
Vibrio parahaemolyticus	Citrate-spherical AuNP	Colorimetric (AuNP growth)	10 CFU mL^{-1}	10–10^6 CFU mL^{-1}	—	186
P. aeruginosa	Chimeric M13 phage-spherical AuNP	Colorimetric (anti-aggregation)	10^2 CFU mL^{-1}	—	Drinking water, nonfat bovine milk	196

Table 1 (*Contd.*)

Target	Nanomaterials	Sensing principle	LOD	Linear range	Real sample	Ref.
Toxins						
Aflatoxin B1	DNA-spherical AuNP	FRET	61 pM	61 pM to 4.0 μM	Wine, beer	95
Aflatoxin M1	(Aptamer + cDNA)-spherical AuNP	Colorimetric (anti-aggregation)	30 ng L^{-1}	300–75 000 ng L^{-1}	Milk	214
Aflatoxin M1	(Aptamer + cDNA)-spherical AuNP	Colorimetric (anti-aggregation)	1.8 nM in milk	—	Milk	215
T-2 toxin	Aptamer-spherical AuNP	Colorimetric (non-crosslinking)	57.8 pg mL^{-1} (0.124 nM)	0.1–5000 ng mL^{-1} (0.21435–10 717.5 nM)	Wheat, corn	197
Zearalenone	(Aptamer + horseradish peroxidase)-spherical AuNP	Indirect colorimetric (nanozyme)	0.08 ng mL^{-1}	20–80 000 ng L^{-1}	Corn oil	216
Fumonisin B1	Cysteamine-spherical AuNP	Colorimetric (crosslinking)	0.90 μg kg^{-1}	2–8 μg kg^{-1}	Corn	198
Saxitoxin	Cysteine-spherical AuNP	SERS (analyte binding)	1×10^{-7} M	—	—	199
Adulterants						
Melamine	(PEG + citrate)-spherical AuNP	Colorimetric (crosslinking)	1.05 nM	1.05 nM to 1 mM	Raw milk	170
Melamine	Spherical AuNP (plant extract)	Colorimetric (crosslinking)	1.82 μM	1.80 to 2.60 μM	Milk	171
Melamine	Spherical AuNP	Colorimetric (crosslinking)	2.38×10^{-7} M 5.56×10^{-6} M (in milk)	3.90×10^{-7} to 3.97×10^{-6} M	Liquid milk	217
Melamine	Triton X-100-spherical AuNP	Colorimetric (crosslinking + de-protection)	UV-vis: 5.1 nM Paper: 1.0 μM	0–2.5 μM 1–1.8 μM	Milk	174
Melamine	*p*-Chlorobenzenesulfonic acid-spherical AuNP	Colorimetric (crosslinking)	2.3 nM	6.0×10^{-7} to 1.5×10^{-6} M	Liquid milk, milk powder	175
Melamine	Thymine derivative-spherical AuNP	Colorimetric (crosslinking)	3.5 nM	0.75–5.00 μM	Milk	172
Melamine	1,4-Dithiothreitol (DTT)-spherical AuNP	Colorimetric (crosslinking)	2.4×10^{-8} M	8×10^{-8} to 6×10^{-7} M 6×10^{-7}–1.5×10^{-6} M	Milk	173
Melamine	Terpyridyl zinc complex-spherical AuNP	Colorimetric (crosslinking)	2.4 ppb	0.1–0.45 μM	Milk	218
Melamine	Citrate-spherical AuNP	FRET	Green: 8 ng mL^{-1} Red: 11 ng mL^{-1}	20–100 ng mL^{-1}	Milk	219
Melamine	Citrate-spherical AuNP	FRET	1.7 nM	5 nM to 1.9 μM	Milk powder	176
Sodium dodecylbenzenesulfonate	Citrate-spherical AuNP	Colorimetric (anti-aggregation)	23 μg mL^{-1}	23–300 μg mL^{-1}	Milk	220
Commercial anionic detergents			92 μg mL^{-1}	92–900 μg mL^{-1}		
Sibutramine	Citrate-spherical AuNP	Colorimetric (crosslinking)	1.15 μM	5–15 μM	Dietary supplement products	221
Urea	FITC-aptamer-spherical AuNP	FRET	20 mM	20–150 mM	Milk	222

Table 1 (*Contd.*)

Target	Nanomaterials	Sensing principle	LOD	Linear range	Real sample	Ref.
Preservatives						
Formaldehyde	Resorcinol-spherical AuNP	SERS (analyte binding)	17 μM	25–1000 μM	—	179
Formaldehyde	Citrate-spherical AuNP	SERS (purge-trap device)	1×10^{-4} μg mL^{-1}	1×10^{-4} to 3×10^{-3} μg mL^{-1}	Duck blood, rice flour	180
Thiabendazole	CTAB-Au nanorod	SERS (analyte binding)	Lemon: 149 μg L^{-1} Carrot: 216 μg L^{-1} Mango: 179 μg L^{-1}	—	Lemon, carrot, mango juice	181
Food dyes						
Allura red sunset yellow	CTAB-Au nanorod	SERS (analyte binding)	0.1 mg L^{-1}	—	Beverages	113
Malachite green	Aptamer-AuNP	Colorimetric (non-crosslinking)	15.95 nM	20–300 nM	Fish	182
Malachite green	Citrate-spherical AuNP	Indirect colorimetric (nanozyme)	1.8 nM	10–500 nM	Fresh water	183

approaches introduce new color ranges which would be useful to develop multi-target detecting systems.

In several immunoassays, AuNPs play the role of a chromatic substrate, in which the characteristic red color of AuNPs would be a reporting signal for the detection. It is convenient to generate immune testing strips.[85–87]

2.2.2. Fluorescence modulation: FRET-based sensors and sensing mechanism. Fluorescence is an optical phenomenon in which a photon is absorbed by a fluorophore and consequently emits another photon at a lower frequency. The emission of a fluorophore can be modulated by AuNPs as it can interact with the LSPR of AuNPs.[88] It has been reported that AuNPs, especially spherical particles, exhibit high fluorescence quenching ability.[89,90] Therefore, AuNPs are ideal candidate for acceptors in a fluorescence resonance energy transfer (FRET)-based system. FRET is a non-radioactive phenomenon involving the energy transfer from an excited donor fluorophore to an acceptor fluorophore. FRET only occurs when the distance between donors and acceptors is sufficiently short, in general, less than 10 nm.[89,91,92] Thanks to the high extinction coefficient and broad absorption spectrum that overlaps the emission spectra of many organic dyes and quantum dots, AuNPs are great quenchers. Without any defined dipole moment, spherical AuNPs are ready for energy transfer from any orientation of the nearby donors.[93] Moreover, the high surface area-to-volume ratio of spherical AuNPs provides a large interacting area for multiple donors at once, increasing the efficiency of the FRET system.[89] More importantly, using spherical AuNPs as acceptors, the distance between the donors and the AuNPs can be extended up to 70–100 nm instead of less than 10 nm.[89,91,94] This allows them to be functionalized with recognition elements such as aptamers or peptides to ensure specific binding to donors without reducing the FRET effect between them. A FRET-based sensor for detection of aflatoxin B1 (AFB1), a mycotoxin that might be found in food and drinks, was fabricated using fluorescein (FAM) molecules as donors and AuNPs as acceptors. FAM molecules were labeled by an aptamer specific for AFB1 while AuNPs were functionalized with complementary DNA strands. In the absence of AFB1, two DNA strands hybridized, resulting in the immobilization of FAM molecules on the surface of AuNPs. FRET phenomenon occurred as AuNPs quenched the fluorescence of FAM. In the presence of AFB1, the aptamers were bound to AFB1, and FAM molecules were released from AuNPs, "turning-on" the fluorescent signal.[95]

Similarly, different kinds of organic dyes, fluorescent proteins, quantum dots, and unconventional NPs have been utilized as donors, from which excited energy is transferred to AuNPs within a short distance.[89,96] AuNPs quench the fluorescence signal, so the system is in "turn-off" state. Hence, the key strategy to "turn-on" a FRET sensor is to elongate the distance between the donor and the acceptor, leading to the recovery of fluorescent signal. Therefore, the target element should bind to either the donor or the acceptor in a competitive mechanism. For example, Dong *et al.* reported a "turn-on" fluorescent sensor to detect glutathione (GSH) based of FRET effect between *N*,*S* dual-doped carbon dots (*N*,*S*-CDs) and AuNPs. Positively

Table 2 Several recently reported AuNPs-based optical nanosensors for *in vitro* disease diagnosis (2015–now)

Target	Nanomaterials	Sensing principle	LOD	Linear range	Real sample	Ref.
Molecule/peptides						
Glucose	GOx-spherical AuNP (on a tapered fiber structure)	LSPR (change in refractive index)	322 μM	0–10 mM	—	230
Glucose	4-Cyanophenyl boronic acid (CPBA)-*b*-cyclodextrin (b-CD)-spherical AuNP	Colorimetric (crosslinking)	—	1–20 mM	Serum	280
Glucose	D-Glucose-spherical AuNP	Colorimetric (AuNP growth)	0.65 mM	1.25–20 mM	Human serum	234
Glucose	Spherical AuNP	Colorimetric (AuNP growth)	0.03 mM	0.1–10 mM	Serum	281
Glucose	Spherical AuNP	Colorimetric (AuNP growth)	0.081 mM	0.3–5.0 mM	Saliva	282
Glucose	Multibranched AuNP	Colorimetric (etching)	0.4 mg dL^{-1} 1.4 mg dL^{-1} (real samples)	—	Saliva	77
Glucose	CTAB-Au nanorod	Colorimetric (etching)	LSPR: 0.1 μM Naked eye: 3 μM	0.3–1.0 μM 1.0–10 μM 3–30 μM	Serum	66
Glucose	Chitosan-spherical AuNP	Indirect colorimetric (nanozyme)	3 μM	—	60% serum	81
Glucose	Citrate-spherical AuNP	FRET (donor: GOQD)	0.65 μM	2.5–75 μM	Serum	232
Glucose	Citrate-spherical AuNP	Colorimetric	0.043 μM	0–40 μM	Urine	283
Glucose (through H_2O_2)	3-Mercaptophenylboronic acid (3-MPBA)-spherical AuNP	SERS (change in ligand)	H_2O_2: 70 nM Glucose: —	70 nM to 150 μM 0.5–5 mM	Serum, urine	231
Glycated hemoglobin	Spherical AuNP	Colorimetric (AuNP growth)	0.124% of total hemoglobin	—	Whole blood	236
Urea	Citrate-spherical AuNP	Indirect colorimetric (nanozyme)	5 μM	0.02–0.4 mM	Human urine	284
Dopamine	Citrate-spherical AuNP	Colorimetric (crosslinking)	22 nM	0.1–4 μM	Human plasma, urine	285
Dopamine	Citrate-spherical AuNP	Colorimetric (crosslinking) FRET	1.85 μM 0.29 μM	0–300 μM 0–80 μM	Urine	225
Glutathione	Spherical AuNP (plant extract)	Indirect colorimetric (nanozyme)	0.013 μM	1–40 μM	Urine	82
Glutathione	Citrate-spherical AuNP	FRET	0.21 μM	3.8–415.1 μM	Serum	97
Protein markers						
Interleukin-6	Aptamer-spherical AuNP	Colorimetric (crosslinking)	1.95 μg mL^{-1}	3.3–125 μg mL^{-1}	—	62
Hemoglobin	2,6-Diaminopurine-spherical AuNP	Indirect colorimetric (nanozyme)	0.96 nM	—	Urine	80
CA15-3	Antibody-Au nanorod	Colorimetric (crosslinking)	—	—	Human serum of breast cancer	256
MUC4	(Antibody + SERS reporter)-spherical AuNP	SERS	—	—	—	257
p53 mutant	Aptamer-spherical AuNP	Colorimetric (crosslinking)	5 nM	—	—	242
CEA	Aptamer-spherical AuNP	Colorimetric (crosslinking)	3 ng mL^{-1}	0.1–120 ng mL^{-1}	Human serum	260
Erα	Aptamer-spherical AuNP	Colorimetric (de-protection)	2.4 ng mL^{-1}	10 ng mL^{-1} to 5 μg mL^{-1}	Cellular extract	245
HER2	Aptamer-spherical AuNP	Colorimetric (de-protection)	10 ng mL^{-1}	0–99 ng mL^{-1}	10% serum	244
AFP	Antibody-spherical AuNP	FRET	400 pg mL^{-1}	0.5–45 ng mL^{-1}	Human serum	246
AFP	Spherical AuNP	SERS (hot-spots with antibody-AgNPs)	5 ng mL^{-1}	0.05–10 μg mL^{-1}	Fetal bovine serum	258
AFP-L3	Antibody-spherical AuNP		05 ng mL^{-1}	0.5–1000 ng mL^{-1}	Human serum	122

Table 2 (*Contd.*)

Target	Nanomaterials	Sensing principle	LOD	Linear range	Real sample	Ref.
		SERS (conformational change in linker)				
PSA	Aptamer-spherical AuNP	Colorimetric (crosslinking)	20 pg mL^{-1}	0.1–100 ng mL^{-1}	Human serum	259
CA-125	DNA-spherical AuNP	FRET	1.5 fg mL^{-1}	5 fg mL^{-1} to 50 ng mL^{-1}	Human serum	261
Acid nucleic markers						
p53	Aptamer-spherical AuNP	FRET (donor: FAM)	1.6 pM	5 pM–1 nM	—	241
BRCA1 mutation	Aptamer-spherical AuNP on 2D material (GO, Bi_2Se_3)	Indirect colorimetric (nanozyme)	10^{-18} M	10^{-18} to 10^{-12} M	Extracted from patients' blood	243
PCA3	Citrate-spherical AuNP	PCR + colorimetric (anti-aggregation)	31.25 ng	—	Urine	247
3 sequences containing melanoma DNA mutations	ssDNA-spherical AuNP	SERS (+PCR)	0.1% mutation (10 copies)	—	—	250
PCA3 mimic DNA	ssDNA-hollow AuNP	SERS	2.7 fM	1 fM to 100 nM	—	251
microRNA	Unfunctionalized spherical AuNP	Colorimetric (de-protection)	0.6 nM	0.5 nM to 1 μM	Total RNA extracted from cancer cells (MCF-7) and normal cells (HEK 293)	252
		FRET (donor: Aptamer-AgNC)	0.4 pM	1 pM–5 ^{252}μM		
Other markers						
Tumor extracellular vesicles	Aptamer-spherical AuNP	SERS (creating hot-spots by organizing around an aptamer-agarose bead)	2.44 pg μL^{-1}	0.043–1240 ng μL^{-1}	Human serum	264
Exosome	Antibody-spherical AuNP	Colorimetric (plasmonic + immunoassay)	8.54×10^5 exosomes per μL	0–1.44×10^8 exosomes per μL	—	286
MCF-7 breast cancer cell	150 nm spherical AuNP	NIR SERS	—	—	Human serum, plasma	128
MCF-7 breast cancer cell	Aptamer-Au nanorod	Colorimetric (crosslinking)	100 cells per mL	10^2–10^5 cells per mL	—	265
MDA-MB-231 breast cancer cell	Au nanostar	SERS	—	10–500 cells per mL	—	287
Red blood cell	2,6-Diaminopurine-spherical AuNP	Indirect colorimetric (nanozyme)	1.6×10^6 cells per L	—	Urine	80
Infectious diseases						
E. coli *V. cholera* *P. aeruginosa*	Chimeric phage-spherical AuNP	Colorimetric (crosslinking)	~10^2 CFU	—	—	169
Tuberculosis (DNA)	Citrate-spherical AuNP	Colorimetric (de-protection)	1.95×10^{-2} ng mL^{-1}	1.95×10^{-2} to 1.95×10^1 ng mL^{-1}	Sample from 01 patient	268
Tuberculosis (ManLAM lipoglycan)	Antibody-spherical AuNP	SERS	0.8 ng mL^{-1} (46 pM)	—	Serum	269
	Antibody-spherical AuNP	Colorimetric (crosslinking)	7.8 HA units	10–80 HA units	Clinical sample	272

Table 2 (*Contd.*)

Target	Nanomaterials	Sensing principle	LOD	Linear range	Real sample	Ref.
H3N2 influenza A virus						
Influenza viruses	Glycans-spherical AuNP	Colorimetric (crosslinking)	8 HA units	—	Clinical sample	273
Tamiflu-resistant influenza virus	Oseltamivir hexylthiol-spherical AuNP	Colorimetric (crosslinking + lateral flow assay)	1×10^4 PFU mL^{-1}	—	—	271
H1N1 influenza A virus	Positive charged spherical AuNP	Indirect colorimetric (nanozyme)	10.79 pg mL^{-1}	10 pg mL^{-1} to 10 μg mL^{-1}	Human serum	270
H3N2 influenza A virus			11.62 PFU mL^{-1}	10–50 000 PFU mL^{-1}		
Newcastle disease virus (viral particle)	Peptide–Cys-spherical AuNP	Colorimetric (crosslinking)	0.125 HA units	—	—	61
DEVN WVN (viral particle)	Citrate-spherical AuNP	SERS (hot-spot: organization of AuNP on viral particles)	10 PFU mL^{-1}	—	—	116
MERS-CoV (upE gene)	Citrate-spherical AuNP	Colorimetric (crosslinking)	1 pmol μL^{-1}	—	Real sample after PCR	274
SARS-CoV-2 influenza B MERS-CoV (viral particle)	Sialic-spherical AuNP	Colorimetric (crosslinking)	—	—	Throat swab	275
SARS-CoV-2 (viral particle)	(3 types of antibodies)-spherical AuNP	Colorimetric (crosslinking)	—	—	Throat swab	224
SARS-CoV-2 (viral particle)	ACE2 protein/mAbs-spherical AuNP	Colorimetric (plasmonic + immunoassay)	370 vp mL^{-1}	0–10^7 vp mL^{-1}	Pseudovirus	276
SARS-CoV-2 (IgM antibody)	(Anti-human IgM)-spherical AuNP	Colorimetric (plasmonic + immunoassay)	—	—	Serum	86
SARS-CoV-2 (IgG antibody)	Virus epitope-spherical AuNP	Colorimetric (crosslinking)	3.2 nM	—	Real plasma samples (including patients)	277
SARS-CoV-2 Spike protein Heat-inactivated virus	Aptamer-spherical AuNP	Colorimetric (anti-aggregation)	16 nM3540 Genome copies per μL	—	—	279
SARS-CoV-2 (protease)	Citrate-spherical AuNP	Colorimetric (aggregation)	10 pM	0.01–0.5 nM	—	288

charged *N*,*S*-CDs bound to negatively charged AuNPs *via* electrostatic interaction.[97] Fluorescence intensity of CDs was quenched by AuNPs due to FRET effect. In the addition of GSH, the strong Au–S bond between GSH and the NPs leads to the release of *N*,*S*-CDs from the NPs surface, so fluorescence recovery occurs (Fig. 5). The limit of detection (*i.e.*, LOD) of this method was as low as 0.21 μM. As the concentration of GSH in human serum is up to mM levels, the sensing system was expected to be able to determine GSH in diluted real samples.[97] This example demonstrates the high sensitivity and accuracy of AuNPs-based FRET sensors that take advantage of the fluorescence efficiency of the donors and the excellent quenching ability of AuNPs. However, further studies are required to achieve the optimal conditions for FRET sensing. Each of donors possess its own advantages and disadvantages. For example, organic dyes are small, simply-prepared and cost-effective, but they have high toxicity, high photobleaching rate and low stability; fluorescent proteins are nontoxic, but they display wide emission spectrum as well as large sizes that can elongate the distance to the acceptors; QDs exhibit high quantum yield, narrow emission spectrum and high photostability, but they are highly toxic, *etc.*[89] Therefore, researchers need to balance out these advantages and disadvantages to choose the suitable donors for FRET sensors based on the desired target elements and the sensing environment. Moreover, other NPs have been investigated as the promising candidates for the role of donors. For instance, unconventional nanoparticles (UCNPs) can emit fluorescence under the excitation wavelengths in the near infrared region, which is less harmful for biological samples.[89,98] Recently, graphene NPs have been regarded as a potential choice as they can be fabricated easily at large scale of production. Moreover, their cost-efficiency, high solubility and biocompatible are advantages. However, the structure of this nanomaterial should be further studied to improve their wide emission spectra.[89,99]

In general, AuNPs are non-luminescent materials, however, ultrasmall AuNPs (<3 nm), which are known as gold nanoclusters (AuNCs), have molecular-like properties, including photoluminescence.[100] Therefore, they have been studied to design fluorescence sensors for many different targets. However, in this review, we only focus on AuNPs. The fluorescent sensing mechanisms using AuNCs have been reviewed in detail by Halawa *et al.*[100]

2.2.3. Surface enhanced Raman scattering: SERS-based sensors and sensing mechanism. Surface enhanced Raman scattering (SERS) is a sensitive spectroscopic technique involving inelastic scattering of incident light and a surface molecule, leading to the vibrational spectral peaks of the molecule. When an analyte is adsorbed onto a rough plasmonic metal, its Raman signal is enhanced. SERS signal provides

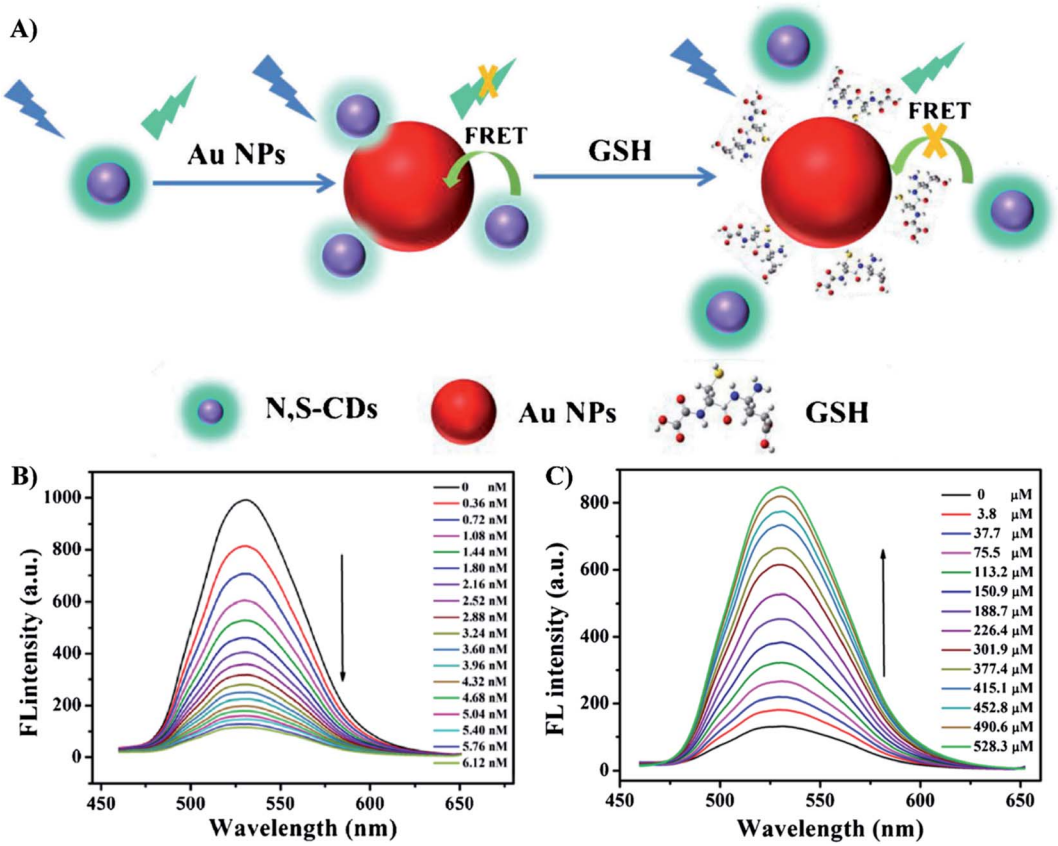

Fig. 5 (A) Schematic principle for the determination of GSH based on FRET of *N*,*S*-CDs and AuNPs; (B) The fluorescence spectra of *N*,*S*-CDs (19 μg mL^{-1}) in presence of different concentrations of AuNPs from 0 to 6.12 nM; (C) the fluorescence spectra of the *N*,*S*-CDs/Au NPs in the presence of different concentrations of GSH (0 μM to 528.3 μM). Reprinted by permission from Springer Nature: ref. 97 Copyright 2019.

information about the structure, the interaction and environment of the analyte, even at trace levels, as well as a platform *via* a rapid detection. AuNPs are widely used as substrates for SERS-based sensors.[25,101] In 1977, the signal enhancement was explained in both chemical and electromagnetic mechanisms (CM and EM) by lbrecht & Creighton[102] and Jeanmaire & Van Duyne,[103] respectively. These two mechanisms are now regarded as the underlying fundamentals of SERS effect. The intensity of Raman scattering is proportional to the square of the induced dipole moment P, which is expressed by the equation:[25,104,105]

$$P = \alpha E \quad (2)$$

in which α is the polarizability of the molecule (chemical), and E is the electric field (electromagnetic). CM requires the analyte to be chemisorbed to the substrate, allowing a charge transfer between them. On the other hand, EM is the result of coupling of the incident electromagnetic field and the surface plasmon of the SERS substrate. This is a local phenomenon that only influences the molecule at or near the metal surface.[105] Therefore, both CM and EM concern the distance between the SERS substance and the analyte/reporter. Minimizing this distance can enhance the SERS signal. In addition, it has been reported that SERS enhancements could originate from the plasmon formed at the small gaps between NPs (usually <10 nm) or sharp tips and corners of NPs, known as "hot spots", with an enhancement factor up to 10^{12}.[106] Therefore, analyte binding and "hot spots" are the keys to design a SERS-based sensor (Fig. 6). Besides, the distance between Raman reporter and the substrate (AuNPs) is also important. In this part, we summarize several strategies to design AuNPs-based SERS sensors and their detecting mechanism (Fig. 3).

The analyte or target element of a SERS-based sensor might be adsorbed directly to the surface of AuNPs or binds indirectly through a recognition element. This element can be an antibody, an aptamer, a small molecule or a polymer. Using AuNPs as SERS substrates, molecules containing thiol or cyanide group can be introduced onto the NP surface directly due to the high affinity between their functional groups and Au.[108,109] Employing unfunctionalized AuNPs is simple to prepare. However, the lack of specificity may lead to the low selectivity of the sensors, especially for samples of complex matrices. More importantly, there are only few functional groups and ions that can attach to the surface of AuNPs. Thus, functionalization of AuNPs is a solution to avoid these two disadvantages because it allows specific binding of target elements on AuNPs. However, the limitation of this approach is that the functional molecule (or receptor) can be extremely large, for example, antibody, which makes the distance between the target element and the substrate too far to experience the signal enhancement.[110] Thus, it has been a demand of investigating smaller molecules to functionalize AuNPs. Van Duyne's group has designed bisboronic acid receptors with two arms of boronic acid forming covalent bonds with glucose and one arm of thiol being immobilized on AuNP surface. In addition, the highly polarizable aromatic structure of the molecule acted as a Raman reporter to enhance SERS signals. The detection of glucose in physically relevant condition range allowed the diagnosis of both hypoglycemia and hyperglycemia.[111] Besides, Raman signal of a target element can be amplified when it is adsorbed on hot-spot regions.[107] Hence, in addition to directing the binding of analyte onto NPs, researchers also pay attention in creating hot-spots *via* material fabrication. Anisotropic AuNPs, such as nanostars, nanorods, have been synthesized and

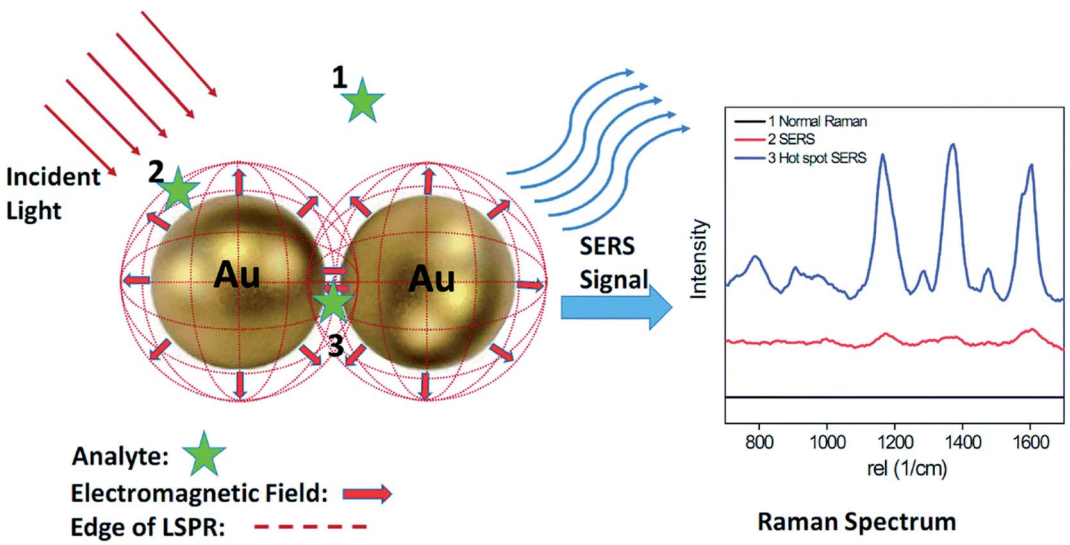

Fig. 6 Schematic of SERS phenomenon for an organic analyte on AuNPs. Analyte molecules located within the dotted red circles (position 2 and 3) show clear Raman signals, while analytes located outside the circles (position 1) exhibit no detectable Raman signal. Commonly, significant Raman enhancements mainly occur within gaps smaller than 10 nm. These localized areas are often referred to as 'hot-spots' (position 3). Analyte molecules located within the hot spot exhibit a much stronger Raman signal than those located on AuNP surface (position 2). Reproduced from ref. 107 with permission from The Royal Society of Chemistry, Copyright 2015.

employed as SERS materials, leading to significant enhancement in SERS signal.[112,113] Besides, hot-spots could be also created between isotropic AuNPs by self-assembly[114] or polymer assisted assembly[115] on the substrates, or even the targets themselves.[116]

In a strategy of hot-spots modulation, hot-spots are created or destroyed by the target elements themselves, consequently, SERS-based sensors are generated *via* either "turn-on" or "turn-off" mechanisms. "Turn-on" approach focuses on decreasing the distance between two adjacent AuNPs to create hot-spots to increase SERS signals. In contrast, in "turn-off" approach, the target elements disrupt the connections between AuNPs, elongate their interparticle distance to destroy the hot-spots, thus, decrease SERS signals. In fact, these mechanisms are similar to aggregation and anti-aggregation mechanisms in colorimetric sensing. An example for the "turn-on" method is the detection of Hg^{2+} ions based on the assembly of AuNPs functionalized with single stranded DNA into chains reported by Xu *et al.* in 2015. Thanks to the T-Hg^{2+}-T bond between two thymine base pairs, double stranded DNA was form between NPs to decrease the interparticle distance. As a result, SERS signals are significantly enhanced, even at low concentration of Hg^{2+}. Hence, the method was extremely sensitive with an LOD of 0.45 pg mL^{-1}.[117] On the other hand, heparin, an anticoagulant, was detected *via* "turn-off" method. Zhang *et al.* induced aggregation state of AuNPs using the interaction between 4-mercaptobenzoic on the surface of AuNPs and protamine. However, the higher affinity to protamine helped heparin to bind to this protein, resulting in anti-aggregation of the NPs and a decrease in SERS signals.[118] To achieve high signals for SERS sensing, it is important to maintain the close distance between the substrates and the reporter. A similar strategy of "turn-on" and "turn-off" using the modulation of this distance can be also generated using the mechanisms mentioned above.[119] However, applying either hot-spots between AuNPs or distance between AuNPs and reporter, "turn-on" approach is commonly preferred. The reason is that at low concentration levels of target elements, the decrease in SERS signals obtained by "turn-off" method is not as noticeable as the presence or not of the signal in "turn-on" approach.

Since SERS is a vibrational spectroscopy, once the structure or conformation of the recognition elements on the surface is changed, the spectral variations in some bands of SERS responds responses can be detected. In a 2019 study, Popp and coworkers reported the detection of Cu^{2+} in white wine using this principle. The interaction of Cu^{2+} and the dipicolylamine-based ligand bound to the surface of AuNPs caused the changes in SERS spectra associated with pyridine breathing mode.[120] This chemo-optical sensing method is a new approach that takes advantage of the chemical sensitivity and specificity of SERS signals. However, it is not all of the chemical and conformational changes that can be detected in SERS responses. In general, changes of the groups linked directly to aromatic ring tend to have greater influence on the polarizability of the probe, therefore the spectral variations are also more noticeable.[104] In addition to the active metal ions that can change the chemical/conformation of the ligands bound to the surface of NPs, large elements have also been detected using this mechanism. For example, the interaction between influenza-H1 antigens and their antibodies, which were linked to 4-ATP, led to the relaxation of the stretched aromatic linker on the surface of AuNPs. This conformational change resulted in significant up-shifts in the peaks corresponding to the C–S stretching and C–C breathing modes.[121] This sensing mechanism has overcome the disadvantages of using large antibodies in SERS sensors as the long distance between target elements and AuNPs did not limit the SERS responses. This mechanism has paved the way to the development of novel methods to detect biological elements using SERS-based sensors.[122,123]

2.3. Advantages and disadvantages of AuNPs-based optical nanosensors

Taking advantage of the optical, chemical and electromagnetic properties of the AuNPs, combining with the knowledge about desired analytes, researchers can design and develop optical nanosensors with various of advantages. However, there are still several disadvantages with which researchers have to cope when working on these types of sensors. Although some advantages and disadvantages have been mentioned previously, in this section, we would like to summarize their pros and cons, in comparison to several other AuNPs-based nanosensors.

Optical AuNPs-based sensors are simple and rapid.[14,124] Especially, the results obtained for colorimetric sensors can be observed by bare-eye.[14,125] However, they have to deal with a risk of false positive/negative results due to aggregation of AuNPs, especially in complex sample matrix.[126,127] Moreover, the inadvertent aggregation of AuNPs may also reduce the sensibility and accuracy of SERS and FRET sensors.[128,129] These risks in precision and accuracy can be avoided by functionalizing AuNPs with a recognition element specific for the desired analyte. Functionalization definitely improves the selectivity of optical AuNPs-based sensors, however, sometimes, it scarifies the stability of AuNPs.[130] Nevertheless, the introduction of fine-tuning techniques resulted in more stable modified-AuNPs.[131] Another drawback of functionalization of AuNPs in optical nanosensors is that large recognition element, such as polymer, protein, antibody, *etc.*, elongate the distance between the surface of the particle and the analyte (in a SERS sensor) or the acceptor (in a FRET sensor), which prevents the analyte from experiencing SERS effect or prevents the fluorescence of the acceptor from being quenched. However, thanks to great quenching ability of AuNPs, the distance between them and the acceptor this distance to be extended up to 70–100 nm,[89,91,94] thus, it is the problem of only the SERS sensors, and the solution is avoiding the large recognition elements despite their high specificity. Besides, the manufacture of multi-target optical sensors requires functionalizing AuNPs with multiple recognition probes. It can increase the complexity and the cost of sensor fabrication procedures, howbeit, to the best of our knowledge, researchers have to accept this drawback to design these optical sensors.[132] In term of instrument, expect for colorimetric sensors, LSPR, FRET and SERS sensors all require specific spectroscopies for measurements.[133] However, being developed for a long period of time, the spectroscopies for these

techniques have become common and popular,[134,135] which can be found in many laboratories all around the world, thus, it is convenient for researchers to generate these optical sensors.

Also using AuNPs as the main substrate for analyte detection, some other nanosensors can help researchers overcome the disadvantages of the optical sensors. Electrochemical sensors are promising for multi-target sensing as they can determine different analytes at the same time.[136] However, they require noticeable electroactivity of the analytes, which limits the range of target molecules.[137] Furthermore, electrode fouling may be a problem for sensing repeatability.[138] Another novel technique based on plasmonic property of AuNPs is chaotic sensor, in which the evolution of absorption spectra of AuNPs was recorded under the excitation of a laser source and analyzed by electronic signals using a chaotic circuit.[139] In another word, it is an opto-electric sensor, which senses the changes in conductivity arising from the absorption of the samples, thus, its sensibility is impressive. This sensor does not require any expensive spectroscopy. However, it is necessary to design a complicated electric modulator.[139] Thus, it needs specialized human resources to design and operate the sensing system. In another approach, AuNPs can also act as an assisting material in terahertz (THz) sensors. THz waves are potential for detecting analytes at trace levels, especially biological elements whose absorption peaks fall in THz region. For example, L-histidine shows a strong absorption band at ~0.78 THz.[140] Unfortunately, AuNPs lack plasmonic property within this region.[140] However, it has been reported that the assist of AuNPs could enhance the performance of metamaterials for THz sensors, leading to impressive LODs of the sensors.[140,141] Avidin, *Staphylococcus aureus* (*S. aureus*), and microRNAs were detected using this kind of sensors at the concentration down to fM, pM, and even aM level, respectively.[140–142] In spite of that excellent sensibility, THz sensors still exhibit several drawbacks. Compared to optical sensors, material fabrication for THz sensors is more complicated and expensive.[140–143] Furthermore, being a novel technique, THz spectroscopy is not as popular.[143] Moreover, due to several reported limitations, THz need to be further studied and modified before being employed for real samples.[144] Therefore, the application of THz sensors is still limited.

Each of the AuNPs-based sensors has its advantages and disadvantages that researchers can consider developing the appropriate sensors based on their desired analytes and the conditions of their laboratories. With the convenience and simplicity of material fabrication and sensing system operation, as well as the popularity of the spectroscopies, AuNPs-based optical sensors still attract the interest of researchers with a huge number of sensors developed for food and health safety monitoring in recent years which will be presented in Tables 1 & 2 in the following sections.

3. AuNPs-based optical nanosensors for food and health safety monitoring

3.1. Food safety monitoring

The rising attention about food quality has triggered many studies on monitoring food safety. In general, they focus on the detection of the contaminants (*i.e.*, heavy metals, pesticides, herbicides, farm animal drugs, *etc.*) and food additives (*i.e.*, preservatives, food dyes). This part will present some examples of recent advances in AuNPs-based sensing to detect these targets (Fig. 7). Detailed information about limits of detection (LOD), linear ranges and real sample matrices is presented in Table 1.

3.1.1. Heavy metals. Heavy metals, such as mercury (Hg), lead (Pb), copper (Cu), iron (Fe), nickel (Ni), cobalt (Co), cadmium (Cd), *etc.*, are omnipresent naturally in the environment. Most of them are even essential for life. However, at high concentrations, they can cause damage to many tissues and organs in human body, including kidney, liver, bones, and central nervous system.[146] Due to industrial and agricultural developments, their contents have increased and accumulated through the food chains. To protect the consumers from food and drinks containing high concentrations of heavy metals, it is important to develop sensing system to monitoring their contents.

In general, most of sensors using AuNPs as probes for detecting heavy metals operate based on the interaction between the ligands on the NP surface. There are several widely-used ligands that can be chosen to be suitable for the desired target. For example, the high specificity of thymine–Hg^{2+}–thymine (T–Hg^{2+}–T) affinity have been applied for many Hg^{2+} sensing systems as in the presence of Hg^{2+}, T–T mismatches are formed. For example, Amiri *et al.* have introduced a FRET aptasensor for Hg^{2+} using carbon dots as donors and AuNPs as acceptors.[145] The carbon dots were labeled with T-rich single stranded DNA, while the AuNPs were functionalized with a complementary DNA sequence (cDNA). When being mixed together, the AuNPs quenched the fluorescence of carbon dots. However, in the presence of Hg^{2+}, the cDNA was replaced due to the formation of T–Hg^{2+}–T on the T-rich single stranded DNA. As a result, fluorescence recovery occurred. The FRET sensor achieved an impressive LOD of 7.5×10^{-13} M of Hg^{2+}.[145] A similar principle has been employed to design an indirect colorimetric sensor, in which T-rich DNA sequence were used as a capturing probe for Hg^{2+}. In the presence of Hg^{2+} ions, it bound to T-rich oligonucleotide to form a T–Hg^{2+}–T complex. The formation of this complex prevented the adsorption of oligonucleotide on the surface of AuNPs. The AuNPs then were available as a nanozyme to oxidize TMB, resulting in a much deeper blue color of the solution compared to the previously coated AuNPs.[147] Besides, the interaction between DNAzyme and Pb^{2+} also attract researchers' concern for anti-aggregation approach.[148] In the presence of Pb^{2+}, DNAzyme would cleavage the target sequence. Therefore, this phenomenon was employed to separate AuNPs and graphene quantum dots in a 2018 study, resulting in fluorescence recovery (Fig. 8A).[149] The sensor had an LOD of 16.7 nM. However, compared to the utilization of T-rich oligonucleotide, using DNAzyme is more complicated and less convenient. Therefore, this approach is not widely used.

In addition to the interaction with oligonucleotide, heavy metals can also be captured by peptides that are rich in reactive groups. Glutathione (GSH) is an example. Each GSH possesses 8 binding sites, including 1 sulfhydryl, 1 amino group, 2 carboxyls

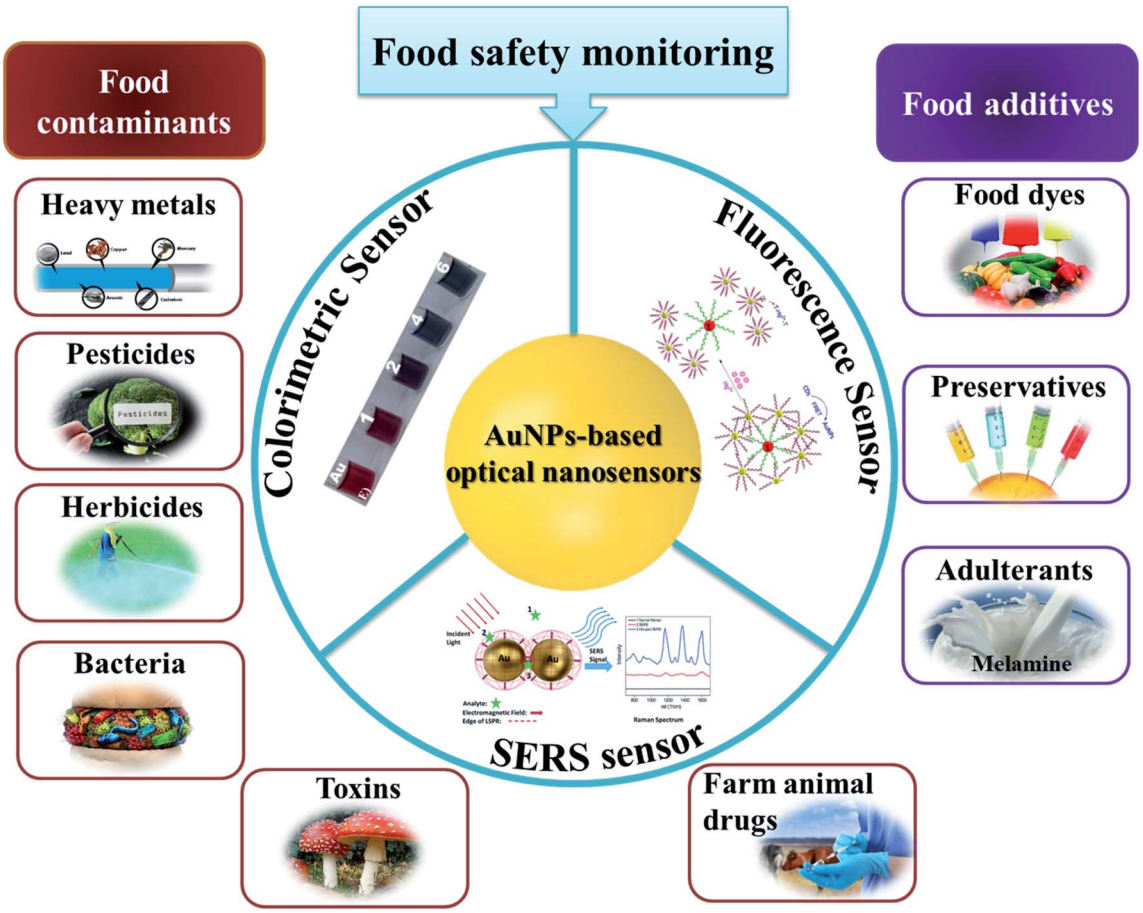

Fig. 7 AuNPs-based optical sensors for food safety monitoring. Inset pictures: colorimetric sensor: reprinted from ref. 72 Copyright 2021, with permission from Elsevier. Fluorescence sensor: reproduced from ref. 145 with permission from The Royal Society of Chemistry, Copyright 2018. SERS sensor: reproduced from ref. 107 with permission from The Royal Society of Chemistry, Copyright 2015.

and 4 carbonyl and amide donors.[150] Therefore, heavy metal ions exhibit high affinity to this peptide. The thiol group allows GSH to be easily introduced onto the surface of AuNPs while other reactive groups are responsible for capturing heavy metal ions, causing the aggregation of AuNPs. Pb^{2+} and As^{3+} have been detected *via* this sensing principle.[151–153] Incubated with GSH before the addition of AuNPs, Cd^{2+} exhibited such a high affinity to the peptide that AuNPs were prevented from binding to GSH, which led to the NP aggregation. The LOD of the method was calculated to be 4.3 pM.[150] Similarly, other molecules containing reactive sites, either natural or synthesized ones, can become promising ligands to detect heavy metals in AuNPs-based assays.[154]

3.1.2. Pesticides and herbicides. Due to the development of agriculture and high demand of grains, vegetables and fruits all around the world, agro-products often contain more pesticides that are harmful to human health. For example, organophosphorus, a group of pesticides, is most used due to its broad spectrum of insecticidal activities. However, it acts as an inhibitor for acetylcholinesterase (AChE), an essential enzyme to decompose acetylcholine for neurotransmission. Thus, the detection of organophosphorus pesticides has attracted a great concern of researchers, resulting in the development of interesting approaches. In addition to the studies using the widely-used concept of AuNP aggregation *via* de-protection of functionalized AuNPs,[155,156] Wu *et al.* took advantage of the characteristics of the pesticides to realize a sensor with high selectivity.[157] This method was based on combination of AChE hydrolysis reaction and dissolution of AuNPs in Au^{3+}-cetyltrimethylammonium bromide (Au^{3+}-CTAB) solution. In the absence of organophosphorus pesticides (OPs), AChE converted acetylthiocholine to thiocholine that reduced Au^{3+} in the solution. Due to the consumption of AChE, there was no Au^{3+} to dissolve AuNPs. Moreover, the reduction of Au^{3+} triggered the growth of AuNPs, which turned the solution into dark red. In contrast, the presence of OPs resulted in the inhibition of AChE. Without reducing thiocholine, Au^{3+} ions remained in the solution and dissolved the AuNPs with the aid of CTAB. Consequently, the solution changed to light pink or colorless. The sensing system achieved a low LOD of 0.7 ppb, and well performed in practical samples including tap water, apple washing solution and sea water.[157] However, this method could not distinguish different kinds of pesticides in the organophosphate group. In a more recent study, Zhang *et al.* designed a multi-analyte sensing system allowing the detection of three organophosphate pesticides (triazophos, parathion, and

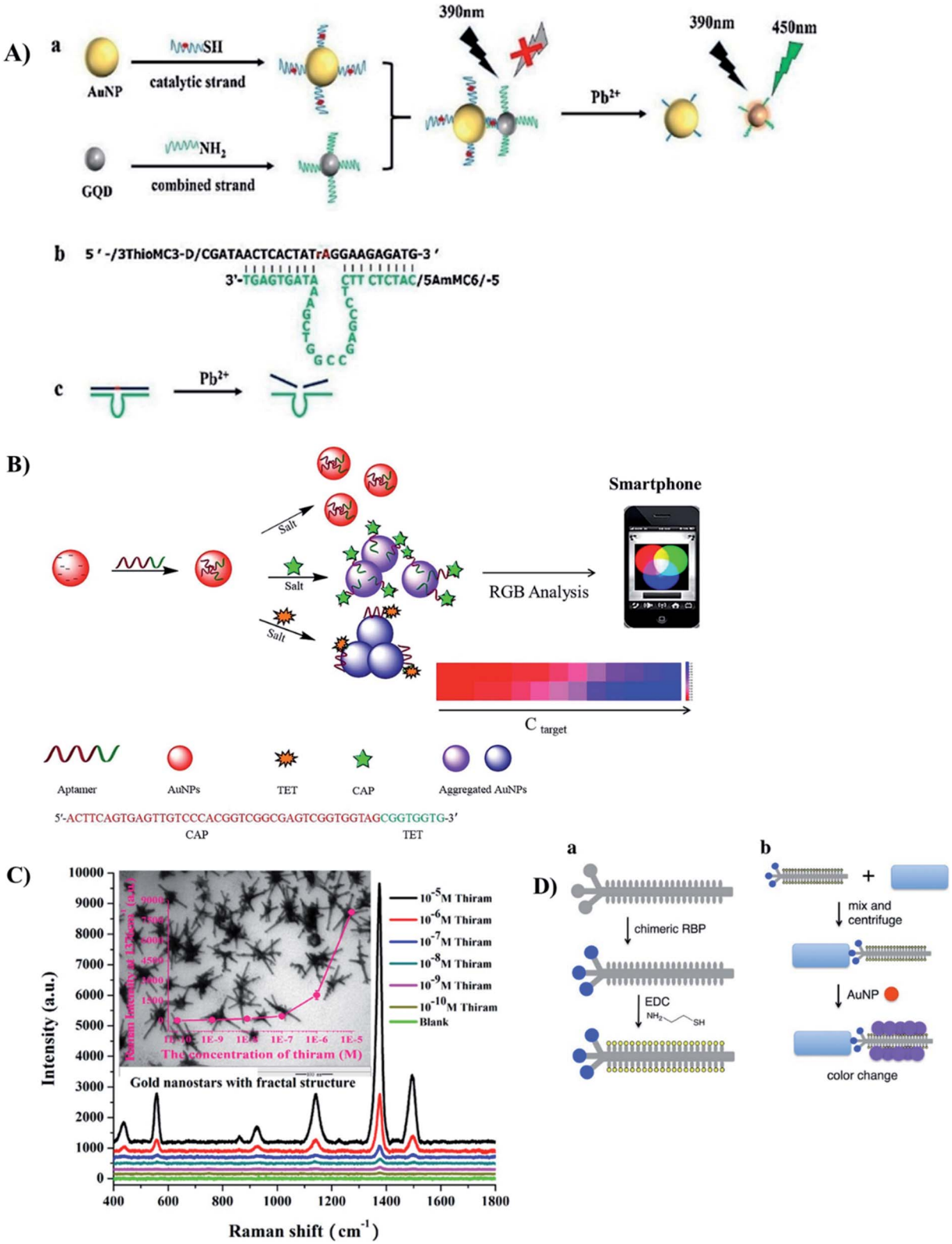

Fig. 8 Different kinds of AuNPs-based optical sensors for detection of food contaminants. (A) FRET-based sensor for Pb^{2+} ions with the use of DNAzyme. Reprinted from ref. 149 Copyright 2018, with permission from Elsevier. (B) Colorimetric (de-protection) aptasensor for 2 kinds of antibiotics TET and CAP. Reprinted from ref. 132 Copyright 2018, with permission from Elsevier. (C) SERS-based sensor using Au nanostars to detect thiram. Reprinted from ref. 112 Copyright 2018, with permission from Elsevier. (D) Colorimetric (crosslinking) sensor for bacteria with the use of thiolated chimeric phage. Reprinted with permission from ref. 169 Copyright (2019) American Chemical Society.

chlorpyrifos).[158] Three kinds of AuNP probes were fabricated with responding antibodies for each pesticide and three different kinds of fluorophores (*i.e.*, FAM, Cys 3 and Texas red), respectively. The detection was based on a competitive reaction between the pesticides and antigens in the plate to bind to AuNP probes. The probes binding to pesticides were washed away while the others were immobilized in the plate. Subsequently, dithiothreitol (DTT) was added and the affinity between DTT and AuNPs led to ligand exchange. As a result, fluorophores were released from the fluorescence quenching AuNPs. The fluorescence signal was recovered and then analyzed to calculate the concentration of each pesticide in the samples. The work proposed a novel method for multi-residue analysis with appropriate performance in various food samples.[158]

Another approach for the detection of pesticides is SERS-based sensors. Different kinds of organophosphorus pesticides and fungicides, such as thiram and carbendazim, have been detected using this method.[112,159,160] In general, these residues can adsorb directly on the surface without any modifications. Therefore, to enhance the SERS signal, researchers have been focusing on the fabrication of the AuNPs. For example, Au nanostars (Fig. 8C), snowflake-like AuNPs, and spherical AuNPs deposited on a "sticky" tape have been employed as substrates for the detection of thiram and several organophosphorus pesticides.[112,159–161]

3.1.3. Farm animal drugs. To meet the growing demand for milk, meat and other livestock products, the number of global livestock has kept increasing for years. As a result, the consumption of farm animal drugs is also in a rising trend. Different from human, for which medicine consumption is carefully calculated and evaluated, veterinary drug consumption is much more massive and less controlled. These drugs can be accumulated in the meat and eggs of the animals or secreted into their milk. In addition, a large part is excreted into the ecosystem *via* urine and feces, which finally ends up in water sources. Therefore, human have to cope with the risk of consuming food and drinks containing high contents of these drugs. Farm animal drugs include β-agonists (*i.e.*, ractopamine, salbutamol, clenbuterol, *etc.*), which promote leanness in livestock, and different kinds of antibiotics.

In general, there has been only few studies mentioning the detection of β-agonists using optical sensing systems. Most of them were based on the crossing-linking principle to cause aggregation of AuNPs. However, using different linking elements including melamine and aptamer has improved the selectivity of the detection,[162,163] allowing them to perform in real complex samples. Recently, Han *et al.* reported on a ractopamine sensing system based on the growth of AuNPs in combination with a competitive immunoassay.[164] In this system, ractopamine in the samples had to compete with ractopamine immobilized in the ELISA to bind to the antibodies. Then, biotinylated second antibodies were added, followed by the introduction of streptavidin label catalase, which could convert H_2O_2 to H_2O and O_2. In the presence of ractopamine, there was less catalase immobilized in the ELISA well, so Au^{3+} ions in the well were reduced by H_2O_2 rapidly, resulting the formation of AuNPs with the red color. In contrast, more catalase consumed a large amount of H_2O_2. The lack of H_2O_2 slowed down the kinetics of AuNP fabrication and induced the formation of aggregation with blue color.[164]

Antibiotics are also widely used in farming in a massive amount. The risk of antibiotic resistance caused by consuming agro-products containing antibiotics cannot be ignored. Therefore, for the last 10 years, many studies have been reported on the detection of antibiotics in food and animal samples. Most of them are colorimetric and fluorescent sensors, however, the detecting approaches are quite diverse. Using aptamers as capturing probes, ampicillin and kanamycin were detected *via* aggregation and anti-aggregation, respectively.[165,166] In another approach, kanamycin, neomycin, streptomycin, and members of tetracycline family were employed to trigger the growth of AuNPs. The color of AuNPs confirmed their presence and concentrations in samples. Although these methods did not exhibit significant difference among different antibiotics,[78,167] it is worth noting that most of those systems could be employed to detect antibiotics in milk and animal tissues. Recently, researchers have expressed a great interest in developing multi-residue sensors. In a 2020 study, Wu *et al.* described a colorimetric aptasensor for multiplex antibiotics, including chloramphenicol (CAP) and tetracycline (TET).[132] A multifunctional aptamer was designed and adsorbed onto the AuNP surface. In the presence of one antibiotic, the specifically recognized fragment of the aptamer bound to that antibiotic and dissociated from the AuNP surface, while the non-specific one still attached and controlled the aggregation of AuNPs. Different antibiotics caused different states of AuNPs aggregation that could be distinguished by the colors of the solutions (Fig. 8B). Therefore, one sensing system was successful for the separate detection of two kinds of antibiotics with low LODs of 32.9 nM and 7.0 nM for TET and CAP, respectively.[132] Similarly, Xiang's group reported an even more complicated system including two kinds of AuNPs labeled with 2 distinct aptamers to detect 5 types of aminoglycoside antibiotics.[168] Due to different binding sites of those types of antibiotics, the obtained signal was distinguished.[168] Therefore, 5 types of antibiotics could be detected separately using one sensing system. However, those two sensing systems were not possible to detect two or more antibiotics at once.

3.1.4. Food additives. Food additives are substances utilized during food processing to improve quality and durability of the product, as well as to control the food color and flavor. However, illegal food additives are toxic substances that are banned in food products. Nevertheless, the use of the illegal ones is not completely stopped that put consumers in health hazards. Hence, it is urgent to develop sensors to detect these poisonous food additives. In this review, we summarize several examples of advanced AuNPs-based sensing systems for melamine, some preservatives and food dyes. Examples of other additives are presented in Table 1.

Melamine is a trimer of cyanamide which has been widely used in manufacture of polymer resins, fertilizers, kitchenware, *etc.* However, due to its high nitrogen contents, it has been added illegally into animal feeds and dairy products to inflate

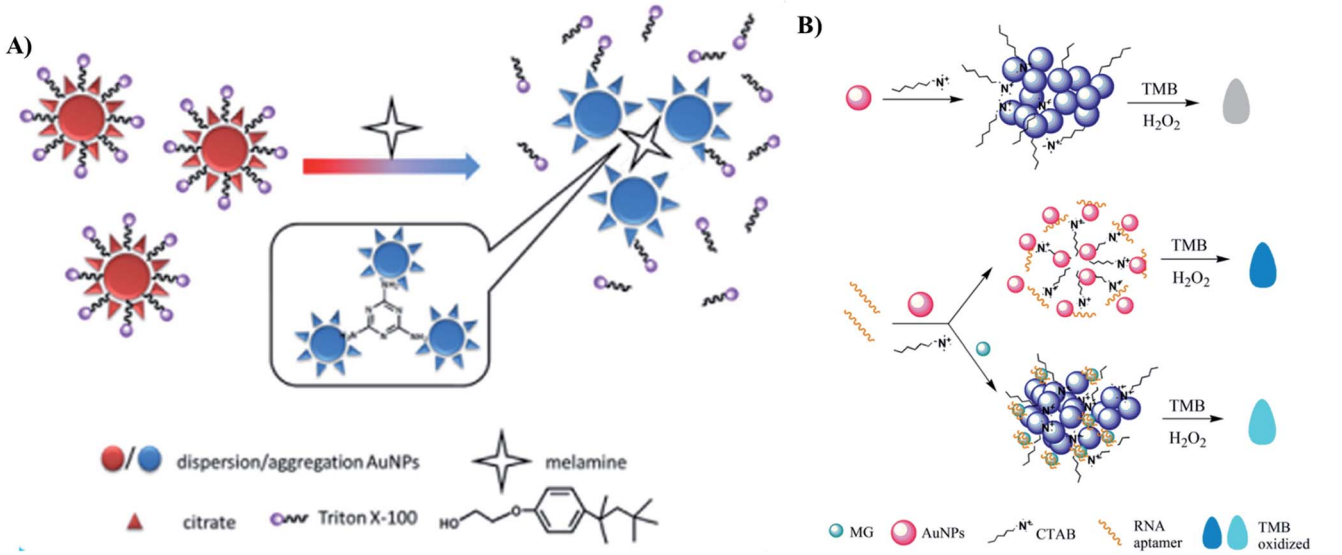

Fig. 9 Different kinds of AuNPs-based optical sensors for detection of food additives. (A) Colorimetric sensor for detection of melanine based on two strategies: crosslinking and de-protection. Reprinted from ref. 174 Copyright 2018, with permission from Elsevier. (B) Colorimetric aptasensor for detecting Malachite Green based on the inhibition of the peroxidase-like activity of gold nanoparticle by CTAB. Reprinted by permission from Springer Nature: ref. 183 Copyright 2019.

the protein contents.[170] Consuming melamine containing food and drinks may cause serious damages to human kidneys and reproductive systems.[170,171] Thus, it is important to develop reliable sensing methods to detect melamine. Due to the structure containing 3 amino groups, it is easily bound to 2–3 AuNPs at once, through the interactions with their coating agents such as citrate,[171] thymine,[172] and 1,4-dithiothreitol (DTT).[173] Therefore, the detection of melamine is usually based on the crosslinking aggregation approach.[171–175] Gao *et al.* even combine crosslinking and de-protection strategies to develop a colorimetric assay for the detection of melanine (Fig. 9A).[174] To improve the sensitivity of the method, several novel strategies have been proposed. Zhang *et al.* took advantage of AuNP aggregation to generate a "turn-off" FRET sensor using conjugated polymer NPs as donors.[176] In the absence of melamine, fluorescence signal was quenched by AuNPs. The introduction of melamine led to aggregation of the AuNPs, resulting in the fluorescence recovery. The method achieved a low LOD of 1.7 nM.[176] Chen *et al.* focused on widening the dynamic detection range.[170] The authors found that after introducing melamine to AuNP solution, AuNPs quickly aggregated and formed large aggregations. The precipitation of these aggregations led to the rapid evanishment of solution color, which reduced the accuracy of the colorimetric signals. Therefore, they introduced polyethylene glycol onto selected area of the AuNP surface, thereby stabilizing the AuNPs. The binding of melamine still occurred at the citrate-site of the AuNPs and induced a purple-to-blue color change. The linear range of the method covered from 1.05 nM to 1 mM.[170]

Preservatives have been playing an important role in the food industry by improving the duration of food products and allowing them to be stored and transported to consumers. However, illegal food preservatives are extremely toxic to human. For example, high intake nitrite and formaldehyde might lead to the risk of gastric cancer and leukemia.[177,178] In general, there are only few studies on optical sensors to detect food preservatives, in comparison to electrochemical ones. Martínes-Aquino *et al.* employed resorcinol functionalized AuNPs for colorimetric detection of formaldehyde with an LOD of 0.05 ppm, but the method has not been applied in real samples.[179] Nie *et al.* detected formaldehyde using non-functionalized AuNPs in a SERS sensor with an LOD of 1×10^{-4} μg mL^{-1}, which exhibited satisfying performance in real samples of duck blood and rice flour.[180] To detect thiabendazole, an antifungal agent and also a food preservative that is not approved in the EU, Alsammarraie *et al.* developed a SERS sensor, in which the utilization of Au nanorods as substrates has enhanced SERS signal.[181] The sensor achieved LODs of 149, 216 and 179 μg L^{-1} in lemon, carrot and mango juice, respectively.[181]

Food dyes provide attractive colors to food and drinking products. However, due to their toxicity, many kinds of food dyes have been prohibited, including Sudan dyes, Malachite Green, Allura Red, Sunset Yellow, *etc.* Malachite Green (MG) is not only a dye but also an antimicrobial in aquaculture. Therefore, MG can be detected in fish and other seafood products. Due to its affinity to RNA aptamer, Jia *et al.* employed aptamer labeled AuNPs to detect MG using an anti-aggregation strategy.[182] In the presence of MG, RNA aptamer would bind to MG instead of protecting AuNPs. As a result, AuNPs were aggregated at a high concentration of NaCl and the solution color turned from red to blue. The LOD of the sensor was as low as 15.95 nM.[182] Also taking advantage of that affinity, Zhao *et al.* developed an indirect colorimetric sensor using CTAB as inhibitors for peroxidase-like activity of AuNPs.[183] The system had 3 states of color. In the absence of RNA aptamer and MG,

CTAB inhibited the enzymatic activity of AuNPs, so TMB could not be oxidized and the solution was nearly colorless (the concentration of AuNPs was low). In the addition of RNA aptamer, AuNPs were stabilized and protected, which consequently reduced the adsorption of CTAB on AuNPs, leading to the oxidization of TMB and a blue color in the solution. In the presence of MG, some of the aptamers bound to MG instead of AuNPs, reducing the level of protection, resulting in a light blue color in the solution. The LOD of the method was 1.8 nM (ref. 183) (Fig. 9B).

3.1.5. Other contaminants. Food and drinks can be contaminated by bacteria, which cause food poisoning or diarrheal disease to human. To control food safety, these food/water-borne pathogens are also the detecting targets. Several AuNPs-based sensors have been designed and developed for the detection of those bacteria. In general, researchers usually choose antibodies[184–186] or aptamers[187–191] to recognize and capture the bacteria. Feng *et al.* reported the development of a simple sensor for *Shigella flexneri* using aptamer labeled AuNPs.[191] Due to the high affinity of the bacteria to the aptamer, they de-protected the AuNPs. The lack of stabilizing agents made AuNPs easily get aggregated under a high-salt condition. In contrast, in the absence of the bacteria, AuNPs were well-protected by the aptamer coating and would not be aggregated even at high concentration of NaCl. The sensor exhibited a low LOD of 80 CFU mL^{-1} and a linear range of 10^2–10^6 CFU mL^{-1}.[191] Concerning the specificity of the detection, it is necessary to mention antibody as an effective recognition ligand. Fu *et al.* proposed a colorimetric immunoassay to sense *Vibrio parahaemolyticus*, in which AuNPs played the role of a chromogenic substrate, and antibody labeled MnO_2 NPs acted as the recognition element.[186] Unbound MnO_2 NPs were eliminated by external magnetic separating. Once being immobilized on the surface of the bacteria, the MnO_2 NPs generated Mn^{2+} due to the etching effect of ascorbic acid. A high concentration of Mn^{2+} induced the aggregation of AuNPs, leading to a red-to-blue color change. The sensor had an LOD as low as 10 CFU mL^{-1} and a detecting range covering from 10 to 10^6 CFU mL^{-1}.[186] Another choice for the capturing element is 4-mercaptophenylboronic acid (4-MPBA). This molecule contains a thiol group to bind to AuNP surface and a boronic acid group that can form covalent bonds with the peptidoglycan cell wall of bacteria. Huang *et al.* reported a colorimetric sensor using AuNPs functionalized with 4-MPBA *via* anti-aggregation strategy.[192] In the absence of bacteria, a high concentration of NaCl induced the aggregation of AuNPs. In contrast, in the presence of bacteria, AuNPs are bound to them through the boronic acid group of 4-MPBA, so the solution remained red instead of turning blue, even at high-salt conditions. The obtained LOD was appropriate at 1.02×10^3 CFU mL^{-1} for *Escherichia coli* (*E. coli*).[192] The utilization of 4-MPBA is more simple, easily-prepared and cost-effective, comparing to using antibody or aptamer. Unfortunately, because of the presence of peptidoglycan in every bacterium, it lacks specificity. Therefore, other molecules have been investigated to find the alternatives for expensive antibodies, which usually requires special experimental conditions. As vancomycin has been confirmed to be able to bind specifically to Gram-positive bacteria,[193,194] Song and coworkers have employed this antibiotic as recognition element in a study of a FRET sensor for *S. aureus* in 2017,[195] followed by the use of another antibiotic in the same family, teicoplanin, in 2021.[190] The newest system consisted of aptamer labeled quantum dots and teicoplanin factionalized AuNPs. In the presence *S. aureus*, both of them specifically bound to the bacteria, and the distance was close enough for AuNPs to quench fluorescent signal of the quantum dots. The method achieved an LOD of 2 CFU mL^{-1}.[190] In addition, chimeric bacteriophage is another potential candidate. Thanks to the developments on phage display technique, Chen's group have introduced a set of engineered M13 phages displaying the receptor-binding protein from a phage naturally targeting several bacteria, including *Pseudomonas aeruginosa (P. aeruginosa)*, *Vibrio cholerae (V. cholerae)*, and *E. coli.*[169,196] The structure of those chimeric M13 phage has been described in a 2019 study (Fig. 8D),[169] followed by a report on the detection of *P. aeruginosa* using a thiolated chimeric phage in a crosslinking aggregation approach in 2020.[196] Chimeric phage is a promising candidate to replace antibody as the recognition element for detecting bacteria due to its specificity and robustness. Moreover, it is non-toxic to human.

Biotoxins occur naturally in the environment, which are secreted by organisms to protect themselves from being eaten by others. For instance, mycotoxins are produced by the ones from fungus kingdom while saxitoxin is the most harmful shellfish toxin. To avoid food poisoning, it is important to determine these toxins in potential food before consuming. Therefore, several studies have been carried out to sense biotoxins using AuNPs-based optical sensors. Mycotoxins, such as fumonisin B1 and T-2, have been detected using colorimetric sensors *via* crosslinking and non-crosslinking approaches, respectively.[197,198] Cao *et al.* employed cysteine-modified AuNPs as detecting probes to sense saxitoxin as the toxin could bind to cysteine *via* electrostatic interactions and hydrogen bonds. As a result, saxitoxin was detected with an LOD as low as 1×10^{-7} M.[199]

3.2. Health safety monitoring

For disease diagnostics, AuNPs-based sensors aim to detect the target molecules related to a specific disease. They can be molecules and peptides (*e.g.*, glucose for diabetes, dopamine for schizophrenia disorder, glutathione for reperfusion injury, *etc.*), protein and nucleic acid biomarkers for non-infectious diseases (*e.g.*, cancers, liver diseases, heart diseases, *etc.*), or infectious pathogens (*e.g.*, bacteria, viruses, *etc.*) and their antibodies for infectious diseases in human blood, serum, saliva, urine, *etc.* Although it has been reported that appropriate nanomaterials for biomedical sensing should have the absorbance adjusted to the near-infrared region by changing their sizes or morphology. Thus, the ideal materials for disease diagnosis are large nanospheres, nanorods, nanocage, *etc.*[75] However, it is the criteria for the substrates for *in vivo* sensing, *i.e.*, bioimaging.[75,223] In this review, we focus on *in vitro* disease diagnosis. Thus, there is no large difference in the nature of the samples in food and health safety monitoring sensors. Therefore, similar to the sensors

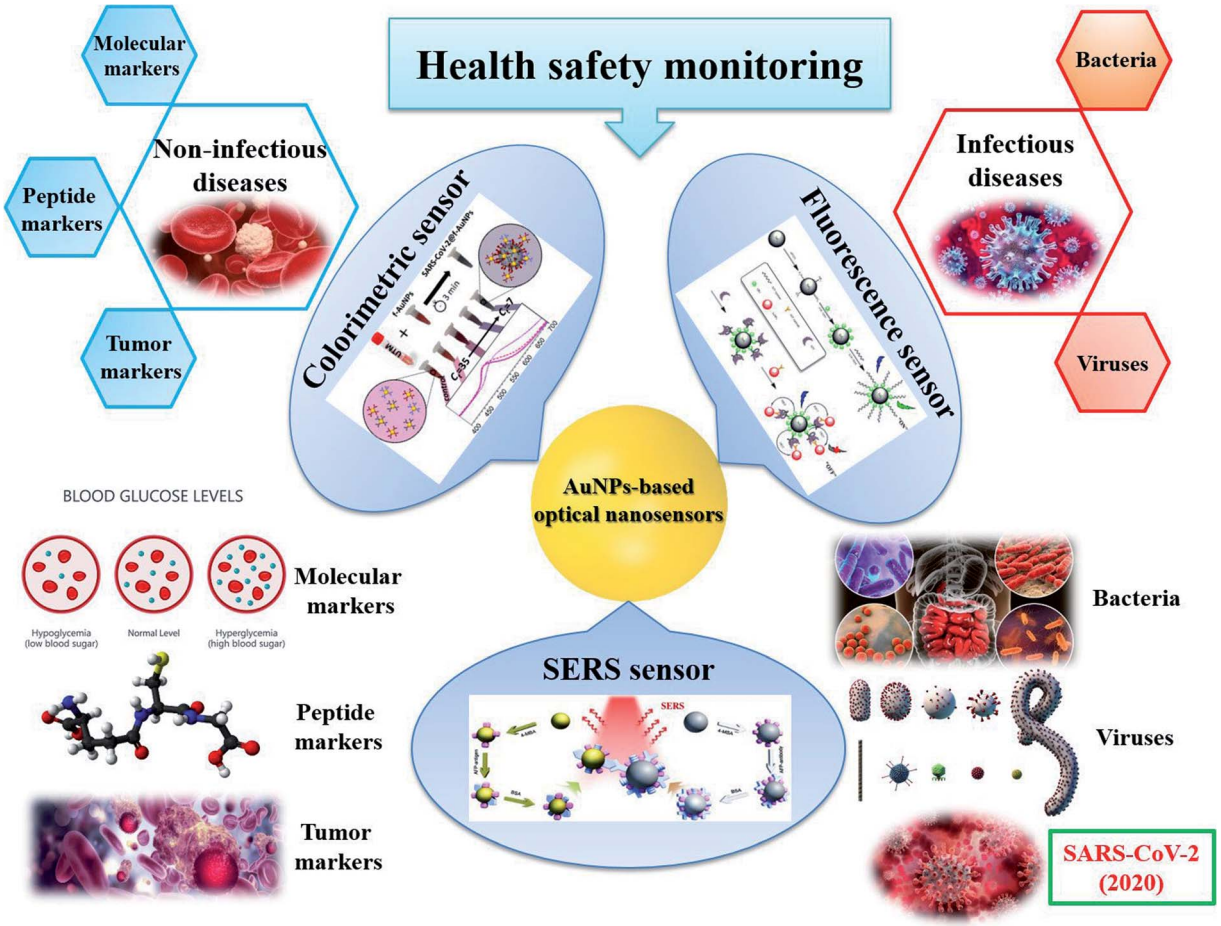

Fig. 10 AuNPs-based optical sensors for health safety monitoring. Inset pictures: colorimetric sensor: reprinted with permission from ref. 224 Copyright (2020) American Chemical Society. Fluorescence sensor: reprinted by permission from Springer Nature: ref. 225 Copyright 2019. SERS sensor: reprinted by permission from Springer Nature: ref. 118 Copyright 2018.

described in the previous section, in this section, the selection of particle shape in each kind of AuNPs-based optical sensors for *in vitro* disease diagnosis is still obeyed what we mentioned in Section 2.2. Herein, we will introduce some AuNPs-based sensing systems for both non-infectious and infectious disease diagnostics, focusing on diabetes, cancers and pathogenic bacteria and viruses, especially SARS-CoV-2 (Fig. 10). The information about other sensors for other diseases is presented in Table 2.

3.2.1. Non-infectious diseases

3.2.1.1. Diabetes. The glucose level in human blood, serum, saliva as well as urine is an indication of health status. Both high and low glycemic levels are harmful for human health. According to World Health Organization, a level below 3.0 mM (54 mg dL^{-1}) of plasma glucose after a period of fasting can be considered as hypoglycemia.[226] In contrast, plasma glucose maintaining at a high concentration of above 7.0 mM (126 mg dL^{-1}) may present hyperglycemia.[227] Persistently high glucose level can be the result of the inability to produce insulin of the pancreas or the inefficiency of utilizing insulin for uptaking glucose into the cells.[228] This is one of the characterized symptoms for diabetes. Therefore, monitoring the glucose level is important to diagnose as well as manage diabetes. In this review, we focus on glucose as a typical example of the molecules that have been detected using many different sensing principles.

Glucose sensors using AuNPs as the detecting probes can be enzymatic or non-enzymatic. Glucose oxidase (GOx) is an enzyme for converting glucose to gluconolactone that releases H_2O_2 as a by-product.[229] Thus, the level of glucose can be determined by the presence of this by-product. In 2020, Yang *et al.* designed a tapered fiber structure decorated with AuNPs and GOx to sense glucose.[230] AuNPs integrated on surface of the tapered fiber were functionalized with GOx. In the addition of glucose solution, GOx decomposed the glucose and produced H_2O_2 that changed the refractive index (RI) of the medium surrounding the AuNPs. As mentioned in the previous part, the RI change Δn always leads to the shift of LSPR band. The absorbance peak shifted toward the longer wavelength region along with the increase in glucose level. This sensor achieved an LOD as low as 322 μM.[230] This sensor also introduced the idea of designing a reusable sensor, which would reduce the cost of the system. However, the limitation of this sensor is that the RI can be affected by various factors. Intrinsic variabilities in complex

biological samples can influence the accuracy of the method. This might be the reason why the sensing system was not employed to detect glucose in real samples.

Another strategy is taking the advantage of the reducing activity of H_2O_2 to accelerate AuNP etching reaction in the presence of halogenic ions. In a recent study, Donati *et al.* use Br^- as the halogenic ion in a sensing system for glucose.[77] Due to the enzymatic reaction between glucose and GOx in the AuNP solutions, H_2O_2 was produce. This by-product converted Br^- ions into Br_2 molecules, which quickly etched the multi-branched AuNPs at their tips and reshaped them into spherical AuNPs. Interestingly, in real samples of saliva, the salivary thiols (*i.e.*, cysteine, glutathione and others) acted as an organic shield that protected and stabilized the NP surface. Therefore, the AuNPs were not aggregated, and the blue-to-red color change of the solution was the result of the transformation of AuNP shapes. At a higher concentration of glucose, a pink color was observed in the reaction solution, indicating a hyperglycemia event (Fig. 11A). The LOD of the sensor calculated after analyzing saliva samples from different donors was 1.4 mg mL^{-1}. Although this LOD is not in line with the best performing glucose sensors mentioned in this review, the system is promising to intrinsic biological variabilities or real clinic samples.[77]

The by-product H_2O_2 can also acts as the analyte in an indirect sensor for glucose. Candem and coworkers designed a sensing system based on 3-mercaptophenylboronic acid (3-MPBA) modified (AuNPs).[231] In the presence of H_2O_2, 3-MPBA is oxidized into 3-hydroxythiophenol (3-HTP). The change in the structure of boronate probe was presented by the change among two SERS spectra of the nanoprobe before and after the H_2O_2 treatment. For the real samples, GOx and nanoprobes were added into glucose-containing urine solutions, resulting in a change in SERS spectra indicating conversion of the boronate into the phenol as expected. A similar result was obtained in serum samples.[231]

Due to the specificity of the enzyme to its substrate, the enzymatic approach provides high selectivity to the AuNPs-based sensors. However, the presence of enzyme requires specific storage and reaction conditions. Thus, we also concern non-enzymatic strategies. Based on the formation of covalent bonds between glucose and boronic acids, Na *et al.* have employed 3-aminobenzeneboronic acid as the recognition element in a sensing assay using AuNPs and graphene oxide quantum dots (GOQDs).[232] GOQDs displayed orange fluorescence, however, this fluorescence was quenched by AuNPs. In the presence of glucose and 3-aminobenzeneboronic acid, they bound together to form a cationic species that could cause aggregation of anionic AuNPs. As a result, the fluoresce signal of GOQD was recovered. This method resulted in an LOD of 0.65 μM,[232] lower than that of a similar sensing system using phenylboronic acid, a boronic acid derivative in colorimetric approach.[233] Besides, the complex of boronic acid and glucose is also useful to reduce the distance between AuNPs and create "hot spots" for SERS sensing.[111]

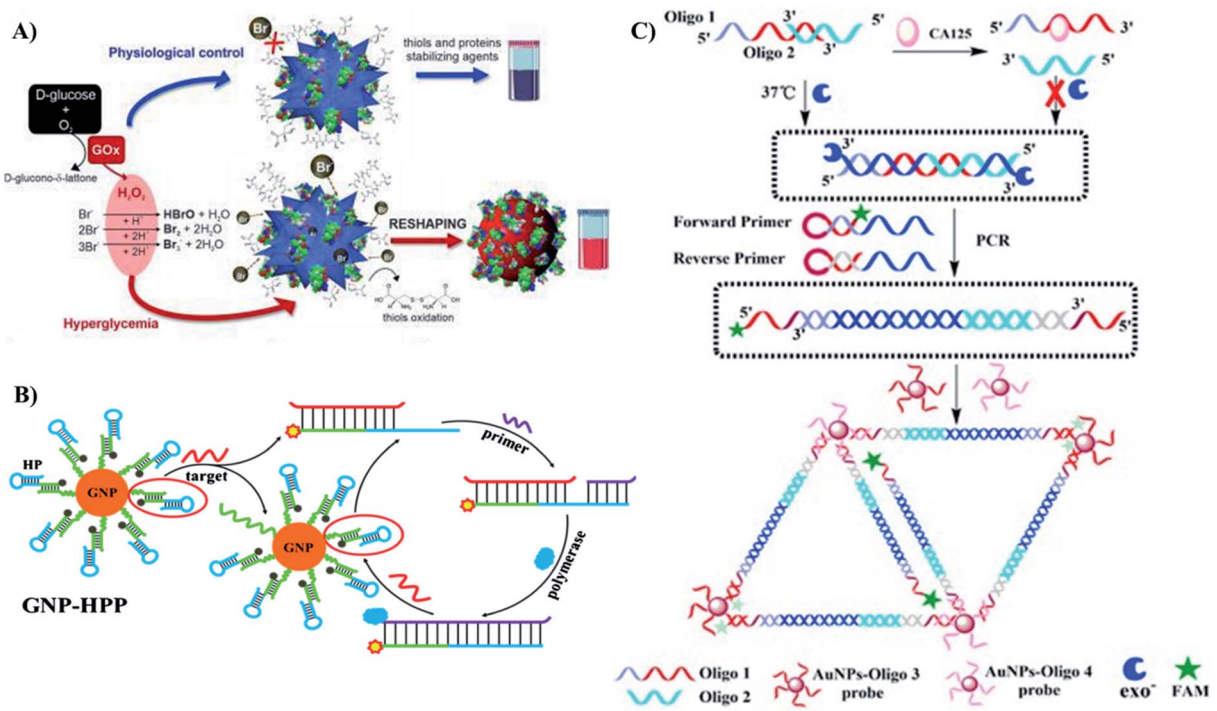

Fig. 11 Several AuNPs-based optical sensors for detection of diabetes and cancers using different kinds of biomarkers. (A) Glucose (molecular biomarker). Colorimetric sensor based on AuNP growth. Reproduced with permission from ref. 77 Copyright 2020 Donati, Pomili, Boselli and Pompa. (B) p53 gene (DNA biomarker). FRET-based sensor with signal amplification strand displacement amplification of the target gene. Reprinted by permission from Springer Nature: ref. 241 Copyright 2019. (C) CA-125 (protein biomarker) FRET-based sensor with signal amplification by PCR. Reprinted from ref. 261 Copyright 2018, with permission from Elsevier.

In another approach, glucose can act as a reducing and capping agent for AuNP synthesis. Hence, Pinheiro *et al.* have designed a colorimetric sensor with the direct detection of glucose without any intermediate product.[234] The authors stated that low concentrations of glucose resulted in large AuNPs while high concentrations of glucose led to the formation of smaller AuNPs. The difference in sizes of AuNPs was claimed based on the LSPR shifts and the color changes of the reaction solutions. The method gave an LOD of 0.65 mM,[234] which is not as low as some others that we have discussed above, but it is still appropriate in physiological range. More importantly, this study has introduced a fast and easily-prepared AuNPs-based sensor without NP modification.

In addition to glucose, glycated hemoglobin is another glycemic indicator, especially to measure the average glucose concentration in the blood of diabetic patients. In comparison to the glucose level, glycated hemoglobin level is more stable due to the 4 months lifespan of the hemoglobin.[235] Therefore, Kwak *et al.* developed a sensor for detection of glycated hemoglobin in an enzymatic approach.[236] Glycated hemoglobin consists of a glucose molecule binding to *N*-terminal valine residue of the hemoglobin β-chains. H_2O_2 was generated due to oxidative cleavage of fructosyl valine in glycated hemoglobin in the presence of fructosyl amino acid oxidase. Subsequently, H_2O_2 reduced Au^{3+} ions into Au atoms and formed AuNPs. The characteristic red color of AuNP solutions and their absorption peak at 520 nm represented for the presence of glycated hemoglobin. Based on the intensity of absorption peak, they calculated the ratio of glycated hemoglobin to total hemoglobin. The sensor exhibited an LOD of 0.124% of total hemoglobin and a linear range of 4.6% to 13.5% of total hemoglobin. Because normal level of glycated hemoglobin levels is within the range of 4–6%, this method was promising *in vitro* diagnosis for diabetes.[236]

3.2.1.2. Cancers. Cancers can be detected through the presence of biomarkers in blood, tissues and other body fluids.[237] Cancer biomarkers can be proteins (either secreted or cell surface proteins), carbohydrates or nucleic acids (*i.e.*, DNA, microRNA, *etc.*).[238] Besides, in some studies, extracellular vesicles and even cancer cells were chosen to be biomarkers for cancer diagnosis.[239,240] Most of AuNPs-based cancer sensors focus on detecting protein and nucleic acid biomarkers due to the well-understood knowledge of the specific interactions such as antigen–antibody, complementary nucleotide sequences, *etc.* The discovery of numerous cancer markers has enabled the detection of cancers, for example, p53 (tumor suppressor gene/protein),[241,242] BRCA,[243] HER2 (ref. 244) and Erα (breast cancer),[245] AFP (liver cancer),[246] PSA (prostate cancer),[247] *etc.*

Nucleic acid biomarkers. To sense nucleic acid cancer biomarkers, the main strategy is based on the interaction between complementary nucleotide sequences. However, because the number of each gene copies in one cell is limited to 2, the concentration of DNA in the samples is consequently low, thus these sensors usually require a step of amplification.[248,249] It can be either the amplification of target, which is carried out before the detection step, or the amplification of signal, which takes place after the detection step. As the most widely-used method to amplify DNA molecules is polymerase chain reaction (PCR), a colorimetric sensor for PSA3 has been designed by combining PCR technique and AuNP functionalization. In this 2019 study, Htoo *et al.* designed primers for PSA3 amplifying using PCR technique, in which the forward primer was thiolated.[247] In the presence of the target gene (PSA3), PRC products were produced as thiolated double-stranded PSA3 sequences, which could bind to AuNPs due to the affinity between their thiol groups and the NP metallic surface. Thanks to the stabilization of the DNA ligands, AuNPs did not aggregate at high-salt condition (red color). In contrast, without the presence of the target gene, no PCR product was formed to stabilize AuNPs, thus, AuNPs aggregated at a high concentration of NaCl (blue color). The red or blue color of AuNP solution represents the presence or absence of PSA3 biomarker in the urine samples, respectively.[247] Instead of thiolated primers, in another study, Trau and coworkers utilized biotin-contained primers to amplify 3 DNA sequences containing 3 important melanoma mutations.[250] These amplicons could be conjugated onto streptavidin coated magnetic bead *via* biotin-streptavidin binding. Meanwhile, AuNPs were functionalized with 3 kinds of DNA tags complementary to 3 different barcodes on the forward primers for recognition. Moreover, each kind of AuNPs was modified with one Raman reporter. As a result, the presence of the targeted mutation was detected through the characteristic peaks of the appropriate reporter. Thanks to DNA amplification step, this multi-target SERS system achieved an impressive LOD of 0.1% mutation (10 copies).[250]

Despite of its advantages, DNA amplification still have several drawbacks including the risk of erroneously amplifying contamination and time-consuming, thus, researchers have developed procedures in which the response signal was amplified instead. For example, instead of amplifying the number of target DNA molecules, Yu and coworkers employed a strategy of "reusing" them.[241] They introduced a sensor for p53 cancer gene using strand displacement amplification on functionalized AuNPs. FAM-labeled hairpin probes were bound on the surfaced of AuNPs, therefore, their fluorescence was quenched by AuNPs *via* FRET principle. In the presence of p53 gene, it hybridized with the hairpin probe due to the complementary sequence. The hybridization opened the hairpin, which not only led to fluorescence recovery, but also allowed the primer to bind to the opened hairpin and trigger the polymerization/displacement reactions. Once being replaced, p53 gene was release, then bound to another hairpin to start another round of reaction (Fig. 11B). The sequences of reactions have amplified the fluorescence signal, which allowed p53 gene to be quantified at a concentration as low as 1.6 pM.[241]

Another approach of signal amplification is focusing on material fabrication. In a 2020 study, Bai *et al.* took advantage of the catalytic activity of AuNPs as they can trigger the reduction of 4-nitrophenol, resulting in a color change from yellow to colorless.[243] They designed a capture probe and a signal probe, each of which contains a DNA sequence that is complementary to the target BRCA1 mutated gene. Capture probes were bound to the surface of the wafer while the signal ones were attached to

0D AuNPs. In the presence of the targets, three DNA sequences form a sandwich structure, and the AuNPs with signal probes were immobilized on the surface of the wafer. The colorimetric reaction catalyzed by these AuNPs provided signals for detection of BRCA1 mutation. Then AuNPs were grafted on the surface of 2D materials including GO and Bi_2Se_3 nanosheets, resulting in 4- and 10-fold amplification in signal, respectively. Thus, by improving the material property, the method reached an impressive LOD of 10^{-18} M and a linear range of 10^{-18} to 10^{-12} M.[243]

To simplify sensing procedures, researchers are also interested in fabrication of amplification-free sensors for DNA biomarkers. Yu *et al.* reported on a SERS sensor, in which the target sequence was sandwiched between 2 probe DNA-immobilized on the surface of 2 kinds of NPs: AuNPs and magnetic beads.[251] AuNPs were modified with a Raman reporter. In fact, the structure of this sensing system is relatively similar to the one developed by Trau and coworkers that we mentioned above.[250] However, Yu *et al.* did not amplify the target gene. Instead, their strategy was enhancing the SERS signal by utilizing hollow AuNPs, which could localize electromagnetic fields through their pinholes. Additionally, the targeted sequence was short (45 nucleotide), so the gaps between two particles were also small enough to create "hot-spots". As a result, the method achieved an LOD of 2.7 fM.[251] Despite the impressive result, it was only an experimental model, in which the target sequence was a PCA3 mimic gene. In real samples, it is difficult to isolate a gene sequence from genome without PCR. This technique might be more appropriate for other kinds of nucleic acid, which are short and single stranded. MicroRNA is a promising candidate.

A dual (colorimetric and FRET) sensor for microRNA-155 was developed by Borghei *et al.*[252] This microRNA was reported to be over-expressed in many human cancers,[253] so amplification was not necessary. They utilized DNA-modified silver nanoclusters (DNA-AgNCs) as donors and AuNPs as acceptors. In the absence of microRNA, the single-stranded DNA sequences were adsorbed onto AuNPs. Consequently, AuNPs quenched the fluorescence emitted from DNA-AgNCs. At the same time, this adsorption also prevented salt-induced aggregation of the AuNPs. In contrast, upon addition of microRNA, the hybridization between microRNA and the DNA immobilized on the AgNCs separated the DNA-AgNCs from the AuNPs. As a result, fluorescence recovery occurred. Also, AuNPs easily aggregated at high concentration of salt, reflected by a red to purple color change. Although this method exhibited an acceptable LODs of 0.6 nM and 0.4 pM for colorimetric and FRET sensor, respectively, it was reported in the article that those LODs were still higher than amplification step-containing methods.[252] Hence, amplification is definitely important for the sensitivity of sensors for nucleic acid biomarkers.

Due to the highly specific interaction between complementary sequences, the selectivity of cancer sensors using nucleic acid targets is undeniable. In all of the studies mentioned above, an obvious difference was observed in the signal of the target genes in comparison with their mutant sequences, even with 1 or 2 mis-matched bases.[241,243,247] However, the necessity of amplification can be a limitation to generate a fast and simple procedure of detecting cancer.

Protein biomarkers. Compared to nucleic acid, protein is a much richer source of biomarkers because many kinds of protein are over-expressed in cancer tissues.[254] However, researchers may encounter the problems of selectivity as the mutations of a few nucleotides only cause a little change in the protein conformation.[255] It requires full understandings of the interactions between these biomarkers and other biological molecules to generate sensitive and selective sensing systems for cancers.

The well-understood immune-interaction of antigen–antibody might be a simple and specific principle to design sensors for protein cancer biomarkers. In a 2015 study, Chen *et al.* reported on a gold nanorods-based LSPR sensor for cancer antigen 15-3 (CA15-3) using gold nanorods modified with CA15-3 antibody. The presence of CA15-3 led to increase of intensity of absorption spectra, red-shifts of the absorption peaks and the broadening of the peaks, corresponding to the assembly of the gold nanorods.[256] Similarly, the mucin protein, MUC4, which is overexpressed in pancreatic cancer, was also recognized thanks to antibody-antigen binding in a SERS sensor.[257] However, due to the large size of the antibody immobilized on AuNPs, the hot-spots for SERS signal enhancement were not created due to the assembly of AuNPs through binding with the same antigen. Instead, they designed a template stripped gold (TSG) substrate to immobilized antibodies. Thus, MUC4 antigens were captured between the substrate and the AuNPs in a sandwich model. The AuNPs were modified with a Raman reporter. Therefore, the signal of the reporter represented for the presence or absence of MUC4. In addition, the concentration of antibody immobilized on the substrate could be controlled to ensure the distance among those antibodies as well as interparticle distance among the AuNPs after the recognition step were close enough to create SERS hot-spots.[257] Another example of the SERS sensor using this interaction is a sensor for AFP developed by Zhang *et al.* in 2018.[258] This system consisted of both AuNPs and AgNPs, in which AgNPs were functionalized with AFP antibodies while AuNPs acted as the capturing probe for the attachment of AFP antigens in the sample. Due to the antibody–antigen interaction, the distance between the nanoparticles was reduced, leading to formation of "hot spots" that enhanced the SERS signal. As expected, the method exhibited high specificity. However, in complex real samples, it expressed poor sensitivity compared to other methods.[258] This can be explained by the high biocompatibility of AuNPs, which allows the attachment of many other molecules rather than AFP antigens.

Recently, based on the interactions between protein molecules and DNA sequences, AuNPs have been functionalized with aptamers and employed as sensing probes for colorimetric sensors. Protein biomarkers such as PSA and p53 was detected using AuNPs-based aptasensors *via* cross-linking strategy.[242,259] Meanwhile, de-protection strategy was employed for detection of others such as HER2,[244] EAα[245] and carcinoma embryonic antigen (CEA).[260] In cross-linking models, the aptamers had to be designed as thiolated DNA[242] or containing poly A

sequences[259] so that they could be attached to AuNPs. In the presence of target biomarker, aptamers-modified AuNPs aggregated due to the specific interaction between their coating agents and the target protein. As a result, a red to purple color change could be observed with bare eye.[242,259] On the other hand, aptamer acted as a protecting agent to prevent salt-induced aggregation of AuNPs by absorbing onto the metallic surface in de-protection models. In the addition of target protein, the aptamer would bind to the target due to a higher affinity, and the AuNPs aggregated easily at high concentration of salt, which also resulted in a red to purple color change. This method is simple and fast with the incubation time of only 5–10 minutes.[244,245,260] Moreover, it can avoid the use of antibodies, which are required strict conditions of storage and utilization. More importantly, the selectivity of aptamer is undeniable. For example, in the study on p53, the mutant p53 could be distinguished from the wild-type.[242] The lack of a functional tetramerization domain in mutated p53 prevented it from inducing aggregation of aptamer-functionalized AuNPs. In contrast, the AuNPs aggregated in the presence of wild-type p53 as the aptamer contained recognition element for the binding of p53.

In another attempt to detect AFP, Zhou *et al.* combined both antibody–antigen and protein–DNA interactions in a FRET sensing system, where the aptamer labeled luminescent CdTe quantum dots (QDs) were the donors and AFP antibody grafted AuNPs were the acceptors.[246] In the presence of AFP antigen, its affinity to antibody and aptamer reduced the distance between the two kinds of NPs. As a result, AuNPs quenched the fluorescence of QDs. This "turn-off" sensor exhibited a linear range of 0.5–45 ng mL^{-1}, with an LOD of 400 pg mL^{-1}. Moreover, it also showed a satisfying performance in human serum samples.[246] It is worth noting that in this study, the author used 2 sites of recognition instead of one, which increased the specificity of the sensing method.

The combination of different strategies may result in interesting results. In a 2021 study, Shen *et al.* were successful to design and develop a FRET sensor for cancer antigen 125 (CA-125) at trace amounts by combining protein-aptamer interaction and DNA amplification.[261] They designed 2 partly complementary sequences, named Oligo 1 and Oligo 2. Oligo 1 contained an aptamer for CA-125. In the absence of CA-125, the partially hybridized sequences were extended with Klenow fragment (exo) polymerase to obtain a new double stranded DNA molecule. This new DNA was employed as the template for PCR-amplification. Both forward and reverse primers contained a spacer, resulting in the formation of single-stranded DNA at two sides of the PCR product, which was complementary with Oligo 3 and Oligo 4 immobilized on the surface of AuNPs. Moreover, each forward primer also contained a fluorescein (FAM). After hybridization, the fluorescence of FAM was quenched by gold nanoparticles due to FRET effect, resulting in a decrease in fluorescence signal. In contrast, in the addition of CA-125, the antigen bound to Oligo 1 and prevented the hybridization between Oligo 1 and Oligo 2. It also terminated all the following process. Thanks to its conformation (Fig. 11C), the forward primer did not hybridize to the DNA probes on the AuNPs directly, thus, their fluorescence intensity remained. Despite its complexity, the method achieved an impressive LOD of 1.5 fg mL^{-1}.[261] Moreover, it has revealed the unlimited potential of combining different strategies and techniques in fabrication of novel systems.

Other biomarkers. In addition to nucleic acid and protein biomarkers, other tumor-related elements have been studied as new markers to detect cancers, including extracellular vesicles (EVs) secreted from cancer cells[262] and cancer cells themselves.[128] Among them, extracellular vesicles are more widely-used because they are the richer source. The advantages of using these large biomarker is that they contain many different membrane proteins, which can be employed as targets for detection.[263] In 2020, Wang and coworkers introduced a sandwich-type SERS sensor for EVs tumor.[264] The system included two kinds of aptamer targeting two different sites of the EVs that were used to label AuNPs and agarose beads, respectively. Even in complex samples, EVs could selectively bind to agarose beads, followed by the attachment of AuNPs to form sandwich complexes. The enhancement in SERS signal was observed due to this formation. The LOD of the sensor was as low as 2.44 pg μL^{-1}.[264] Similarly, Oliveira-Rodríguez *et al.* also employed two tetraspanins on the membrane of exosome as detecting target in their colorimetric sensor.[263] The utilization of two binding sites on one target can increase the selectivity of the sensing systems.

On the other hand, cancer cells were the biomarkers in several studies. Butler *et al.* developed a near infrared SERS sensor based on 150 nm AuNPs to detect MCF-7 breast cancer cells.[128] A significant enhancement of Raman signal was observed in the presence of MCF-7 cells. However, without specific functionalization, this sensing system were not effective in protein-rich samples, such as serum, with a low signal-to-noise ratio.[128] Also in an effort of sensing MCF-7 cells, Li *et al.* introduced a colorimetric sensor, in which the cancer cells were recognized by Mucin 1 protein (MUC-1) aptamer-modified gold nanorods.[265] In the presence of the cancer cells, the gold nanorods bound onto their membrane, which can be observed by UV-vis spectroscopy. Thanks to the specific binding of the aptamer and MUC-1 protein, the sensors could distinguish the target MCF-7 and untumorigenic cells HepG-2.[265]

3.2.2. Infectious pathogens control. Infectious diseases are caused by different kinds of pathogens such as bacteria and viruses. Therefore, there are several approaches for diagnosis of one specific infectious disease, including detecting the whole or a part of the pathogen particle, the whole or a part of its genome or the antibody produced by the body in the presence of pathogen.[266] As mentioned in the part about food safety, one whole bacterium can be captured and determined by a sensing system.[169,196] However, considering the high infectivity of pathogenic bacteria in human clinic samples, it is safer to inactivate them and use their genome for detection. For example, *Mycobacterium tuberculosis* (TB) collected from oral swabs should be heat-treated before being further studied.[267,268] Tsai *et al.* proposed a colorimetric method to sense a TB sequence containing IS6110, using the non-crosslinking strategy.[268] Similar to other studies on detecting DNA sequences mentioned above,[247]

the target sequence had to be amplified by PCR before the detection. The authors designed a single stranded DNA probe that was complementary to IS6110. The DNA probes were adsorbed on the surface of AuNPs. Once the sample containing IS6110 was added to the solution, the DNA probe would bind to the target sequence, thus de-protected the AuNPs, and AuNPs were easily aggregated (Fig. 12A). As a result, the absorption spectra of the solution shifted towards the longer wavelength region while its color became more blueish. The method had an LOD of 1.95 ng mL^{-1} for TB DNA.[268] In another study, Owens

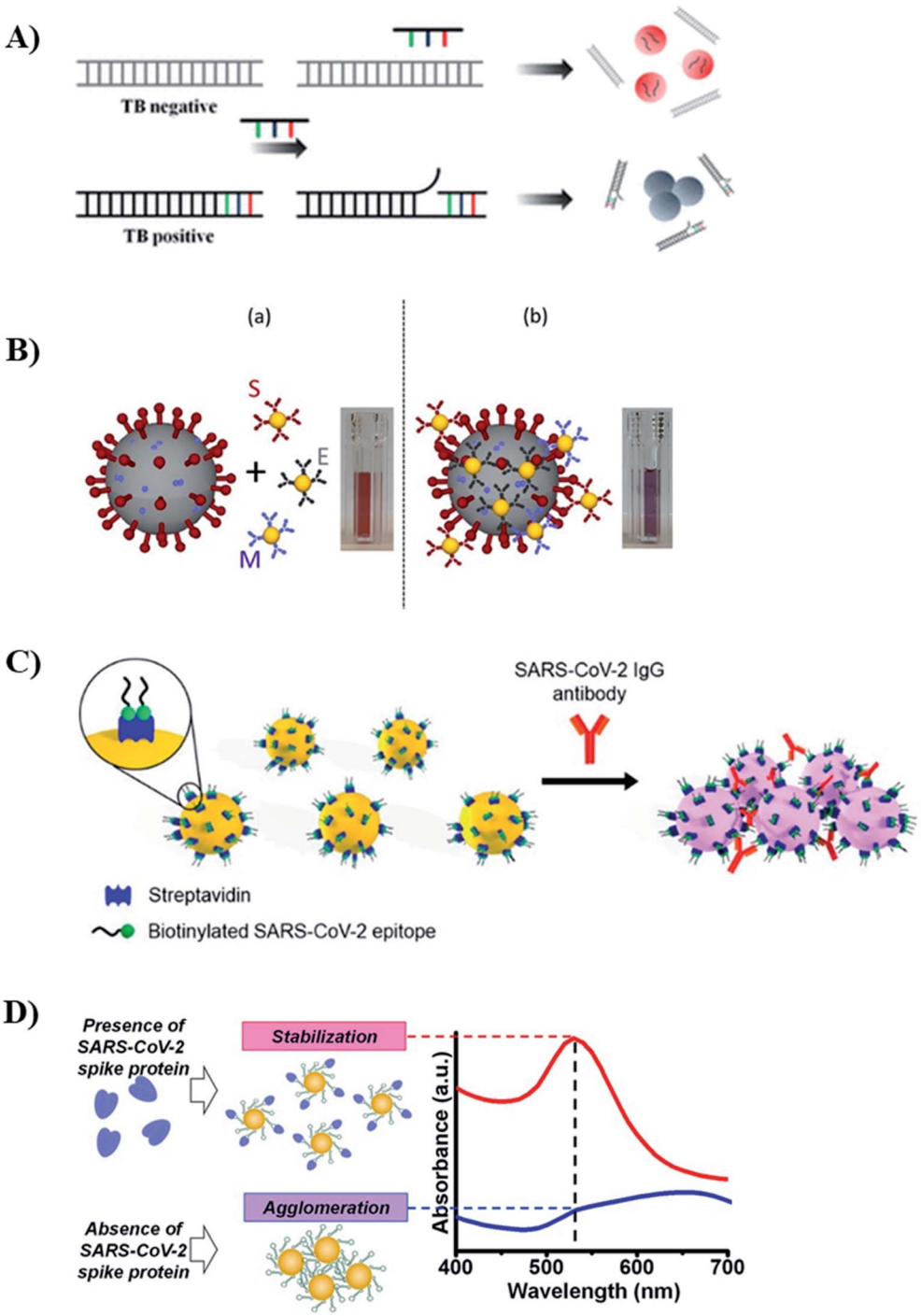

Fig. 12 Several AuNPs-based colorimetric sensors for infectious pathogens designed for detecting different kinds of target. (A) Genome. Colorimetric (de-protection) sensor for detection of Tuberculosis. Reprinted with permission from ref. 268 Copyright (2017) American Chemical Society. (B) Whole virus particle. Colorimetric (crosslinking) sensor for detection of SARS-CoV-2. Reprinted with permission from ref. 224 Copyright (2020) American Chemical Society. (C) Antibody. Colorimetric (crosslinking) sensor for detection of SARS-CoV-2. Reprinted with permission from ref. 277. Copyright (2021) American Chemical Society. (D) Spike protein. Colorimetric (anti-aggregation) sensor for detection of SARS-CoV-2. Reprinted from ref. 279 Copyright 2021, with permission from Elsevier.

et al. chose mannose-capped lipoarabinomannan (ManLAM), an TB antigenic marker, as the target to detect TB.[269] Two kinds of anti-ManLAM antibodies were employed to functionalize the AuNPs and the capture substrate, respectively. Hence, ManLAM antigen would be captured between them. The SERS signal was measured to determine the presence of ManLAM with an LOD of 10 ng mL^{-1}.[269]

Similarly, for virus detection, it is possible to detect the whole virus or its genome. Many kinds of influenza viruses were detected as whole virus particles,[270–272] in which AuNPs were functionalized with recognition elements to sense the viruses. The most frequently-used capturing probe is antibody so that AuNPs would assemble on the surface of the virus. Thus, the presence of viruses could be determined due to a red to purple color change caused by that assembly.[271,272] In another approach, Ahmed *et al.* reported that the organization of AuNPs on the surface of virus had enhanced the peroxidase-mimic enzymatic activity of positively-charged AuNPs.[270] Compared to AuNPs only, AuNPs-decorated influenza viruses exhibited stronger catalytic activity when catalyzing the oxidation of TMB by H_2O_2, resulting in a deeper blue color in solution, reflecting in higher absorption intensity at 665 nm. It was the main principle to determine the presence of influenza virus H1N1 and H3N2.[270] Instead of using antibody, Li and coworkers employed AuNPs modified with glycan containing terminal sialic acid (SA).[273] The structure of this terminal SA played a decisive role for the binding of the functionalized AuNPs to the viruses. The binding of SA receptors to the viruses resulted in the aggregation of the AuNPs on the virus surface, and subsequently the blue color of the solution. In contrast, in case the SA receptor was not specific to the virus, the AuNPs would not bind to the viruses and the solution would remain the red color. Using a set of AuNPs with 7 different structures of SA receptors, the authors differentiated 14 influenza virus strains, including the most major subtypes in human and avian populations.[273] Besides, an example for virus detection through its genome is a colorimetric assay to detect MERS-CoV developed by Kim *et al.*[274] They designed a pair of thiolated probes at 5′ or 3′ end, which were complementary to MERS-CoV sequence. In the presence of the target DNA sequence, they reorganized into a double stranded DNA, which was assembled on the surface of AuNPs and prevented them from aggregation at high-salt condition. In contrast, the absence of target sequence led to the aggregation of AuNPs. The difference in color could be observed using bare eye or UV-Vis spectroscopy. The assay had a low LOD of 1 pmol μL^{-1}.[274]

3.2.3. Emerging COVID-19 disease control. Since December 2019, the whole world has been under the threat of a new Severe Acute Respiratory Syndrome Coronaviridae virus, known as SARS-CoV-2. Many detecting approaches for this kind of virus have been investigated, including the use of AuNPs. However, short research time and limited understanding about the structure of this virus only allowed researchers to provide simple reports of SARS-CoV-2 sensing. For fast detection, most of them described the sensors to detect the whole virus particle.[224,275,276] For example, Alfassam *et al.* proposed taking advantage of hemagglutinin (HA) protein on the surface of the virus as target for detection.[275] Therefore, they fabricated sialic acid (SA) coated AuNPs, so the binding of HA of the virus to SA on AuNPs would lead to the aggregation of AuNPs, resulting in the spectral shift of LSPR. However, this sensor lacked of selectivity because it exhibited the same positive result for all three types of respiratory virus: SARS-CoV-2, influenza B, and MERS-CoV.[275] Ventura *et al.* described another sensor using 3 kinds of antibodies targeting 3 kinds of protein on SARS-CoV-2 surface, including spike (S), membrane (M) and envelop (E).[224] Obvious changes in solution color and absorbance have been observed in the presence of the virus (Fig. 12B).[224] To increase sensitivity and selectivity of the sensor, Huang *et al.* have immobilized the virus on a sensing chip *via* antibodies coated on the chip surface in an immunoassay.[276] AuNPs were functionalized with another kind of antibodies to bind to a different epitope of the virus. Using the whole virus directly as a target element, this method is time effective (<15 min) with a low LOD of 30 particles.[276]

Jiao and coworkers have avoided the threat of being infected while working with viruses by choosing a different target, IgM antibody against SARS-CoV produced in the human body in the presence of the virus.[86] They fabricated a testing strip, where SARS-CoV-2 nucleoprotein (SARS-CoV-2 NP) was coated on a membrane to capture the target antibody. Antihuman IgM was attached to AuNPs. In the presence of the antibody, it was immobilized between the nucleoprotein and AuNPs, which introduced a line in characteristic red color on the strip.[86] Through this study, the authors have reported a fast testing of SARS-CoV-2 using serum samples rather than oral swabs. The limitation of this approach was that it required a relatively high concentration of antibody in human serum to form a visible red line on the testing strip. Therefore, SARS-CoV-2 could not be detected in early stage of infection using this method. In an effort to fabricate a more sensitive sensor for SARS-CoV-2 antibody, Lew *et al.* designed a colorimetric sensor to detect SARS-CoV-2 IgGs in patients' plasma.[277] The IgG binding affinity of four immunodominant linear B-cell epitopes, located on the spike (S) and nucleocapsid (N) proteins, were characterized to find the two most sensitive ones, which were subsequently biotinylated and conjugated to streptavidin-coated AuNPs. In the presence of SARS-CoV-2 IgGs, these epitopes played the role of recognizing target antibodies, triggering to the aggregation of AuNPs (Fig. 12C). Moreover, co-immobilization of two epitopes led to an improvement in the sensitivity of the method, in comparison to single-epitope modified AuNPs. The assay achieved an LOD of 3.2 nM. Hence, it could be potentially used to detect IgG for convalescent COVID-19 patients. Using for 35 clinic samples, including Covid-19 patients' samples, the novel method successfully identified SARS-CoV-2 infection with 100% specificity and 83% sensitivity.[277]

In addition to the method using antigen–antibody interaction, recently, detecting SARS-CoV-2 using aptamers has attracted the interest of researchers.[278,279] In a recent study, Aithal *et al.* employed aptamer-functionalized AuNPs to target S protein of the virus in a colorimetric sensor.[279] In an anti-aggregation approach, the binding of S protein to the aptamer prevented to the aggregation of the AuNPs at high-salt condition

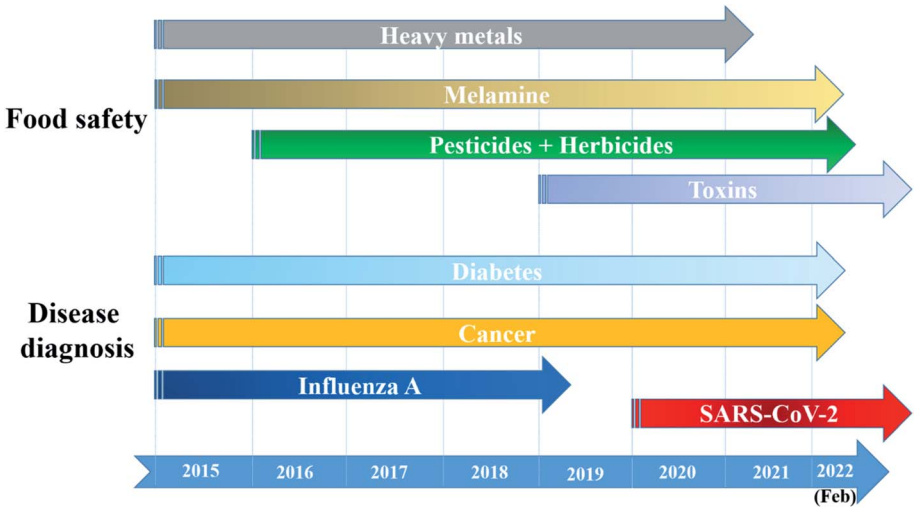

Fig. 13 The most concerned detecting targets of AuNPs-based optical nanosensors for food and health safety (2015 – February 2022).

(Fig. 12D). The sensor was well-performed in the presence of isolated S protein as well as heat-inactivated SARS-CoV-2 viruses. The nanoprobes could detect 3540 genome copies/μL inactivated SARS-CoV-2 virus. However, it should be further validated with real patients' samples.[279]

3.3. Potential of multi-metallic gold-based optical sensors for food and health safety monitoring

Recently, the introduction of multi-metallic nanomaterials, in general, and multi-metallic gold-based nanoparticles, in particular, has opened a potential of developing a new generation of optical sensors. To achieve the best plasmonic effect, noble metals such as silver (Ag), platinum (Pt), copper (Cu), *etc.* have been selected to combine with Au in the manufacture of multi-metallic nanostructures.[289,290] It has been reported that these nanomaterials exhibited stronger LSPR bands than mono-metallic ones.[289,291] Moreover, the position of LSPR band in UV-Vis spectrum of a multi-metallic material can be controlled by adjusting the ratio and the arrangement of its components.[289–291] Besides, in another study, Bai *et al.* calculated electromagnetic field distributions of AuNPs and several multi-metallic NPs using Lorenz-Mie theory.[292] The results revealed significant electromagnetic enhancement of alloy and core–shell multi-metallic structures (*i.e.*, Ag–Au NPs and Au@Ag NP, respectively), and especially alloy core–shell structure (*i.e.*, Au@Ag–Au NPs), in comparison with mono-metallic AuNPs.[292] Therefore, multi-metallic gold-based NPs are promising to develop colorimetric (or LSPR) and SERS nanosensors. However, there has been no report on the property of quenching fluorescence of these NPs, especially in comparison to AuNPs. As a results, studies on multi-metallic gold-based NPs as substrates for optical sensors for food and health safety monitoring have focused on colorimetric and SERS sensors. For instance, the strong LSPR band of bimetallic Ag–Au NPs allowed George *et al.* to develop ultrasensitive colorimetric sensors for Mn^{2+} and ciprofloxacin, an antibiotic banned for animal food.[293] Mn^{2+} and ciprofloxacin were detected at low concentrations down to 18.40 and 10.26 nM, respectively.[293] In another approach, core–shell Au@Ag nanorods were employed to detect AFP, a protein marker of hepatocellular cancer.[294] By controlling the thickness of Ag shell and the aspect ratio of Au core, the authors adjusted the color of nanorod solution to achieve the appropriate color range for bare-eyed observation.[294] Besides, the noticeable electromagnetic enhancement of core–shell structures, especially at the internal gap between the core and the shell, has attracted the attention of researchers in the effort of designing and developing effective SERS substrates.[292,295] For example, Au@Ag NPs was designed and optimized to detect pesticides, including tricyclazone and thiram in pear extracts, resulting in impressive LODs of 0.005 and 0.003 ppm, respectively.[296] In addition, Cu@Au NPs exhibited a great potential to be appropriate SERS substrates for various biomolecules, including acetaminophen, dopamine, cholesterol, *etc.*[290] Furthermore, the complex core–shell alloy structure of Au@Ag–Au NPs showed the best performance compared with core–shell (Au@Ag NPs), alloy (Ag–Au NPs) and mono-metallic structures (AuNPs) in SERS sensing system for cardiac troponin I, a biomarker for cardiac injury.[292]

Despite the great potential, the application of multi-metallic gold-based NPs for development of optical nanosensors for food and health safety is still limited with only a few studies, and very few of them were carried out in real samples.[296] Compared to mono-metallic AuNPs, complicated procedures of multi-metallic NP manufacture[297] might have been prevented them from being widely-employed in sensing systems. Readers who are interested in the manufacture of multi-metallic NPs may find useful information in the established review by Srinoi *et al.*[297] Nevertheless, the superior optical properties of multi-metallic gold-based NPs are undeniable, therefore, they still have space to grow as substrates for optical sensors for food and health safety monitoring in the future.

4. Trends and challenges of gold nanoparticles-based optical sensing systems for food and health safety monitoring

4.1. Trends

The huge amount of information in the tables has provided a picture of recent developments of AuNPs-based sensing systems for food safety control and *in vitro* disease diagnosis. Fig. 13 exhibits the most concerned detecting targets in both fields with the presence of long-term and emerging ones. In general, the development of AuNPs-based optical sensors have always caught up with urgent needs of the society. For example, virus outbreaks have triggered the investigation of their detecting sensors. High toxicity, even at low concentrations, of pesticides[298] and melamine have led to the demand of monitoring these food contaminant/additive, especially when melamine contamination is usually related to enfant milk.[299] Diabetes and cancers are also concerning as the number of patients suffering and dying of these disease keeps rising every year.[300,301] Herein, we present several trends of developing AuNPs-based optical sensors in the recent 7 years.

With a large number of reported studies, obviously, AuNPs-based optical nanosensors are widely studied to monitor food safety. Since 2015, many food contaminants and additives have been detected using colorimetric, FRET- and SERS-based sensors. Starting with analytes possessing simple chemical structure such as heavy metals (*e.g.*, Hg^{2+}, Pb^{2+}) and melamine, researchers have design various sensing systems based on their well-understood interactions with DNA,[201] DNAzyme[205] and peptides[207] (for heavy metals) as well as citrate,[219] methanobactin[217] and DTT,[173] *etc.* (for melamine). Thus, heavy metals and melamine were the targets for many reported optical nanosensors. Moreover, recent studies about melamine detection also concern the improvements in technologies, including newly-investigated ligands[218] and the combination of known ligands[170] to evaluate the performance of the optical sensors. They not only introduced effective sensing tools for the most popular contaminants and additive in food but also provided the concepts for the following studies. The enlarged knowledge about other food contaminants and their specific interactions to other compounds allow the fabrication of other sensing systems in the later period. We can clearly observe an upward trend in determination of toxins as many analytes in this category have been detected using different kinds of optical sensors and in various forms of real samples in recent 3 years.[95,199,214] This trend may continue to grow in the following years. Detection of pesticides and herbicides is also a long-term concern of researchers. In fact, before 2016, pesticides and herbicides were determined using AuNPs-based optical sensors.[156,302] However, it was not until 2017 that we observed a wave of research on pesticide and herbicide detection as many kinds of targets have been detected. The developments in nanotechnology have led to the significant improvements in the sensitivity of the sensors. For instance, SERS sensors for pesticide detection designed by Huang *et al.* in 2020[159] resulted in impressive LODs which were 10 times lower than those of the studies reported in 2018 (ref. 112) and 2016,[161] thanks to the fabrication of snowflake-like AuNPs and the utilization of specific ligands. Recently, many states and countries has participated in numerous Free Trade Agreements, which allows the trading of goods, including various kinds of food, all over the world. Therefore, cost- and time-effective sensing tools to monitor food safety and quality have been in high demand. It opens an opportunity for AuNPs-based optical sensors to be further investigated and applied in this large area in the near future.

Besides, the AuNPs have maintained their position as one of the most appropriate substrates to develop optical nanosensors for *in vitro* disease diagnosis during the observed period (*i.e.*, 2015–now) thanks to their excellent biocompatibility.[22,39,88] The non-infectious diseases such as diabetes and cancers have been always long-term concerns of researchers as many kinds of optical sensors have been generated to monitor the glucose level or determine varied tumor markers. Because diabetes and cancers are still unsolved problems of modern mankind,[303,304] these studies may be continued in several years. On the other hand, the trends of investigating optical sensors for detection of infectious diseases usually follow their outbreaks. For examples, influenza viruses, which have been the perpetrators for the outbreaks of flu, including bird flu,[273] swine flu,[270] and seasonal flu,[271] *etc.*, have attract the interest of researchers for several years. The turning point came in December 2019 with the outbreak of a new corona virus (*i.e.*, SARS-CoV-2), which then developed into COVID-19 pandemic, one of the most serious health crisis in the human history.[305,306] Consequently, we are witnessing an explosion of researches on detecting COVID-19, including AuNPs-based optical sensors. Until now (February 2022), the world is still under the threat of the pandemic with the appearance of the new variants, and the virus shows no sign of stop. Therefore, the studies on SARS-CoV-2 will be continued, and the AuNPs-based optical sensing systems for rapid COVID-19 detection is still on the road to optimization.

Following the recent advances, we can see that antibody is losing their place as the most ideal recognition element. Although antibody provides selective targeting, more and more groups are choosing aptamer, which is more stable and smaller in size compared to antibodies. However, it cannot be denied that biological molecules are not as stable as chemical ones. Their affinity to analytes would reduce after a long time of storage, especially in hot weather. Researchers have started solving this challenge by finding alternative such as synthetic organic compounds,[111] antibiotics[190,195] and chimeric phages.[169,196]

Another trend is the utilization of smart phone in recording and analyzing signals, especially with colorimetric sensors, in RGB color model.[132,158,221] Because almost everyone today possesses a smart phone, it is a step closer to the application of sensor in real life.

4.2. Challenges

Along with the developments of knowledge and new technology, researchers have focused on various AuNPs-based sensing

systems for food and health safety monitoring. However, we are still facing several challenges to improve and optimize the performance of these sensing systems, including their sensibility, reliability and practicality.

4.2.1. Sensibility. An effective sensor requires a low limit of detection and a large linear detecting range. In general, the reported AuNPs-based optical sensors listed in the tables exhibits appropriate LODs. For example, all the LODs of those melamine sensors are lower than the maximum acceptable concentration in food set by US FDA (50 ppb ~0.3 μM).[307] However, in colorimetric sensors, the linear range is usually limited due to the aggregation of AuNPs. The introduction of analytes at high concentration leads to the rapid formation of large aggregates and precipitates of AuNPs, causing a fast reduction in the intensity of absorption spectrum, which is usually out of the linear range. Chen *et al.* have suggested a solution for this challenge by improving the stability of AuNPs against aggregation by partially functionalizing the AuNPs with PEG.[170] In this study, they attached citrate-stabilized AuNPs onto a APTES-activated glass substrate *via* electrostatic attraction. Subsequently, thiol-PEG-acid chains were introduced onto the "untouched" surface of AuNPs. Definitely, this approach has enlarged the linear range of the AuNPs-based melamine sensor toward the higher-concentration side. However, the preparation of AuNPs was complicated. Moreover, it is difficult to apply this concept to other sensing systems using any ligands other than citrate. Therefore, improving linear ranges for colorimetric sensors is still challenging.

4.2.2. Reliability. In order to develop appropriate AuNPs-based optical sensors, the parameters of reliability such as selectivity, stability, reproducibility, *etc.* cannot be ignored. Following the recent reports presented in the tables, it is not difficult to notice that in many sensing systems, citrate has been chosen as the recognition element for the detection of varied analytes such as melamine,[170] dopamine,[225] paraquat,[212] *etc.* This choice has simplified the fabrication of AuNPs-based sensors. Moreover, those sensors have exhibited appropriate LODs. However, it is obvious that those sensors are lacked of selectivity. To improve the selectivity of the methods, it requires the utilization of more specific ligands on the AuNPs surface. Nevertheless, in SERS sensors, there is a conflict between the selectivity and the sensibility of the method. SERS sensors require an intimate contact between the AuNPs surface and the analyte for signal enhancement while the specific recognition element may enlarge the distance between them. The trend of investigating alternative ligands mentioned in the previous part of this Section may be the solution to balance this conflict. In addition, being performed on dried substrates, SERS sensors usually exhibit lower reproducibility compared to the ones performed in solutions. Neither drop-casting[159] nor pasting-and-peeling[161] technique is able to ensure the homogeneity and reproducibility of SERS signal on the substrate.

4.2.3. Practicability. Many studies have described rapid, sensitive, selective sensors. However, they are still laboratory-based, and practicality is still a major challenge. Researchers are in the struggle between generating simple and user-friendly sensors *versus* selective and sensitive ones. We are impressed by the LODs and linear ranges of many sensors, but their complicated preparation limits the potential for wider application.[241,243,246] Among all sensing systems mentioned above, many of them were claimed to have been employed in real samples (Table 1 & 2). However, most of these "real samples" need to be managed in the laboratory with many steps of pretreatment.[170,222,308] Even though there are a few sensors fabricated using simply-prepared samples,[170,222,308] they are all clinical samples, which have been managed strictly through a standard procedure. It would be much more difficult for a real sample of food. Real food samples are extremely complicated and unpredictable. They might contain a large amount of salts that induces the aggregation of AuNPs. In addition, they can include oil and oil-soluble elements. Therefore, even when a sensor is designed for one specific food product, the pH of the sample can change due to the influence of unexpected contaminations. Similarly, saliva samples for rapid sensing of drugs or biomarkers are also uncontrollable with many variables.[258]

Besides, due to the complexity of real samples, each of which might contain more than one desired target, optical sensors have been designed and developed towards multi-target directions. However, among numerous examples that we have mentioned above, there is only one sensor that can detect more than one molecule at once. It is the sensing systems for 3 kinds of pesticides by Zhang *et al.* in 2020,[158] in which 3 different fluorescence signals from 3 kinds of fluorophores were recorded, analyzed in RGB model to calculate the contents of each kind of pesticides. However, a fluorescence-based sensor always requires some instruments and tools to record and analyze the signals. Colorimetric sensor is a more user-friendly approach. Therefore, several groups have investigated multi-target colorimetric sensor. Wu *et al.* employed multi-functional aptamer labeled AuNPs[132] while Yan *et al.* proposed a pattern recognition methods using two kinds of AuNPs functionalized with two different aptamers.[168] However, due to the "red-to-blue" trap, these sensors are not accurate in complex samples contained two or more targets.

5. Conclusions and future prospects

Gold nanoparticles are excellent transducers for optical nanosensors including LSPR, colorimetric, FRET-based and SERS-based sensors for detection of food contaminants and diseases. Examples on advanced sensing systems have been summarized to draw a general picture of the recent developments of AuNPs-based optical nanosensors. In-laboratory works have shown impressive achievements in detecting many kinds of analytes. However, on the road of optimizing their sensing performance, there are several challenges. In the future, by solving all those challenges and taking advantage of the developments of every field of science and technology, sensor-developers may fabricate a new generation of AuNPs-based optical sensors, which is smarter, achieves significant improvements in sensing performance and accomplishes the goal of practical applications. To generate smart sensors, researchers need to combine the latest technologies including Internet of Things (IoT), Artificial Intelligence (AI) and machine

learning to their sensing systems. These tools are able to collect, manage and analyze a large amount of data. Therefore, the data recorded by the sensors may be rapidly collated to the data bank, followed by the fast determination of the sensing system. Besides, the sensing performance of the sensors will be improved in every aspect. Knowledge about the interactions between analytes and recognition elements will be fulfilled, so more highly-specific elements (either natural or synthetic ones) at appropriate sizes will be employed for the detection of desired targets. Obviously, stable and durable ligands are highly desirable to enhance to stability of the systems. In addition, further studies on multi-metallic gold-based nanomaterials and their applications of optical sensing may be a direction to elevate the sensibility of the sensors. Finally, the new sensors will be more practicable. Standard but irreducible preparation procedures will be investigated in order to minimize the influence of environmental factors on the sensing performance, but still be user-friendly. Besides, the success of glucose meter has established the idea of developing hand-held spectrometers for LSPR, fluorescence and SERS measurements. The manufacture of these devices in combination with the development of professional analysis tools in smartphones might make AuNPs-based optical nanosensors become accessible for everyone. Furthermore, multi-target sensors will be the new direction to monitor complex samples, especially food products. Beside the red-to-blue range, sensor-developer may add more color ranges by combining indirect colorimetric sensing to the systems. In another approach, taking advantage of the different colors of fluorophores may be the key for the detection of several targets at once using fluorescence sensors. In term of material fabrication, AuNPs should be synthesized using robotic systems. It will ensure the homogeneity among different synthesis batches. Moreover, it will not only reduce the requirement of specialized human resources, but also allow highly-yielded manufacture. As a result, AuNP fabrication will be more cost- and time-effective, which is essential for the goal of high practicability. After several decades of research, the practical applications of optical sensors based on AuNPs are still limited. Hence, greater efforts should be made towards their practical utilization in the future.

Author contributions

N. H. Anh: conceptualization, methodology, formal analysis, writing-original draft; M. Q. Doan: conceptualization, validation, investigation, writing-original draft; N. X.Dinh: conceptualization, writing-review & editing; T. Q. Huy: writing-review & editing, formal analysis; D. Q. Tri: funding acquisition, visualization, writing-review & editing; L. T. N. Loan: methodology, writing-review & editing; B. V. Hao: formal analysis, writing-review & editing; L. A. Tuan: conceptualization, methodology, supervision, project administration, writing-review & editing.

Conflicts of interest

The authors declare that they have no known competing financial interests or personal relationships that could have appeared to influence the work reported in this paper.

Acknowledgements

This research was funded by Vietnam National Foundation for Science and Technology Development (NAFOSTED) under grant number 103.02-2018.48. The authors would like to thank application-driven research program on Smart Sensing Technologies between ITIMS-HUST, IMS-VAST and MSE-NANO at the Phenikaa University.

References

1 W. Xing, H. Zhang, K. G. Scheckel and L. Li, *Environ. Monit. Assess.*, 2015, **188**, 23.
2 C. Xiu and K. K. Klein, *Food Pol.*, 2010, **35**, 463–470.
3 A. European Food Safety, H. Reich and G. A. Triacchini, *EFSA J.*, 2018, **16**, e05164.
4 F. Federspiel and M. Ali, *BMC Public Health*, 2018, **18**, 1338.
5 Q. Song, Y.-J. Zheng, Y. Xue, W.-G. Sheng and M.-R. Zhao, *Neurocomputing*, 2017, **226**, 16–22.
6 A. N. Tchana, P. F. Moundipa and F. M. Tchouanguep, *Int. J. Environ. Res. Public Health*, 2010, **7**, 178–188.
7 T. Ghazi, T. Arumugam, A. Foolchand and A. A. Chuturgoon, *Cells*, 2020, **9**, 2004.
8 T. Borahan, T. Unutkan, A. Şahin and S. Bakırdere, *J. Sep. Sci.*, 2019, **42**, 678–683.
9 D. T. Usmanov, S. Akhunov, U. Khasanov, V. M. Rotshteyn and B. Kasimov, *Eur. J. Mass Spectrom.*, 2019, **26**, 153–157.
10 H. Nakagawa, R. Hashimoto, Y. Matsuo, Y. Sago, K. Yokoyama and H. Takahashi, *Curr. Microbiol.*, 2020, **77**, 3057–3064.
11 V. C. Fernandes, M. Freitas, J. P. G. Pacheco, J. M. Oliveira, V. F. Domingues and C. Delerue-Matos, *J. Chromatogr. A*, 2018, **1566**, 1–12.
12 A. Agarwal, R. Agrawal, D. V. Gunasekaran, D. Raje, B. Gupta, K. Aggarwal, S. L. Murthy, M. Westcott, S. P. Chee, P. McCluskey, H. S. Ling, S. Teoh, L. Cimino, J. Biswas, S. Narain, M. Agarwal, P. Mahendradas, M. Khairallah, N. Jones, I. Tugal-Tutkun, K. Babu, S. Basu, E. Carreño, R. Lee, H. Al-Dhibi, B. Bodaghi, A. Invernizzi, D. A. Goldstein, C. P. Herbort, T. Barisani-Asenbauer, J. J. González-López, S. Androudi, R. Bansal, B. Moharana, S. Mahajan, S. Esposti, A. Tasiopoulou, S. Nadarajah, M. Agarwal, S. Abraham, R. Vala, R. Singh, A. Sharma, K. Sharma, M. Zierhut, O. M. Kon, E. Cunningham, Q. D. Nguyen, C. Pavesio and V. Gupta, *Ocul. Immunol. Inflamm.*, 2019, **27**, 465–473.
13 Y. Li, Z. Wang, L. Sun, L. Liu, C. Xu and H. Kuang, *TrAC, Trends Anal. Chem.*, 2019, **113**, 74–83.
14 G. Liu, M. Lu, X. Huang, T. Li and D. Xu, *Sensors*, 2018, **18**, 4166.
15 D. O'Hare, in *Body Sensor Networks*, ed. G.-Z. Yang, Springer London, London, 2014, DOI: 10.1007/978-1-4471-6374-9_2, pp. 55–115.
16 S. Mohammadi, A. Salimi, S. Hamd-Ghadareh, F. Fathi and F. Soleimani, *Anal. Biochem.*, 2018, **557**, 18–26.
17 Q. Liu, L. Li, Y. Zhao and Z. Chen, *Mikrochim. Acta*, 2018, **185**, 301.

18 S. Dalirirad and A. J. Steckl, *Sens. Actuators, B*, 2019, **283**, 79–86.
19 K. Saha, S. S. Agasti, C. Kim, X. Li and V. M. Rotello, *Chem. Rev.*, 2012, **112**, 2739–2779.
20 N. Elahi, M. Kamali and M. H. Baghersad, *Talanta*, 2018, **184**, 537–556.
21 P. Zhao, N. Li and D. Astruc, *Coord. Chem. Rev.*, 2013, **257**, 638–665.
22 M. Azharuddin, G. H. Zhu, D. Das, E. Ozgur, L. Uzun, A. P. F. Turner and H. K. Patra, *Chem. Commun.*, 2019, **55**, 6964–6996.
23 C. C. Chang, C. P. Chen, T. H. Wu, C. H. Yang, C. W. Lin and C. Y. Chen, *Nanomaterials*, 2019, **9**, 861.
24 P. Jiang, Y. Wang, L. Zhao, C. Ji, D. Chen and L. Nie, *Nanomaterials*, 2018, **8**, 977.
25 E. Petryayeva and U. J. Krull, *Anal. Chim. Acta*, 2011, **706**, 8–24.
26 Y. Zhang, W. Chu, A. D. Foroushani, H. Wang, D. Li, J. Liu, C. J. Barrow, X. Wang and W. Yang, *Materials*, 2014, **7**, 5169–5201.
27 L. Li, M. Zhang and W. Chen, *J. Food Drug Anal.*, 2020, **28**, 642–654.
28 M. Cordeiro, F. Ferreira Carlos, P. Pedrosa, A. Lopez and P. V. Baptista, *Diagnostics*, 2016, **6**, 43.
29 L. Tessaro, A. Aquino, A. P. A. d. Carvalho and C. A. Conte-Junior, *Sens. Actuators Rep.*, 2021, **3**, 100060.
30 B. Negahdari, M. Darvishi and A. A. Saeedi, *Artif. Cells, Nanomed., Biotechnol.*, 2019, **47**, 455–461.
31 V. Ramalingam, *Adv. Colloid Interface Sci.*, 2019, **271**, 101989.
32 D. T. Nguyen, D.-J. Kim and K.-S. Kim, *Micron*, 2011, **42**, 207–227.
33 P. Slepička, N. Slepičková Kasálková, J. Siegel, Z. Kolská and V. Švorčík, *Materials*, 2019, **13**, 1.
34 T. Schmutzler, T. Schindler, T. Zech, S. Lages, M. Thoma, M.-S. Appavou, W. Peukert, E. Spiecker and T. Unruh, *ACS Appl. Nano Mater.*, 2019, **2**, 3206–3219.
35 J.-E. Park, M. Atobe and T. Fuchigami, *Ultrason. Sonochem.*, 2006, **13**, 237–241.
36 Y. Ren, C. Xu, M. Wu, M. Niu and Y. Fang, *Colloids Surf., A*, 2011, **380**, 222–228.
37 P. Priecel, H. Adekunle Salami, R. H. Padilla, Z. Zhong and J. A. Lopez-Sanchez, *Chin. J. Catal.*, 2016, **37**, 1619–1650.
38 C. Kohout, C. Santi and L. Polito, *Int. J. Mol. Sci.*, 2018, **19**, 3385.
39 X. Hu, Y. Zhang, T. Ding, J. Liu and H. Zhao, *Front. Bioeng. Biotechnol.*, 2020, **8**, 990.
40 J. Turkevich, P. C. Stevenson and J. Hillier, *Discuss. Faraday Soc.*, 1951, **11**, 55–75.
41 G. Frens, *Nat. Phys. Sci.*, 1973, **241**, 20–22.
42 M. Brust, M. Walker, D. Bethell, D. J. Schiffrin and R. Whyman, *J. Chem. Soc., Chem. Commun.*, 1994, 801–802, DOI: 10.1039/C39940000801.
43 M. Shah, V. Badwaik, Y. Kherde, H. K. Waghwani, T. Modi, Z. P. Aguilar, H. Rodgers, W. Hamilton, T. Marutharaj, C. Webb, M. B. Lawrenz and R. Dakshinamurthy, *Front. Biosci.*, 2014, **19**, 1320–1344.
44 R. Herizchi, E. Abasi, M. Milani and A. Akbarzadeh, *Artif. Cells, Nanomed., Biotechnol.*, 2014, **44**, 1–7.
45 M. Grzelczak, J. Pérez-Juste, P. Mulvaney and L. M. Liz-Marzán, *Chem. Soc. Rev.*, 2008, **37**, 1783–1791.
46 S. E. Lohse and C. J. Murphy, *Chem. Mater.*, 2013, **25**, 1250–1261.
47 C. Kan, C. Wang, J. Zhu and H. Li, *J. Solid State Chem.*, 2010, **183**, 858–865.
48 M. A. Wall, S. Harmsen, S. Pal, L. Zhang, G. Arianna, J. R. Lombardi, C. M. Drain and M. F. Kircher, *Adv. Mater.*, 2017, **29**, 1605622.
49 J. Gubitosa, V. Rizzi, P. Fini, R. Del Sole, A. Lopedota, V. Laquintana, N. Denora, A. Agostiano and P. Cosma, *Mater. Sci. Eng., C*, 2020, **106**, 110170.
50 J. Yu, D. Xu, H. N. Guan, C. Wang, L. K. Huang and D. F. Chi, *Mater. Lett.*, 2016, **166**, 110–112.
51 S. Palanisamy, S. K. Ramaraj, S.-M. Chen, T.-W. Chiu, V. Velusamy, T. C. K. Yang, T.-W. Chen and S. Selvam, *J. Colloid Interface Sci.*, 2017, **496**, 364–370.
52 M. Annadhasan, J. Kasthuri and N. Rajendiran, *RSC Adv.*, 2015, **5**, 11458–11468.
53 F. Correard, K. Maximova, M.-A. Estève, C. Villard, M. Roy, A. Al-Kattan, M. Sentis, M. Gingras, A. V. Kabashin and D. Braguer, *Int. J. Nanomed.*, 2014, **9**, 5415–5430.
54 V. Amendola, S. Polizzi and M. Meneghetti, *J. Phys. Chem. B*, 2006, **110**, 7232–7237.
55 M. Vinod, R. S. Jayasree and K. G. Gopchandran, *Curr. Appl. Phys.*, 2017, **17**, 1430–1438.
56 M. Morita, T. Tachikawa, S. Seino, K. Tanaka and T. Majima, *ACS Appl. Nano Mater.*, 2018, **1**, 355–363.
57 J. C. Love, L. A. Estroff, J. K. Kriebel, R. G. Nuzzo and G. M. Whitesides, *Chem. Rev.*, 2005, **105**, 1103–1170.
58 E. Colangelo, J. Comenge, D. Paramelle, M. Volk, Q. Chen and R. Lévy, *Bioconjugate Chem.*, 2017, **28**, 11–22.
59 O. S. Muddineti, B. Ghosh and S. Biswas, *Int. J. Pharm.*, 2015, **484**, 252–267.
60 Q. Shao and C. K. Hall, *Langmuir*, 2016, **32**, 7888–7896.
61 B. Sajjanar, B. Kakodia, D. Bisht, S. Saxena, A. K. Singh, V. Joshi, A. K. Tiwari and S. Kumar, *J. Nanopart. Res.*, 2015, **17**, 234.
62 S. Giorgi-Coll, M. J. Marín, O. Sule, P. J. Hutchinson and K. L. H. Carpenter, *Mikrochim. Acta*, 2019, **187**, 13.
63 J. Cao, T. Sun and K. T. V. Grattan, *Sens. Actuators, B*, 2014, **195**, 332–351.
64 X. Huang and M. A. El-Sayed, *J. Adv. Res.*, 2010, **1**, 13–28.
65 X. Lu, M. Rycenga, S. E. Skrabalak, B. Wiley and Y. Xia, *Annu. Rev. Phys. Chem.*, 2009, **60**, 167–192.
66 Z. Zhang, Z. Chen, F. Cheng, Y. Zhang and L. Chen, *Biosens. Bioelectron.*, 2017, **89**, 932–936.
67 Y. A. Attia, D. Buceta, F. G. Requejo, L. J. Giovanetti and M. A. López-Quintela, *Nanoscale*, 2015, **7**, 11273–11279.
68 L. M. Liz-Marzán, *Langmuir*, 2006, **22**, 32–41.
69 A. Bigdeli, F. Ghasemi, H. Golmohammadi, S. Abbasi-Moayed, M. A. F. Nejad, N. Fahimi-Kashani, S. Jafarinejad, M. Shahrajabian and M. R. Hormozi-Nezhad, *Nanoscale*, 2017, **9**, 16546–16563.

70 S. Megarajan and A. Veerappan, *Opt. Mater.*, 2020, **108**, 110177.
71 W. H. Wu, M. Li, Y. Wang, H. X. Ouyang, L. Wang, C. X. Li, Y. C. Cao, Q. H. Meng and J. X. Lu, *Nanoscale Res. Lett.*, 2012, **7**, 658.
72 L. Mao, Q. Wang, Y. Luo and Y. Gao, *Talanta*, 2021, **222**, 121506.
73 J. Zhang, X. Sun and J. Wu, *Appl. Sci.*, 2019, **9**, 489.
74 L. Guo, X. Wu, L. Liu, H. Kuang and C. Xu, *Small*, 2018, **14**, 1701782.
75 A. J. Mieszawska, W. J. M. Mulder, Z. A. Fayad and D. P. Cormode, *Mol. Pharm.*, 2013, **10**, 831–847.
76 C.-C. Chang, C.-P. Chen, T.-H. Wu, C.-H. Yang, C.-W. Lin and C.-Y. Chen, *Nanomaterials*, 2019, **9**, 861.
77 P. Donati, T. Pomili, L. Boselli and P. P. Pompa, *Front. Bioeng. Biotechnol.*, 2020, **8**, 601216.
78 L. Shen, J. Chen, N. Li, P. He and Z. Li, *Anal. Chim. Acta*, 2014, **839**, 83–90.
79 C. Jiang, Z. Li, Y. Wu, W. Guo, J. Wang and Q. Jiang, *Bull. Korean Chem. Soc.*, 2018, **39**, 625–630.
80 Y. Wu, Y. Chen, Y. Li, J. Huang, H. Yu and Z. Wang, *Sens. Actuators, B*, 2018, **270**, 443–451.
81 C. Jiang, J. Zhu, Z. Li, J. Luo, J. Wang and Y. Sun, *RSC Adv.*, 2017, **7**, 44463–44469.
82 V. Kumar, D. Bano, D. K. Singh, S. Mohan, V. K. Singh and S. H. Hasan, *ACS Sustain. Chem. Eng.*, 2018, **6**, 7662–7675.
83 Y. Zhao, Y. Huang, H. Zhu, Q. Zhu and Y. Xia, *J. Am. Chem. Soc.*, 2016, **138**, 16645–16654.
84 S. M. Taghdisi, N. M. Danesh, M. Ramezani, A. S. Emrani and K. Abnous, *ACS Appl. Mater. Interfaces*, 2018, **10**, 12504–12509.
85 E. Guler, T. Yilmaz Sengel, Z. P. Gumus, M. Arslan, H. Coskunol, S. Timur and Y. Yagci, *Anal. Chem.*, 2017, **89**, 9629–9632.
86 C. Huang, T. Wen, F.-J. Shi, X.-Y. Zeng and Y.-J. Jiao, *ACS Omega*, 2020, **5**, 12550–12556.
87 C. Shende, C. Brouillette and S. Farquharson, *Analyst*, 2019, **144**, 5449–5454.
88 M. Cordeiro, F. Ferreira Carlos, P. Pedrosa, A. Lopez and P. V. Baptista, *J. Diagn.*, 2016, **6**, 43.
89 J. Shi, F. Tian, J. Lyu and M. Yang, *J. Mater. Chem. B*, 2015, **3**, 6989–7005.
90 A. B. Chinen, C. M. Guan, J. R. Ferrer, S. N. Barnaby, T. J. Merkel and C. A. Mirkin, *Chem. Rev.*, 2015, **115**, 10530–10574.
91 J. Xu, Y. Li, L. Wang, Y. Huang, D. Liu, R. Sun, J. Luo and C. Sun, *Dyes Pigm.*, 2015, **123**, 55–63.
92 G. Chen, F. Song, X. Xiong and X. Peng, *Ind. Eng. Chem. Res.*, 2013, **52**, 11228–11245.
93 S. Mayilo, M. A. Kloster, M. Wunderlich, A. Lutich, T. A. Klar, A. Nichtl, K. Kürzinger, F. D. Stefani and J. Feldmann, *Nano Lett.*, 2009, **9**, 4558–4563.
94 P. C. Ray, A. Fortner and G. K. Darbha, *J. Phys. Chem. B*, 2006, **110**, 20745–20748.
95 C. Wang, Y. Li, C. Zhou and Q. Zhao, *Mikrochim. Acta*, 2019, **186**, 728.
96 N.-T. Chen, S.-H. Cheng, C.-P. Liu, J. S. Souris, C.-T. Chen, C.-Y. Mou and L.-W. Lo, *Int. J. Mol. Sci.*, 2012, **13**, 16598–16623.
97 W. Dong, R. Wang, X. Gong and C. Dong, *Anal. Bioanal. Chem.*, 2019, **411**, 6687–6695.
98 Y. Wang, M. Lv, Z. Chen, Z. Deng, N. Liu, J. Fan and W. Zhang, *Front. Chem.*, 2020, **8**, 238.
99 J. Shi, C. Chan, Y. Pang, W. Ye, F. Tian, J. Lyu, Y. Zhang and M. Yang, *Biosens. Bioelectron.*, 2015, **67**, 595–600.
100 M. I. Halawa, J. Lai and G. Xu, *Mater. Today Nano*, 2018, **3**, 9–27.
101 C. Muehlethaler, M. Leona and J. R. Lombardi, *Anal. Chem.*, 2016, **88**, 152–169.
102 M. G. Albrecht and J. A. Creighton, *J. Am. Chem. Soc.*, 1977, **99**, 5215–5217.
103 D. L. Jeanmaire and R. P. Van Duyne, *J. Electroanal. Chem. Interfacial Electrochem.*, 1977, **84**, 1–20.
104 X. Gu, M. J. Trujillo, J. E. Olson and J. P. Camden, *Annu. Rev. Anal. Chem.*, 2018, **11**, 147–169.
105 S. Kumar, P. Kumar, A. Das and C. S. Pathak, 2020, DOI: 10.5772/intechopen.92614.
106 S. L. Kleinman, R. R. Frontiera, A.-I. Henry, J. A. Dieringer and R. P. Van Duyne, *Phys. Chem. Chem. Phys.*, 2013, **15**, 21–36.
107 H. Wei, S. M. Hossein Abtahi and P. J. Vikesland, *Environ. Sci.: Nano*, 2015, **2**, 120–135.
108 Q. Xiao, H. Gao, C. Lu and Q. Yuan, *TrAC, Trends Anal. Chem.*, 2012, **40**, 64–76.
109 D. Senapati, S. S. R. Dasary, A. K. Singh, T. Senapati, H. Yu and P. C. Ray, *Chem. – Eur. J.*, 2011, **17**, 8445–8451.
110 C. Catala, B. Mir-Simon, X. Feng, C. Cardozo, N. Pazos-Perez, E. Pazos, S. Gómez-de Pedro, L. Guerrini, A. Soriano, J. Vila, F. Marco, E. Garcia-Rico and R. A. Alvarez-Puebla, *Adv. Mater. Technol.*, 2016, **1**, 1600163.
111 B. Sharma, P. Bugga, L. R. Madison, A.-I. Henry, M. G. Blaber, N. G. Greeneltch, N. Chiang, M. Mrksich, G. C. Schatz and R. P. Van Duyne, *J. Am. Chem. Soc.*, 2016, **138**, 13952–13959.
112 J. Zhu, M.-J. Liu, J.-J. Li, X. Li and J.-W. Zhao, *Spectrochim. Acta, Part A*, 2018, **189**, 586–593.
113 Y. Ou, X. Wang, K. Lai, Y. Huang, B. A. Rasco and Y. Fan, *J. Agric. Food Chem.*, 2018, **66**, 2954–2961.
114 N. Ha Anh, M. Quan Doan, N. Xuan Dinh, T. Quang Huy, D. Quang Tri and A.-T. Le, *Appl. Surf. Sci.*, 2022, **584**, 152555.
115 M. Chen, W. Luo, Q. Liu, N. Hao, Y. Zhu, M. Liu, L. Wang, H. Yang and X. Chen, *Anal. Chem.*, 2018, **90**, 13647–13654.
116 A. M. Paul, Z. Fan, S. S. Sinha, Y. Shi, L. Le, F. Bai and P. C. Ray, *J. Phys. Chem. C*, 2015, **119**, 23669–23675.
117 L. Xu, H. Yin, W. Ma, H. Kuang, L. Wang and C. Xu, *Biosens. Bioelectron.*, 2015, **67**, 472–476.
118 C. Zhang, X. Liang, T. You, N. Yang, Y. Gao and P. Yin, *Anal. Methods*, 2017, **9**, 2517–2522.
119 Y. Shi, H. Wang, X. Jiang, B. Sun, B. Song, Y. Su and Y. He, *Anal. Chem.*, 2016, **88**, 3723–3729.

120 V. Dugandžić, S. Kupfer, M. Jahn, T. Henkel, K. Weber, D. Cialla-May and J. Popp, *Sens. Actuators, B*, 2019, **279**, 230–237.
121 K. W. Kho, U. S. Dinish, A. Kumar and M. Olivo, *ACS Nano*, 2012, **6**, 4892–4902.
122 H. Ma, X. Sun, L. Chen, W. Cheng, X. X. Han, B. Zhao and C. He, *Anal. Chem.*, 2017, **89**, 8877–8883.
123 C. Song, S. Guo, S. Jin, L. Chen and Y. M. Jung, *Chemosensors*, 2020, **8**, 118.
124 G. Zhang, *Nanotechnol. Rev.*, 2013, **2**, 269–288.
125 G. Liu, R. Zhang, X. Huang, L. Li, N. Liu, J. Wang and D. Xu, *Sensors*, 2018, **18**, 1595.
126 S. H. Hwang, S. Jeong, H. J. Choi, H. Eun, M. G. Jo, W. Y. Kwon, S. Kim, Y. Kim, M. Lee and K. S. Park, *J. Nanomater.*, 2019, **2019**, 3676384.
127 M. S. Cordray, M. Amdahl and R. R. Richards-Kortum, *Anal. Biochem.*, 2012, **431**, 99–105.
128 H. J. Butler, S. W. Fogarty, J. G. Kerns, P. L. Martin-Hirsch, N. J. Fullwood and F. L. Martin, *Analyst*, 2015, **140**, 3090–3097.
129 M. Swierczewska, S. Lee and X. Chen, *Phys. Chem. Chem. Phys.*, 2011, **13**, 9929–9941.
130 J. Manson, D. Kumar, B. J. Meenan and D. Dixon, *Gold Bull.*, 2011, **44**, 99–105.
131 H. Daima, P. R. Selvakannan, R. Shukla, S. Bhargava and V. Bansal, *PLoS One*, 2013, **8**, e79676.
132 Y.-Y. Wu, P. Huang and F.-Y. Wu, *Food Chem.*, 2020, **304**, 125377.
133 J. B. Wiester, in *Raman Spectroscopy in the Undergraduate Curriculum*, American Chemical Society, 2018, vol. 1305, ch. 2, pp. 13–33.
134 A. Saletnik, B. Saletnik and C. Puchalski, *Molecules*, 2021, **26**, 1537.
135 M. Nachtmann, J. Deuerling and M. Rädle, *Micromachines*, 2020, **11**, 353.
136 G. Maduraiveeran and R. Ramaraj, *J. Anal. Sci. Technol.*, 2017, **8**, 14.
137 D. Grieshaber, R. MacKenzie, J. Vörös and E. Reimhult, *Sensors*, 2008, **8**, 1400–1458.
138 J. Barek, *Chemosensors*, 2021, **9**, 12.
139 H. Martines-Arano, B. E. García-Pérez, M. A. Vidales-Hurtado, M. Trejo-Valdez, L. H. Hernández-Gómez and C. Torres-Torres, *Sensors*, 2019, **19**, 4728.
140 W. Xu, L. Xie, J. Zhu, X. Xu, Z. Ye, C. Wang, Y. Ma and Y. Ying, *ACS Photonics*, 2016, **3**, 2308–2314.
141 K. Yang, J. Li, M. Lamy de la Chapelle, G. Huang, Y. Wang, J. Zhang, D. Xu, J. Yao, X. Yang and W. Fu, *Biosens. Bioelectron.*, 2021, **175**, 112874.
142 K. Yang, W. Yu, G. Huang, J. Zhou, X. Yang and W. Fu, *RSC Adv.*, 2020, **10**, 26824–26833.
143 K. Smart, J. Du, L. Li, D. Wang, K. Leslie, F. Ji, X. D. Li and D. Z. Zeng, *Sensors*, 2016, **16**, 579.
144 V. A. Trofimov and S. A. Varentsova, *Sensors*, 2016, **16**, 502.
145 S. Amiri, R. Ahmadi, A. Salimi, A. Navaee, S. Hamd Qaddare and M. K. Amini, *New J. Chem.*, 2018, **42**, 16027–16035.
146 H. Chen, K. Zhou and G. Zhao, *Trends Food Sci. Technol.*, 2018, **78**, 83–94.
147 Y. Qi, D. Song and Y. Chen, *Sci. Total Environ.*, 2021, **766**, 142579.
148 Z. Huang, J. Chen, Z. Luo, X. Wang and Y. Duan, *Anal. Chem.*, 2019, **91**, 4806–4813.
149 X. Niu, Y. Zhong, R. Chen, F. Wang, Y. Liu and D. Luo, *Sens. Actuators, B*, 2018, **255**, 1577–1581.
150 L. Li, B. Liu and Z. Chen, *Mikrochim. Acta*, 2018, **186**, 37.
151 L. Beqa, A. K. Singh, S. A. Khan, D. Senapati, S. R. Arumugam and P. C. Ray, *ACS Appl. Mater. Interfaces*, 2011, **3**, 668–673.
152 L. Gong, B. Du, L. Pan, Q. Liu, K. Yang, W. Wang, H. Zhao, L. Wu and Y. He, *Mikrochim. Acta*, 2017, **184**, 1185–1190.
153 W. Chu, Y. Zhang, D. Li, C. J. Barrow, H. Wang and W. Yang, *Biosens. Bioelectron.*, 2015, **67**, 621–624.
154 A. Anwar, A. Minhaz, N. A. Khan, K. Kalantari, A. B. M. Afifi and M. R. Shah, *Sens. Actuators, B*, 2018, **257**, 875–881.
155 L. Yang, X. Zhang, H. Li and L. Jiang, *Anal. Methods*, 2017, **9**, 6139–6147.
156 W. Bai, C. Zhu, J. Liu, M. Yan, S. Yang and A. Chen, *Environ. Toxicol. Chem.*, 2015, **34**, 2244–2249.
157 S. Wu, D. Li, J. Wang, Y. Zhao, S. Dong and X. Wang, *Sens. Actuators, B*, 2017, **238**, 427–433.
158 C. Zhang, Z. Jiang, M. Jin, P. Du, G. Chen, X. Cui, Y. Zhang, G. Qin, F. Yan, A. M. Abd El-Aty, A. Hacimüftüoğlu and J. Wang, *Food Chem.*, 2020, **326**, 126813.
159 D. Huang, J. Zhao, M. Wang and S. Zhu, *Food Control*, 2020, **108**, 106835.
160 X. Chen, M. Lin, L. Sun, T. Xu, K. Lai, M. Huang and H. Lin, *Food Chem.*, 2019, **293**, 271–277.
161 J. Chen, Y. Huang, P. Kannan, L. Zhang, Z. Lin, J. Zhang, T. Chen and L. Guo, *Anal. Chem.*, 2016, **88**, 2149–2155.
162 Y. Zhou, P. Wang, X. Su, H. Zhao and Y. He, *Talanta*, 2013, **112**, 20–25.
163 P. Wang, X. Su, L. Shi and Y. Yuan, *Mikrochim. Acta*, 2016, **183**, 2899–2905.
164 S. Han, T. Zhou, B. Yin and P. He, *Mikrochim. Acta*, 2018, **185**, 210.
165 K.-M. Song, E. Jeong, W. Jeon, M. Cho and C. Ban, *Anal. Bioanal. Chem.*, 2012, **402**, 2153–2161.
166 N. Zhou, J. Zhang and Y. Tian, *Anal. Methods*, 2014, **6**, 1569–1574.
167 X. Zhang, Y. Zhang, H. Zhao, Y. He, X. Li and Z. Yuan, *Anal. Chim. Acta*, 2013, **778**, 63–69.
168 S. Yan, X. Lai, G. Du and Y. Xiang, *Anal. Chim. Acta*, 2018, **1034**, 153–160.
169 H. Peng and I. A. Chen, *ACS Nano*, 2019, **13**, 1244–1252.
170 X.-Y. Chen, W. Ha and Y.-P. Shi, *Talanta*, 2019, **194**, 475–484.
171 M. Zhou, J. Yin, X. Zhao, Y. Fu, X. Jin, X. Liu and T. Jiao, *Colloids Surf., A*, 2020, **603**, 125293.
172 J. Du, Z. Wang, X. Peng and J. Fan, *Ind. Eng. Chem. Res.*, 2015, **54**, 12011–12016.
173 C. Xiao, X. Zhang, J. Liu, A. Yang, H. Zhao, X. Li, Y. He and Z. Yuan, *Anal. Methods*, 2015, **7**, 924–929.
174 N. Gao, P. Huang and F. Wu, *Spectrochim. Acta, Part A*, 2018, **192**, 174–180.
175 J. Li, P. Huang and F. Wu, *J. Nanopart. Res.*, 2016, **18**, 156.

176 C.-j. Zhang, Z.-y. Gao, Q.-b. Wang, X. Zhang, J.-s. Yao, C.-d. Qiao and Q.-z. Liu, *Polymers*, 2018, **10**, 873.
177 P. Song, L. Wu and W. Guan, *Nutrients*, 2015, **7**, 9872–9895.
178 S.-C. Kwon, I. Kim, J. Song and J. Park, *Ann. Occup. Environ. Med.*, 2018, **30**, 5.
179 C. Martínez-Aquino, A. M. Costero, S. Gil and P. Gaviña, *Nanomaterials*, 2019, **9**, 302.
180 X. Nie, Z. Chen, Y. Tian, S. Chen, L. Qu and M. Fan, *Food Chem.*, 2021, **340**, 127930.
181 F. K. Alsammarraie, M. Lin, A. Mustapha, H. Lin, X. Chen, Y. Chen, H. Wang and M. Huang, *Food Chem.*, 2018, **259**, 219–225.
182 J. Jia, S. Yan, X. Lai, Y. Xu, T. Liu and Y. Xiang, *Food Anal. Methods*, 2018, **11**, 1668–1676.
183 C. Zhao, C.-y. Hong, Z.-z. Lin, X.-m. Chen and Z.-Y. Huang, *Mikrochim. Acta*, 2019, **186**, 322.
184 N. Bhardwaj, S. K. Bhardwaj, M. K. Nayak, J. Mehta, K.-H. Kim and A. Deep, *TrAC, Trends Anal. Chem.*, 2017, **97**, 120–135.
185 Y. Zou, J. Liang, Z. She and H.-B. Kraatz, *Talanta*, 2019, **193**, 15–22.
186 K. Fu, Y. Zheng, J. Li, Y. Liu, B. Pang, X. Song, K. Xu, J. Wang and C. Zhao, *J. Agric. Food Chem.*, 2018, **66**, 9516–9521.
187 B. Jin, S. Wang, M. Lin, Y. Jin, S. Zhang, X. Cui, Y. Gong, A. Li, F. Xu and T. J. Lu, *Biosens. Bioelectron.*, 2017, **90**, 525–533.
188 R. Gupta, A. Kumar, S. Kumar, A. K. Pinnaka and N. K. Singhal, *Sens. Actuators, B*, 2021, **329**, 129100.
189 J. Yi, P. Wu, G. Li, W. Xiao, L. Li, Y. He, Y. He, P. Ding and C. Chen, *Mikrochim. Acta*, 2019, **186**, 711.
190 X. Tao, Z. Liao, Y. Zhang, F. Fu, M. Hao, Y. Song and E. Song, *Chin. Chem. Lett.*, 2021, **32**, 791–795.
191 J. Feng, Q. Shen, J. Wu, Z. Dai and Y. Wang, *Food Control*, 2019, **98**, 333–341.
192 J. Huang, J. Sun, A. R. Warden and X. Ding, *Food Control*, 2020, **108**, 106885.
193 M. Esmaeillou, G. Zarrini, M. Ahangarzadeh Rezaee, J. Shahbazi Mojarrad and A. Bahadori, *Adv. Pharm. Bull.*, 2017, **7**, 479–483.
194 C. Wang, B. Gu, Q. Liu, Y. Pang, R. Xiao and S. Wang, *Int. J. Nanomed.*, 2018, **13**, 1159–1178.
195 M. Yu, H. Wang, F. Fu, L. Li, J. Li, G. Li, Y. Song, M. T. Swihart and E. Song, *Anal. Chem.*, 2017, **89**, 4085–4090.
196 H. Peng, R. E. Borg, A. B. N. Nguyen and I. A. Chen, *ACS Sens.*, 2020, **5**, 1491–1499.
197 W. Zhang, Y. Wang, M. Nan, Y. Li, J. Yun, Y. Wang and Y. Bi, *Food Chem.*, 2021, **348**, 129128.
198 T. Chotchuang, W. Cheewasedtham, T. J. Jayeoye and T. Rujiralai, *Mikrochim. Acta*, 2019, **186**, 655.
199 C. Cao, P. Li, H. Liao, J. Wang, X. Tang and L. Yang, *Anal. Bioanal. Chem.*, 2020, **412**, 4609–4617.
200 S. Liu, X. Leng, X. Wang, Q. Pei, X. Cui, Y. Wang and J. Huang, *Mikrochim. Acta*, 2017, **184**, 1969–1976.
201 Y. Liu, Q. Ouyang, H. Li, M. Chen, Z. Zhang and Q. Chen, *J. Agric. Food Chem.*, 2018, **66**, 6188–6195.
202 W. Jin, P. Huang, Y. Chen, F. Wu and Y. Wan, *J. Nanopart. Res.*, 2015, **17**, 358.
203 M. H. Hu, W. H. Huang, L. L. Suo, L. H. Zhou, L. F. Ma and H. F. Zhu, *Anal. Methods*, 2017, **9**, 5598–5603.
204 S. Thatai, P. Khurana, S. Prasad, S. K. Soni and D. Kumar, *Microchem. J.*, 2016, **124**, 104–110.
205 W. Diao, G. Wang, L. Wang, L. Zhang, S. Ding, T. Takarada, M. Maeda and X. Liang, *ACS Appl. Bio Mater.*, 2020, **3**, 7003–7010.
206 N. Ratnarathorn, O. Chailapakul and W. Dungchai, *Talanta*, 2015, **132**, 613–618.
207 B. Feng, R. Zhu, S. Xu, Y. Chen and J. Di, *RSC Adv.*, 2018, **8**, 4049–4056.
208 H. Yu, M. Wang, J. Cao, Y. She, Y. Zhu, J. Ye, A. M. Abd El-Aty, A. Hacımüftüoğlu, J. Wang and S. Lao, *Food Chem.*, 2021, **364**, 130326.
209 D. Li, S. Wang, L. Wang, H. Zhang and J. hu, *Anal. Bioanal. Chem.*, 2019, **411**, 2645.
210 G. Liu, R. Zhang, L. Li, X. Huang, T. Li, M. Lu, D. Xu and J. Wang, *Nanomaterials*, 2018, **8**, 499.
211 S.-H. Hung, J.-Y. Lee, C.-C. Hu and T.-C. Chiu, *Food Chem.*, 2018, **260**, 61–65.
212 H. Luo, X. Wang, Y. Huang, K. Lai, B. A. Rasco and Y. Fan, *J. Sci. Food Agric.*, 2018, **98**, 3892–3898.
213 L. Zou, X. Li and Y. Lai, *Microchem. J.*, 2021, **162**, 105858.
214 S. H. Jalalian, P. Lavaee, M. Ramezani, N. M. Danesh, M. Alibolandi, K. Abnous and S. M. Taghdisi, *Spectrochim. Acta, Part A*, 2021, **246**, 119062.
215 M. Ramezani, S. H. Jalalian, S. M. Taghdisi, K. Abnous and M. Alibolandi, in *Biomedical Engineering Technologies: Volume 1*, ed. M. R. Ossandon, H. Baker and A. Rasooly, Springer US, New York, NY, 2022, pp. 417–436, DOI: 10.1007/978-1-0716-1803-5_21.
216 S. Sun and Y. Xie, *Anal. Methods*, 2021, **13**, 1255–1260.
217 J.-y. Xin, L.-x. Zhang, D.-d. Chen, K. Lin, H.-c. Fan, Y. Wang and C.-g. Xia, *Food Chem.*, 2015, **174**, 473–479.
218 X. Bao, J. Liu, Q. Zheng, L. Duan, Y. Zhang, J. Qian and T. Tu, *Chin. Chem. Lett.*, 2021, 3023–3026.
219 J. Zhu, H. Chang, J.-J. Li, X. Li and J.-W. Zhao, *Sens. Actuators, B*, 2017, **239**, 906–915.
220 P. Kumar, P. Kumar, S. Manhas and N. K. Navani, *Sens. Actuators, B*, 2016, **233**, 157–161.
221 K. Chaisiwamongkhol, S. Labaidae, S. Pon-in, S. Pinsrithong, T. Bunchuay and A. Phonchai, *Microchem. J.*, 2020, **158**, 105273.
222 P. Kumar, P. Ramulu Lambadi and N. Kumar Navani, *Biosens. Bioelectron.*, 2015, **72**, 340–347.
223 H. S. Ali, B. M. El-Haj, S. Saifullah and M. Kawish, in *Metal Nanoparticles for Drug Delivery and Diagnostic Applications*, ed. M. R. Shah, M. Imran and S. Ullah, Elsevier, 2020, pp. 43–58, DOI: 10.1016/B978-0-12-816960-5.00004-5.
224 B. D. Ventura, M. Cennamo, A. Minopoli, R. Campanile, S. B. Censi, D. Terracciano, G. Portella and R. Velotta, *ACS Sens.*, 2020, **5**, 3043–3048.
225 J. Peng, N. Zhou, Y. Zhong, Y. Su, L. Zhao and Y.-T. Chang, *Mikrochim. Acta*, 2019, **186**, 618.

226 Division of Child Health and Development and Maternal Health and Safe Motherhood Program, *Hypoglycaemia of the newborn: review of the literature*, World Health Organization, Geneva, 1997, https://apps.who.int/iris/handle/10665/63362.

227 WHO and IDF, *Definition and diagnosis of diabetes mellitus and intermediate hyperglycemia*, 2006.

228 S. Kawahito, H. Kitahata and S. Oshita, *World J. Gastroenterol.*, 2009, **15**, 4137–4142.

229 E.-H. Yoo and S.-Y. Lee, *Sensors*, 2010, **10**, 4558–4576.

230 Q. Yang, X. Zhang, S. Kumar, R. Singh, B. Zhang, C. Bai and X. Pu, *Plasmonics*, 2020, **15**, 841–848.

231 X. Gu, H. Wang, Z. D. Schultz and J. P. Camden, *Anal. Chem.*, 2016, **88**, 7191–7197.

232 W. Na, H. Liu, M. Wang and X. Su, *Mikrochim. Acta*, 2017, **184**, 1463–1470.

233 Y.-P. Li, L. Jiang, T. Zhang, M. Lin, D.-B. Tian and H. Huang, *Chin. Chem. Lett.*, 2014, **25**, 77–79.

234 T. Pinheiro, J. Ferrão, A. C. Marques, M. J. Oliveira, N. M. Batra, P. M. F. J. Costa, M. P. Macedo, H. Águas, R. Martins and E. Fortunato, *Nanomaterials*, 2020, **10**, 2027.

235 F. B. Araujo, D. S. Barbosa, C. Y. Hsin, R. C. Maranhão and D. S. P. Abdalla, *Atherosclerosis*, 1995, **117**, 61–71.

236 J. Kwak, H. J. Park and S. S. Lee, *Bull. Korean Chem. Soc.*, 2018, **39**, 156–160.

237 M. Nagpal, S. Singh, P. Singh, P. Chauhan and M. A. Zaidi, *Natl. J. Maxillofac. Surg.*, 2016, **7**, 17–20.

238 Y. Zhang, M. Li, X. Gao, Y. Chen and T. Liu, *J. Hematol. Oncol.*, 2019, **12**, 137.

239 N. L. Henry and D. F. Hayes, *Mol. Oncol.*, 2012, **6**, 140–146.

240 R. E. Lane, D. Korbie, M. M. Hill and M. Trau, *Clin. Transl. Med.*, 2018, **7**, 14.

241 W. Zhao, H. Li, Y. Tang, M. Liu, S. Wang and R. Yu, *Mikrochim. Acta*, 2019, **186**, 517.

242 E. Assah, W. Goh, X. T. Zheng, T. X. Lim, J. Li, D. Lane, F. Ghadessy and Y. N. Tan, *Colloids Surf., B*, 2018, **169**, 214–221.

243 Y. Bai, H. Li, J. Xu, Y. Huang, X. Zhang, J. Weng, Z. Li and L. Sun, *Biosens. Bioelectron.*, 2020, **166**, 112424.

244 V. Ranganathan, S. Srinivasan, A. Singh and M. C. DeRosa, *Anal. Biochem.*, 2020, **588**, 113471.

245 R. Ahirwar and P. Nahar, *Anal. Bioanal. Chem.*, 2016, **408**, 327–332.

246 L. Zhou, F. Ji, T. Zhang, F. Wang, Y. Li, Z. Yu, X. Jin and B. Ruan, *Talanta*, 2019, **197**, 444–450.

247 K. P. P. Htoo, V. Yamkamon, S. Yainoy, T. Suksrichavalit, W. Viseshsindh and W. Eiamphungporn, *Clin. Chim. Acta*, 2019, **488**, 40–49.

248 A. Kumar, B. Mazinder Boruah and X.-J. Liang, *J. Nanomater.*, 2011, **2011**, 202187.

249 B. P. Crulhas, C. R. Basso, G. R. Castro and V. A. Pedrosa, *ECS J. Solid State Sci. Technol.*, 2021, **10**, 047004.

250 E. J. H. Wee, Y. Wang, S. C.-H. Tsao and M. Trau, *Theranostics*, 2016, **6**, 1506–1513.

251 J. Yu, J. Jeon, N. Choi, J. O. Lee, Y.-P. Kim and J. Choo, *Sens. Actuators, B*, 2017, **251**, 302–309.

252 Y.-S. Borghei, M. Hosseini, M. R. Ganjali and H. Ju, *Mikrochim. Acta*, 2018, **185**, 286.

253 G. Higgs and F. Slack, *J. Clin. Bioinf.*, 2013, **3**, 17.

254 M. C. Boonstra, S. W. L. de Geus, H. A. J. M. Prevoo, L. J. A. C. Hawinkels, C. J. H. van de Velde, P. J. K. Kuppen, A. L. Vahrmeijer and C. F. M. Sier, *Biomarkers Cancer*, 2016, **8**, 119–133.

255 R. Sasidharan and C. Chothia, *Proc. Natl. Acad. Sci. U.S.A.*, 2007, **104**, 10080–10085.

256 S. Chen, Q. Zhao, L. Zhang, L. Wang, Y. Zeng and H. Huang, *Sens. Actuators, B*, 2015, **221**, 1391–1397.

257 A. V. Krasnoslobodtsev, M. P. Torres, S. Kaur, I. V. Vlassiouk, R. J. Lipert, M. Jain, S. K. Batra and Y. L. Lyubchenko, *Nanomedicine*, 2015, **11**, 167–173.

258 C. Zhang, Y. Gao, N. Yang, T. You, H. Chen and P. Yin, *Mikrochim. Acta*, 2018, **185**, 90.

259 O. H. Shayesteh and R. Ghavami, *Spectrochim. Acta, Part A*, 2020, **226**, 117644.

260 C. Luo, W. Wen, F. Lin, X. Zhang, H. Gu and S. Wang, *RSC Adv.*, 2015, **5**, 10994–10999.

261 R. Shen, J. Zhang, W. Huang, S. Wu, G. Li, S. Zou and L. Ling, *Anal. Chim. Acta*, 2021, **1145**, 87–94.

262 K. Abhange, A. Makler, Y. Wen, N. Ramnauth, W. Mao, W. Asghar and Y. Wan, *Bioact. Mater.*, 2021, **6**, 3705–3743.

263 M. Oliveira-Rodríguez, S. López-Cobo, H. T. Reyburn, A. Costa-García, S. López-Martín, M. Yáñez-Mó, E. Cernuda-Morollón, A. Paschen, M. Valés-Gómez and M. C. Blanco-López, *J. Extracell. Vesicles*, 2016, **5**, 31803.

264 M. Hou, D. He, H. Bu, H. Wang, J. Huang, J. Gu, R. Wu, H.-W. Li, X. He and K. Wang, *Analyst*, 2020, **145**, 6232–6236.

265 Y. Li, Y. Zhang, M. Zhao, Q. Zhou, L. Wang, H. Wang, X. Wang and L. Zhan, *Chem. Commun.*, 2016, **52**, 3959–3961.

266 W.-J. Shieh and S. R. Zaki, in *Advanced Techniques in Diagnostic Microbiology*, ed. Y.-W. Tang and C. W. Stratton, Springer US, Boston, MA, 2013, pp. 873–890, DOI: 10.1007/978-1-4614-3970-7_45.

267 W. Sabiiti, K. Azam, E. Esmeraldo, N. Bhatt, A. Rachow and S. H. Gillespie, *J. Clin. Microbiol.*, 2019, **57**, e01778–01718.

268 T.-T. Tsai, C.-Y. Huang, C.-A. Chen, S.-W. Shen, M.-C. Wang, C.-M. Cheng and C.-F. Chen, *ACS Sens.*, 2017, **2**, 1345–1354.

269 N. A. Owens, A. Pinter and M. D. Porter, *J. Raman Spectrosc.*, 2019, **50**, 15–25.

270 S. R. Ahmed, J. Kim, T. Suzuki, J. Lee and E. Y. Park, *Biotechnol. Bioeng.*, 2016, **113**, 2298–2303.

271 S. G. Hwang, K. Ha, K. Guk, D. K. Lee, G. Eom, S. Song, T. Kang, H. Park, J. Jung and E.-K. Lim, *Sci. Rep.*, 2018, **8**, 12999.

272 Y. Liu, L. Zhang, W. Wei, H. Zhao, Z. Zhou, Y. Zhang and S. Liu, *Analyst*, 2015, **140**, 3989–3995.

273 L. Zheng, J. Wei, X. Lv, Y. Bi, P. Wu, Z. Zhang, P. Wang, R. Liu, J. Jiang, H. Cong, J. Liang, W. Chen, H. Cao, W. Liu, G. F. Gao, Y. Du, X. Jiang and X. Li, *Biosens. Bioelectron.*, 2017, **91**, 46–52.

274 H. Kim, M. Park, J. Hwang, J. H. Kim, D.-R. Chung, K.-s. Lee and M. Kang, *ACS Sens.*, 2019, **4**, 1306–1312.

275 H. A. Alfassam, M. S. Nassar, M. M. Almusaynid, B. A. Khalifah, A. S. Alshahrani, F. A. Almughem, A. A. Alshehri, M. O. Alawad, S. Massadeh, M. Alaamery, I. M. Aldeailej, A. A. Alamri, A. Z. Binjomah and E. A. Tawfik, *Pharmaceutics*, 2021, **13**, 06.

276 L. Huang, L. Ding, J. Zhou, S. Chen, F. Chen, C. Zhao, J. Xu, W. Hu, J. Ji, H. Xu and G. L. Liu, *Biosens. Bioelectron.*, 2021, **171**, 112685.

277 T. T. S. Lew, K. M. M. Aung, S. Y. Ow, S. N. Amrun, L. Sutarlie, L. F. P. Ng and X. Su, *ACS Nano*, 2021, **15**, 12286–12297.

278 Z. Chen, Q. Wu, J. Chen, X. Ni and J. Dai, *Virol. Sin.*, 2020, **35**, 351–354.

279 S. Aithal, S. Mishriki, R. Gupta, R. P. Sahu, G. Botos, S. Tanvir, R. W. Hanson and I. K. Puri, *Talanta*, 2022, **236**, 122841.

280 P. A. Nair and K. Sreenivasan, *Anal. Methods*, 2016, **8**, 2082–2087.

281 Y. Xiong, Y. Zhang, P. Rong, J. Yang, W. Wang and D. Liu, *Nanoscale*, 2015, **7**, 15584–15588.

282 B. Brasiunas, A. Popov, A. Ramanavicius and A. Ramanaviciene, *Food Chem.*, 2021, **351**, 129238.

283 M. L. Firdaus, E. Saputra, S. M. Ginting, S. Wyantuti, D. R. Eddy, L. Rahmidar and B. Yuliarto, *Sens. Bio-Sens. Res*, 2022, **35**, 100472.

284 H.-H. Deng, G.-L. Hong, F.-L. Lin, A.-L. Liu, X.-H. Xia and W. Chen, *Anal. Chim. Acta*, 2016, **915**, 74–80.

285 N. Mohseni and M. Bahram, *Spectrochim. Acta, Part A*, 2018, **193**, 451–457.

286 M. Oliveira-Rodríguez, S. López-Cobo, H. T. Reyburn, A. Costa-García, S. López-Martín, M. Yáñez-Mó, E. Cernuda-Morollón, A. Paschen, M. Valés-Gómez and M. C. Blanco-López, *J. Extracell. Vesicles*, 2016, **5**, 31803.

287 M. K. Hameed, J. B. M. Parambath, M. T. Gul, A. A. Khan, Y. Park, C. Han and A. A. Mohamed, *Appl. Surf. Sci.*, 2022, **583**, 152504.

288 Y. Feng, G. Liu, M. La and L. Liu, *Molecules*, 2022, **27**, 615.

289 S. Kunwar, P. Pandey and J. Lee, *ACS Omega*, 2019, **4**, 17340–17351.

290 G. Cabello, K. C. Nwoko, J. F. Marco, M. Sánchez-Arenillas, A. M. Méndez-Torres, J. Feldmann, C. Yáñez and T. A. D. Smith, *J. Alloys Compd.*, 2019, **791**, 184–192.

291 M. Sui, S. Kunwar, P. Pandey and J. Lee, *Sci. Rep.*, 2019, **9**, 16582.

292 T. Bai, M. Wang, M. Cao, J. Zhang, K. Zhang, P. Zhou, Z. Liu, Y. Liu, Z. Guo and X. Lu, *Anal. Bioanal. Chem.*, 2018, **410**, 2291–2303.

293 J. M. George, R. N. Priyanka and B. Mathew, *Microchem. J.*, 2020, **155**, 104686.

294 F. Zhang, J. Zhu, J.-J. Li and J.-W. Zhao, *J. Mater. Chem. C*, 2015, **3**, 6035–6045.

295 B. Liu, H. Ni, D. Zhang, D. Wang, D. Fu, H. Chen, Z. Gu and X. Zhao, *ACS Sens.*, 2017, **2**, 1035–1043.

296 N. Hussain, H. Pu and D.-W. Sun, *Food Chem.*, 2021, **350**, 129025.

297 P. Srinoi, Y.-T. Chen, V. Vittur, M. D. Marquez and T. R. Lee, *Appl. Sci.*, 2018, **8**, 1106.

298 I. Ansari, M. M. El-Kady, C. Arora, M. Sundararajan, D. Maiti and A. Khan, in *Global Climate Change*, ed. S. Singh, P. Singh, S. Rangabhashiyam and K. K. Srivastava, Elsevier, 2021, pp. 361–391, DOI: 10.1016/B978-0-12-822928-6.00017-4.

299 Q. Li, P. Song and J. Wen, *Curr. Opin. Food Sci.*, 2019, **30**, 79–84.

300 J. Reed, S. Bain and V. Kanamarlapudi, *Diabetes, Metab. Syndr. Obes.: Targets Ther.*, 2021, **14**, 3567–3602.

301 H. Sung, J. Ferlay, R. L. Siegel, M. Laversanne, I. Soerjomataram, A. Jemal and F. Bray, *Ca-Cancer J. Clin.*, 2021, **71**, 209–249.

302 Q. Xu, S. Du, G.-d. Jin, H. Li and X. Y. Hu, *Mikrochim. Acta*, 2011, **173**, 323–329.

303 A. T. Kharroubi and H. M. Darwish, *World J. Diabetes*, 2015, **6**, 850–867.

304 V. Schirrmacher, *Int. J. Oncol.*, 2019, **54**, 407–419.

305 M. Simeoni, T. Cavinato, D. Rodriguez and D. Gatfield, *Commun. Biol.*, 2021, **4**, 715.

306 T.-A. T. Le, K. Vodden, J. Wu and G. Atiwesh, *Int. J. Environ. Res. Public Health*, 2021, **18**, 559.

307 Y.-C. Tyan, M.-H. Yang, S.-B. Jong, C.-K. Wang and J. Shiea, *Anal. Bioanal. Chem.*, 2009, **395**, 729–735.

308 J. Khodaveisi, S. Dadfarnia, A. M. H. Shabani and D. Saberi, *Sens. Actuators, B*, 2017, **239**, 1300–1306.